Composition and Cycling of Natural Organic Matter: Insights from NMR Spectroscopy

A Thesis
Presented to
The Academic Faculty

by

Poulomi Sannigrahi

In Partial Fulfillment
of the Requirements for the Degree
Doctor of Philosophy

School of Earth and Atmospheric Sciences
Georgia Institute of Technology
December 2005

Composition and Cycling of Natural Organic Matter: Insights from NMR Spectroscopy

Approved by:

Professor Ellery D. Ingall, Advisor
School of Earth & Atmospheric Sciences
Georgia Institute of Technology

Dr. Martial Taillefert
School of Earth & Atmospheric Sciences
Georgia Institute of Technology

Dr. Rodney J. Weber
School of Earth & Atmospheric Sciences
Georgia Institute of Technology

Dr. Andrew G. Stack
School of Earth & Atmospheric Sciences
Georgia Institute of Technology

Dr. Ronald Benner
Department of Biological Sciences
University of South Carolina

Date Approved: November 16, 2005

To my Family

ACKNOWLEDGEMENTS

I would like to thank several people who helped make this dissertation possible. First, I would like to thank my advisor Dr. Ellery Ingall for his guidance, mentorship, and support at all stages of my doctoral research. Ellery's enthusiasm for science and a unique sense of humor has helped me through the ups and downs of research. I would like to thank Dr. Ron Benner for his valuable suggestions and advice. My interactions with him have helped improve the quality of my research. Dr. Rodney Weber supported me during the summer of 2004 and gave me the opportunity to work with atmospheric aerosols. It was a pleasure to work with him and Amy Sullivan. Dr. Martial Taillefert and Dr. Andrew Stack are also thanked for serving on my committee, their comments and suggestions have added to the quality of this dissertation.

My sincere thanks go out to Dr. Johannes Leisen of the Georgia Tech NMR center, for training me in the use of solid-state NMR spectrometers, helping with data interpretation, and allowing me ready access to the NMR lab. Dr. Les Gelbaum, director of the NMR center, has also been very helpful, especially during my occasional forays into solution NMR. Karl Kaiser at the University of South Carolina, carried out the molecular-level analyses used in this dissertation and also assisted with sample collection.

I would like to thank the School of Earth and Atmospheric Sciences for providing me with teaching assistantships and conference travel support, when needed. Rita Anderson, Susan Ryan, Laura Cederquist and Kathy Plummer have helped in various administrative issues.

My fellow graduate students in EAS, especially Melanie, Cynthia, Jean-Francois, JR, Patrick and Amy have not only been great to work with, but also a lot of fun to be around. Thanks are also due to Sameer and Mamta for their unwavering friendship over the years, and my family for always being there for me. Last, but definitely not the least, I would like to thank my husband Manuj for his friendship, love and support. He has spent countless

hours helping me with any and all computer related issues. His suggestion to write this dissertation using LaTeXsignificantly eased the writing process.

TABLE OF CONTENTS

LIST OF TABLES

LIST OF FIGURES

LIST OF ABBREVIATIONS

CP-MAS	Cross polarization-magic angle spinning
DIC	Dissolved inorganic carbon
DIP	Dissolved inorganic phosphate
DOC	Dissolved organic carbon
DOM	Dissolved organic matter
DON	Dissolved organic nitrogen
DOP	Dissolved organic phosphorus
GC-MS	Gas chromatography-mass spectrometry
HMW-DOM	High molecular weight-dissolved organic matter
IR	Infrared
LMW-DOM	Low molecular weight-dissolved organic matter
MUC	Molecularly uncharacterized component
NMR	Nuclear magnetic resonance
NOM	Natural organic matter
OC	Organic carbon
POC	Particulate organic carbon
POM	Particulate organic matter
TDP	Total dissolved phosphorus
THAA	Total hydrolysable amino acids

THAS	Total hydrolysable amino sugars
THNS	Total hydrolysable neutral sugars
UDOM	Ultrafiltered dissolved organic matter
UPOM	Ultrafiltered particulate organic matter
WSOC	Water-soluble organic carbon

SUMMARY

Different aspects of natural organic matter composition and cycling have been studied using solid-state ^{13}C and ^{31}P Nuclear Magnetic Resonance (NMR) spectroscopy. Depending on the specific study, complementary analytical techniques such as elemental, isotopic and molecular analyses have also been applied. Samples from a variety of environments were examined including ocean waters, marine sediments and atmospheric aerosols. Studies from all these environments illustrate differences in natural organic matter composition resulting from various factors such as sources, cycling mechanisms and redox conditions. In the marine water column, organic matter of two different size fractions (dissolved and particulate) is found to have distinctly different bulk chemical and isotopic compositions. Overall, this indicates that particulate organic matter does not form from the simple physical aggregation of dissolved organic matter, and dissolved organic matter is not the primary source for particulate organic matter. Comparison of carbon and phosphorus compositional changes with depth in the ocean within the dissolved and particulate fractions reveals differences in cycling mechanisms. In the marine water column, selective mineralization of specific carbon compounds such as carbohydrates and amino acids occurs relative other species such as lipids. Whereas for phosphorus, the relative proportion of the different functional groups are unvarying with depth. In marine sediments, NMR spectroscopy reveals P cycling for specific phases such as polyphosphates is a function of sediment redox conditions. In atmospheric aerosols ^{13}C NMR spectroscopy shows differences in water-soluble organic carbon composition from urban versus biomass burning sources. Urban aerosols have higher aliphatic and lower aromatic compound contents relative to samples derived from biomass burning. The results of these studies provide new insights into carbon and phosphorus cycling in the environment and demonstrate the capabilities of solid-state NMR as a tool for investigating natural organic matter composition.

CHAPTER 1

INTRODUCTION

1.1 Natural Organic Material in the Environment

Organic material is an important constituent of all natural environments. Organic molecules are found in both soluble and insoluble forms in a variety of environments such as, atmospheric aerosols, soils, sediments and aquatic systems [151, 169]. Both living and non-living organic matter play important roles in the global biogeochemical cycles of carbon (C), nitrogen (N), phosphorus (P) and many other elements. Natural organic matter (NOM) bioavailability and composition affects soil fertility, carbon dioxide sequestration, nutrient cycling and metal speciation. NOM is produced by the activities of micro as well as macro fauna and flora and can undergo a wide variety of alteration processes such as physical degradation and aggregation, microbial remineralization, diagenesis, and photochemical reactions. The large number of different primary sources, coupled with the various alteration processes, leads to large variations in NOM composition.

Two important properties that dictate the behavior of organic molecules in the environment are functional group chemistry and macromolecular structure [148]. Evaluation of these two properties is complicated by the compositional and structural heterogeneity of the natural organic molecules, and their ability to form intramolecular and intermolecular hydrogen bonds, which further modify their structure and chemical reactivity [126]. One of the biggest challenges facing geochemists is to gain a better understanding of the relationship between chemical composition and structure, and the biogeochemical behavior of NOM [126].

This dissertation presents studies of different aspects of NOM cycling especially in marine systems and atmospheric aerosols. For all these studies, the versatile and powerful technique of solid-state ^{13}C and ^{31}P nuclear magnetic resonance (NMR) spectroscopy was the primary analytical technique used. Depending on nature of the study, complementary

analytical tools such as elemental C, N, P measurements, C stable isotope analyses and molecular level carbohydrate and amino acid analyses were applied. This chapter provides background information and motivation for the different NOM composition and cycling studies carried out as part of this dissertation.

1.2 Extraction and Analysis of NOM

Due to the chemical and structural complexity of NOM, scientists have devised several classification schemes in an effort to simplify their characterization. These classifications are based on different physical and chemical properties, such as size, molecular weight and acid or base solubility. NOM in aqueous environments is often classified as dissolved or particulate based on its passage or retention by filters with pore sizes in the 0.2 to 1.0 μm size range [12]. The fraction that passes through the filter is designated as *dissolved organic matter* (DOM) and the retained fraction is termed *particulate organic matter* (POM). In soils, atmospheric aerosols, and freshwater environments, NOM has been chemically separated into different fractions using reverse phase solid phase extractions with XAD-8 resins, whose primary partitioning force is hydrophobic interactions [159, 170]. The resin retains the hydrophobic organic molecules, while the hydrophilic molecules pass through. The hydrophilic and hydrophobic fractions are usually referred to as humic and fulvic acids, respectively.

Detailed NOM analyses often involve chromatographic separation and measurement of different biomolecular classes. Several biomolecular classes such as carbohydrates, amino acids, lipids, pigments and hydrocarbons have been successfully isolated from the complex NOM matrix and analyzed eg. [13,76,93,108,130,154,169,176]. While these molecular-level techniques have provided great insights in to the composition of NOM, prolonged hydrolysis by strong acids and bases used in these extractions, may lead to drastic pH changes and potential alteration of the pristine state of NOM. Despite substantial research efforts and increasing analytical sophistication, more than half of the OM in the natural environment remains uncharacterized at the molecular level [72]. In the marine water column, the molecularly uncharacterized fraction of NOM constitutes an increasing proportion of the

organic carbon in deeper waters [107, 177]. This is also true for NOM from other environments, such as soils, sediments and even aerosol water-soluble organic carbon(WSOC), where only a very small fraction of the organic carbon has been identified as individual compounds [45, 72, 144]. Identifying the composition of the molecularly uncharacterized component is thus fundamental to understanding the sources and cycling of NOM.

Spectroscopic analytical techniques such as NMR and infrared (IR), are excellent in providing information about the broad structural features of complex mixtures such as NOM. Chapter 2 of this dissertation provides an overview of the basic theory and principles of nuclear magnetic resonance (NMR) spectroscopy and its applications to natural organic material. This chapter also describes the experiments necessary to optimize NMR operating parameters for the semi-quantitative analyses of natural material. Elemental C:N:P ratios of organic material may also provide important information about bulk chemical composition and can sometimes be used to distinguish between organic material with different sources. Stable isotopic ratios (e.g. δ^{13}C and δ^{15}N) of NOM may also yield invaluable information about the sources and cycling pathways of organic material [61]. These techniques are described in individual chapters where appropriate. Comparison of compositional information gained independently from these different techniques is the key to characterizing the composition of the molecularly uncharacterized fraction of NOM.

1.3 Organic Matter in the Oceans

Chapters 3 to 6 of this dissertation examine the cycling of organic carbon and phosphorus in the marine environment. The oceans play a major role in the biogeochemical cycling of several key elements including carbon, nitrogen and phosphorus. Photosynthetic phytoplankton living in the surface oceans are responsible for almost half of the Earth's net primary productivity [147]. The crucial balance between carbon dioxide and oxygen in the atmosphere is largely controlled by marine primary productivity, which in turn in linked to the availability of limiting nutrients such as P and N. Thus, an understanding of the marine C and P cycles is central to determining the long term controls and variability of marine primary productivity.

Organic C (OC)dissolved in the oceans, suspended as particles and deposited in sediments together constitute a very significant fraction of the global C budget [73]. Both particulate and dissolved OM are continuously produced and remineralized in the marine water column, making OM a very dynamic component of the biogechemical cycles of C, N, and P. DOM is the dominant form of organic matter in the oceans and comprises approximately 730 Gt of C, making it one of the largest dynamic reservoirs of organic C on Earth [73]. The DOM reservoir of C is comparable in size to the atmospheric CO_2 and land biota reservoirs. Though a much smaller reservoir in size than DOM, marine particulate organic matter is also important as the sinking of POM from the surface to deep ocean waters is a major pathway for transporting C and other biologically associated elements within the ocean [107, 176]. Burial of C in the deep oceans and marine sediments is an effective long term sink in the global carbon cycle.

Chapter 3 presents a comprehensive study of ultrafiltered dissolved and particulate marine OM collected from a depth profile at the United States Joint Global Ocean Flux Study (USJGOFS) site, Station Aloha in the Pacific ocean. These OM fractions have been studied using ^{13}C NMR spectroscopy, together with elemental, isotopic and molecular level carbohydrate and amino acid analyses. Comparison of bulk compositional analyses from ^{13}C NMR spectroscopy, to specific molecular level carbohydrate and amino acid analyses, to understand the composition of the large molecularly uncharacterized fraction of marine OM is unique to this study. The results presented here are also the first reported NMR spectra of ultrafiltered particulate organic matter from the marine water column. The findings from chapter 3 have been published in Deep Sea Research I [141]. An overview of the organic C cycling at the Bermuda Atlantic time series study (BATS) site in the Atlantic Ocean is presented in Chapter 5. In this study solid state ^{13}C NMR spectroscopy has been used to understand the composition of ultrafiltered dissolved organic matter. The information gained from NMR was interpreted along with elemental C/N ratios and stable C isotopic ratios on DOM and suspended POM.

In the marine water column, P occurs in both organic and inorganic compounds. Marine organisms can utilize both dissolved organic phosphorus (DOP) and dissolved inorganic

phosphate (DIP), but DIP is their preferred substrate. DIP concentrations are almost undetectable in vast areas of oligotrophic surface ocean. As a result, surface water DOP concentrations often greatly exceed that of DIP in vast oligotrophic oceanic regions and many coastal areas making DOP an important potential source of P for organisms. P-esters and phosphonates are the major P functional groups in DOP [35, 36, 102]. While P-esters can be associated with a variety of biomolecules such as DNA, RNA, sugar phosphates and phospholipids, the source of phosphonates in the oceans remains uncertain. Chapter 4 of this dissertation describes the composition and cycling of P in the water column at Station Aloha. The composition of dissolved and particulate OM was investigated using solid-state ^{31}P NMR and elemental C, N, P analyses. The results, presented in Chapter 4 correlate the P compositional information to recent literature developments in P cycling at this site and to C biomolecule contents (Chapter 3) and reveal novel insights as to the possible biomolecular associations of P-esters and phosphonates.

The burial of P compounds resistant to remineralization during diagenesis in marine sediments is a significant sink in the global marine P cycle [58, 63, 87, 137, 163]. The release and benthic flux of P from sediments relative to C or N remineralization may change significantly as a function of bottom water oxygen availability. Preferential regeneration of P from sediments overlain by anoxic bottom waters has been suggested from flux measurements [38, 85, 122] and solid phase P distribution studies of marine sediments [88, 123, 124, 133]. However, there is very limited information on organic P speciation as a function of redox conditions and the relative importance of the different proposed mechanisms to explain enhanced benthic P fluxes. Chapter 6 investigates the composition of organic P as a function of redox conditions in sediments from the Effingham Inlet, British Columbia, using solid-state ^{31}P NMR spectroscopy. The NMR results have also been used in conjunction with organic C and P concentrations and benthic P flux measurements to evaluate the contribution of redox-dependant polyphosphate cycling to the enhanced P fluxes under anoxic conditions. While this mechanism of producing enhanced P fluxes has been proposed in the literature [65, 82, 86, 162], this study provides some of the first evidence for this process in marine sediments. The results from Chapter 6 were published in

Geochemical Transactions [140].

1.4 Water-soluble Organic Carbon in Aerosols

Chapter 7 examines the composition of water soluble organic C (WSOC) in urban Atlanta and biomass burning aerosols. Organic C is also an important constituent of atmospheric aerosol particles comprising a significant fraction of the ambient particle mass. Organic C in aerosols is composed of primary emissions (both elemental C and organic C) and secondary organic compounds formed in the atmosphere. Primary emissions are produced by automobile exhaust, biomass burning, industrial activities and even vegetation. These aerosols can have a range of particle sizes. Secondary aerosols are produced from primary aerosols by photochemical reactions taking place in the atmosphere. The formation of secondary organic aerosols is a source for fine particles, such as those less than 2.5 μm in diameter (referred to as $PM_{2.5}$). A major fraction of both primary and secondary organic C compounds in aerosols are soluble in water [111]. The fine WSOC fraction in atmospheric aerosols can affect their optical, radiative, and, cloud nucleating properties, thus impacting the regional air quality and climate. As a result of their fine size, these particles can also enter the human respiratory system and cause adverse health effects. With increasing industrialization and population growth in urban areas, the problems associated with particle pollution, or, smog are also on the rise. In large cities such as Atlanta, the air quality especially deteriorates during summer months when the meteorological conditions are favorable for the formation of secondary organic aerosols. WSOC has been reported to account for up to ~80% of OC in aerosols during the day and 40% at night, from an urban site during summer [158].

In several regions of the world, such as the Amazon Basin, biomass burning is a major source of organic C to the atmosphere. The majority of biomass burning in these areas is due to primary deforestation and seasonal burning of forests and grasslands [56]. The products of these burning activities may be rapidly uplifted to high altitudes and be transported over long distances, thus impacting global air quality, climate and biogeochemical cycling of nutrients. Aerosols derived from biomass burning have very high concentrations of WSOC (up to 100%; [129]).

Despite being a major constituent of the bulk organic mass of ambient aerosols, WSOC is one of the least chemically characterized fractions of aerosol OC. One of the major uncertainties in estimating the climatic effects of tropospheric aerosol is that the chemical composition and properties of bulk OM in fine aerosol are still largely unknown [100]. Chemical characterization of aerosol OC is usually performed using an individual compound approach utilizing techniques such as, gas chromatography coupled with mass spectrometry (GC-MS). However, this technique is not suited for the analyses of the large fraction of polar oxygenated OC compounds present in WSOC [45, 144]. Therefore, only a small fraction of aerosols has been identified in the form of specific compounds. A more comprehensive approach to studying aerosol WSOC is the combination of solid-phase extractions and spectroscopic techniques such as NMR and IR spectroscopy [45, 52, 67, 100, 142]. Chapter 7 presents characterization of WSOC and its chromatographically separated hydrophilic and hydrophobic fractions from urban and biomass burning aerosols using ^{13}C NMR spectroscopy. ^{13}C NMR is a more suitable spectroscopic tool for WSOC analysis as the carboxylic acid functional groups present in these samples cannot usually be detected using ^{1}H NMR. The results presented in this dissertation represent the first comprehensive study of the composition of aerosol WSOC and its separated hydrophobic and hydrophilic fractions from two different sources using solid-state ^{13}C NMR. This work reveals clear differences between the fractions and between WSOC from the two sources and demonstrates the potential of solid-state NMR techniques as a valuable tool for studying the organic C composition of aerosols. The contents of Chapter 7 have been accepted for publication in Environmental Science and Technology.

Insights in to the composition and cycling of NOM from different environments gained from the various studies involving solid-state NMR spectroscopy and allied geochemical analyses are summarized in Chapter 8, along with proposed future research directions.

CHAPTER 2

NUCLEAR MAGNETIC RESONANCE SPECTROSCOPY: OVERVIEW OF METHODOLOGY AND APPLICATIONS TO NATURAL ORGANIC MATTER

2.1 Introduction

Nuclear magnetic resonance (NMR) spectroscopy is a technique based on the magnetic properties of atomic nuclei. It is used to distinguish between different functional groups/compound classes present in organic compounds and can be applied to liquid as well as solid samples. Since most of the results presented in this dissertation are based on data from NMR experiments, a brief overview of NMR spectroscopy and its applications to the study of natural organic material is given in this chapter. It is intended to aid the reader in interpretation of this work. For more detailed reviews the reader is referred to several textbooks and review articles on this subject cited at the end of this chapter.

2.1.1 Basic NMR Theory

The phenomenon of nuclear magnetic resonance occurs when the nuclei of certain atoms are immersed in a static magnetic field and exposed to a second oscillating magnetic field. Some nuclei experience this phenomenon, while others do not, depending on whether or not they possess non-zero values of a quantum mechanical property known as *spin*. Nuclear spin has a magnetic moment associated with it which will interact with an applied magnetic field. When a nucleus with spin, I = 1/2, such as a proton is placed in a magnetic field, two energy levels are generated. These energy levels can be characterized by the magnetic spin quantum number, m_I, and are separated by an amount ΔE, which is given by:

$$\Delta E = \frac{h\gamma B_0}{2\pi} \tag{1}$$

where γ is the gyromagnetic ratio and B_0 is the applied static magnetic field.

Table 1: NMR parameters and magnetic properties of some common nuclei, adapted from [64]

Nucleus	**Natural Isotopic abundance**(%)	**Spin**	**Gyromagnetic ratio** (MHz/Tesla)	**Relative sensitivity**
^{1}H	99.8	1/2	267.48	1.000
^{13}C	1.11	1/2	67.30	0.032
^{31}P	100.00	1/2	108.32	0.100
^{15}N	0.37	1/2	27.08	3.3×10^{-3}
^{29}Si	4.7	1/2	53.16	0.018
^{17}O	0.037	5/2	36.25	0.079

The gyromagnetic ratio is a proportionality constant which relates the observation frequency for a particular nucleus to the applied field. The gyromagnetic ratios and relative NMR sensitivity of some nuclei commonly studied in NOM are presented in Table 1.

The lower energy state, in which the nuclear magnetic moment is parallel to the applied magnetic field B_0, corresponds to $m_I = +1/2$. The higher energy state in which the magnetic moment is antiparallel to B_0 corresponds to $m_I = -1/2$. The observation frequency can be expressed in terms of the gyromagnetic ratio and the applied field as:

$$\nu = \frac{\gamma B_0}{2\pi} \tag{2}$$

or

$$\omega = \gamma B_0 \tag{3}$$

where, ω is the resonant frequency in radians/second and ν is the resonant frequency in hertz. The two energy states will be unequally populated, with the ratio of their populations given by the Boltzman equation:

$$\frac{N_\beta}{N_\alpha} = e^{(\frac{-\Delta E}{kT})} \tag{4}$$

where, N_α is the population of the lower state and N_β is the population of the higher state. The population difference is dependent both on the field and the nucleus being observed and corresponds to a bulk magnetization (**M**), which is the sum of the magnetizations of the individual spins.

Since the magnetic moment has magnitude and direction, its behavior in a magnetic field is usually described using vector diagrams. Initially, the bulk magnetization **M**, will be aligned with the applied magnetic field, till the system is perturbed(Figure 1). The direction of the applied field is defined as the z direction. If the induced magnetization is misaligned from the applied field, a force generated by B_0 develops on M. This magnetization is generated from nuclear spins and as a result, it behaves in a manner similar to that of a spinning top in the Earth's gravitational field. The force generated by B_0 on M is a torque, which causes M to precess around B_0 (Figure 1) at a frequency of $\gamma B_0/2\pi$ hertz. This motion is known as Larmor precession. There is another component of this precessing magetization in the xy plane. If a coil of wire is wound around an axis perpendicular to the B_0 field, the precessing magnetization would induce an oscillating current in the coil (Figure 1). After necessary amplification and processing (described below), this current becomes the NMR signal. The coordinates x, y, z are in the three-dimensional 'laboratory frame of reference'. From the perspective of the nuclei, these coordinates are rotating at the Larmor frequency (μ). If the x, y coordinates are changed to those in the rotating frame x', y', the magnetization appears static. The net magnetization now lies along z' and its behavior at equilibrium is shown in Figure 1

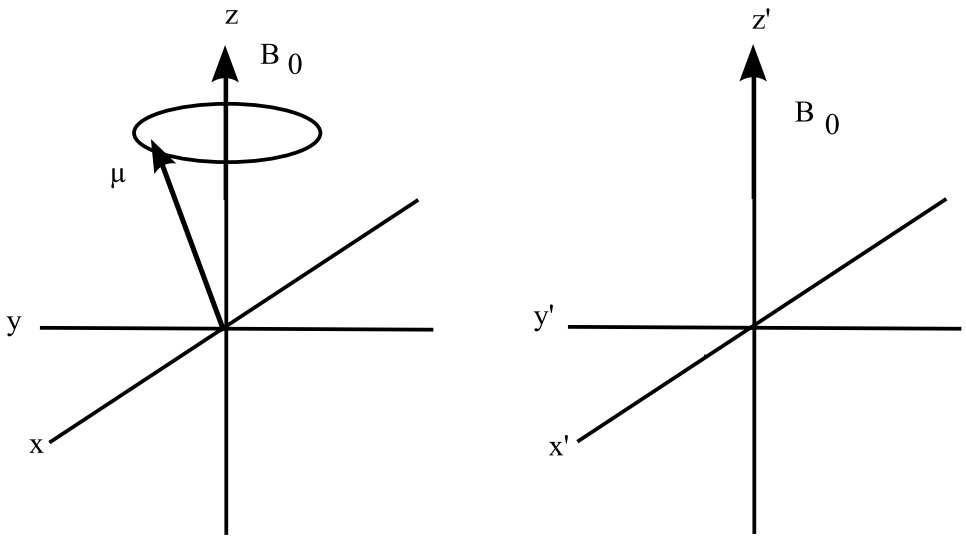

Figure 1: Behavior of the bulk magnetization (M): a) at equilibrium in laboratory frame of reference; b) at equilibrium in the rotating frame of reference [180]

In an NMR experiment, the magnetization is displaced from its equilibrium position by applying a second magnetic field B_1, which oscillates at radio frequency (rf; 10^6 to 10^{10} Hz). This field is induced from a current in a coil would perpendicular to B_0 and is applied for a few microseconds. This rf field is also at the Larmor frequency. When the introduced rf radiation exactly matches the energy difference between the two states, the energy is absorbed and the nuclei are in resonance with the electromagnetic radiation. The frequency of radiation needed to induce resonance also depends on the nature of electronic shielding around the nucleus. Different functional groups or bond types in organic molecules have different electron distributions and thus their constituent nuclei resonate at different frequencies. Therefore it is possible to identify a particular functional group from its resonance frequency. The chemical environment around a given nucleus is primarily a function of the surrounding atoms. Because the electron cloud shields the nucleus, the actual magnetic field experienced by a nucleus in a molecule is generally less than the applied magnetic field B_0 by a fraction σ. This alteration of the external field is called chemical shift. The actual resonance frequency of a nucleus in a molecule is given as

$$\nu = \frac{\gamma B_0(1-\sigma)}{2\pi} \tag{5}$$

Therefore, the greater the shielding of the nucleus by electrons (i.e. larger values of σ), the lower is its resonance frequency. In order to compare NMR spectra from spectrometers with different magnetic fields (B_0), the quantity *chemical shift* was developed which is related to the difference between the resonance frequency ν of the nucleus of interest and that of a reference standard ν_0. The chemical shift δ, is defined as:

$$\delta = \frac{\nu - \nu_0}{\nu_0} \times 10^6 \tag{6}$$

Due to the small values of chemical shift (about 10^{-3} to 10^{-6} of the applied magnetic field strength), the factor of 10^6 is used, as a result of which, the δ values are expressed in parts per million or ppm. The chemical shifts reported on the δ scale are independent of the applied field since both the numerator and denominator are proportional to the field. Tetramethylsilane (TMS) is the commonly used reference standard for ^{1}H and ^{13}C NMR

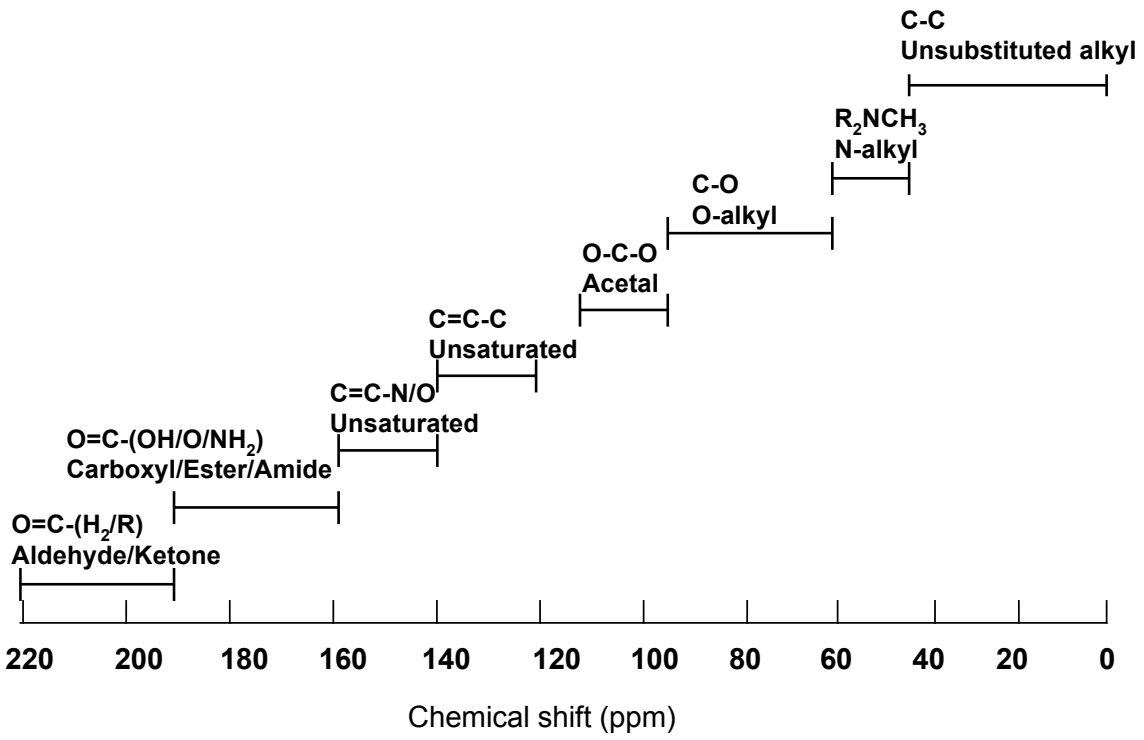

Figure 2: ^{13}C NMR chemical shift ranges (on the ppm scale) and chemical structures of common C functional groups observed in natural samples [114]

while the standard for ^{31}P NMR is phosphoric acid. The chemical shift ranges of ^{13}C and ^{31}P functional groups in natural organic material are shown in Figures 2 and 3 respectively.

In modern day NMR spectrometers, the nuclei under investigation are subjected to a short intense pulse of rf radiation under conditions chosen such that all the nuclei resonate simultaneously. The excitation frequency is set to exactly equal the nuclear precession frequency. The field B_1 interacts with the magnetization M to produce a torque which moves the magnetization towards the x', y' plane. Since the precession frequency about the static B_0 field is equal to the rotating B_1frequency, the magnetization will remain perpendicular to the B_1 field component. Therefore the magnetization will precess around the rf field at an angular frequency γB_1. At the same time, it is also precessing about the static magnetic field with an angular frequency γB_0. This simultaneous precession about the two axes is referred to as nutation.

The final position of the magnetization will depend on the duration of the rf pulse t_p. The angle θ (called the tip angle) through which the magnetization is flipped from the z

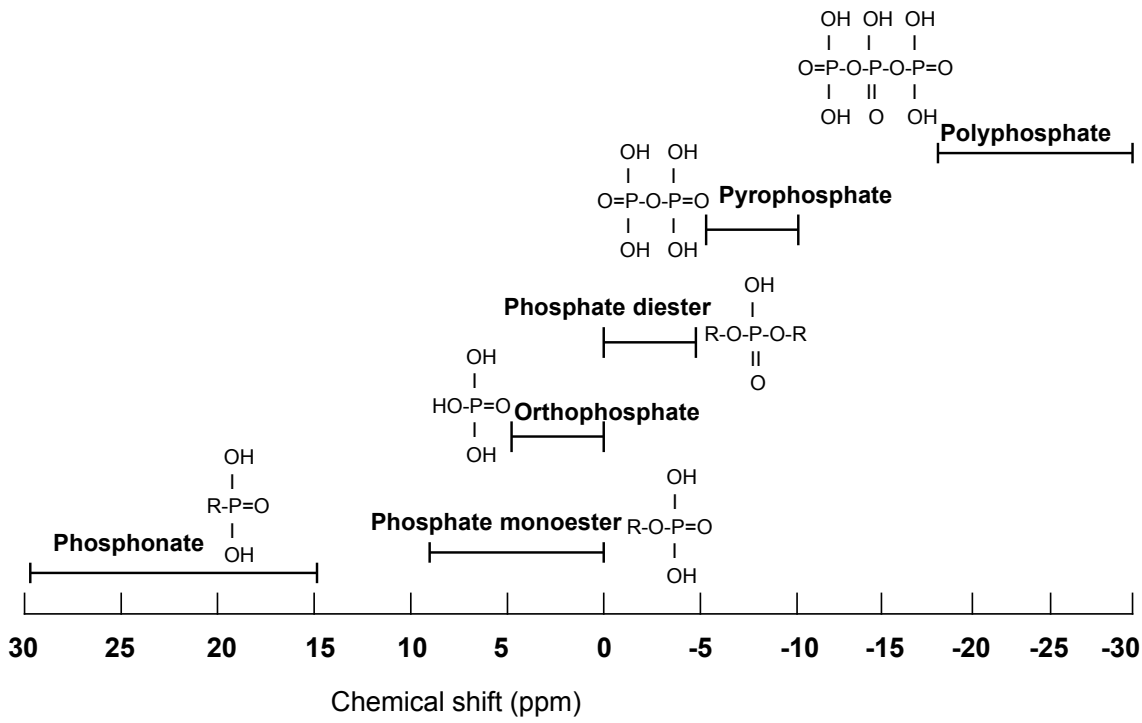

Figure 3: ^{31}P NMR chemical shift ranges (on the ppm scale) and chemical structures of common P functional groups observed in natural samples [127, 131, 171]

axis, can be calculated as

$$\theta = \gamma B_1 t_p \tag{7}$$

The magnitude of B_1 is chosen to be large enough to tip the magnetization from the z' to the x', y' plane in a few microseconds. The duration of the pulse or the pulse width is usually referred to in terms of its effective tip angle in radians. Since the magnetization is measured in the x', y' plane looking along the x' axis, there will ideally be a sinusoidal variation in the intensity with pulse width. Therefore, the signal will be maximum for a tip angle of $\pi/2$, zero at π when the magnetization is along $-z'$, a negative maximum at $3\pi/2$ and back to zero at 2π. The time constant which describes how the net magnetization along the z' axis returns to its equilibrium value is called the spin lattice relaxation time (T_1). The relaxation of the x', y' magnetization is called spin-spin relaxation, which is described by the time constant (T_2). The motion of the x', y' component of the magnetization induces a current in the detection coil. This induced signal loses intensity as a function of

time according to the (T_2) relaxation process. This decaying signal pattern is called a free induction decay or FID. The FID can be transformed in to a spectrum of signal intensity versus the frequency of emitted radiation by the mathematical operation of computerized fast Fourier transformation. In order to increase the signal to noise ratio of the spectrum, several FID's are collected and added prior to performing the Fourier transformation. The signal to noise ratio of an NMR spectrum increases as the square root of the number of scans [139]. In pulsed NMR experiments, a large number of scans are collected and the resulting FID is digitized and stored in a computer for data processing.

2.2 Application of NMR Spectroscopy to Natural Organic Matter

As mentioned earlier, NMR spectroscopy can be applied to both liquid as well as solid state samples. Although solution NMR generally provides greater resolution, solid-state NMR is more suited for studying natural OM and humic substances due to reasons discussed below. Since the development of technological advancements such as magic-angle spinning, dipolar decoupling and cross-polarization (described below) together with powerful NMR instruments capable of producing higher magnetic fields, high-resolution solid-state NMR experiments on natural organic matter have advanced rapidly.

One of the major advantages of solid-state NMR especially in case of NOM is that little or no sample preparation is required other than drying. It is a non-destructive probe and the sample remains available for other complementary analyses. Also, solid-state NMR spectroscopy does not have some of the problems encountered during solution NMR analyses of NOM samples including:

1) the low solubility of various kinds of natural OM in suitable NMR solvents,

2) the differential solubility of various components of these complex mixtures resulting in sample fractionation and formation of colloidal suspensions,

3) pH effects on the chemical shifts of nuclei,

4) the obscuring of certain chemical shifts by solvent chemical shifts in the same region,

If solid samples are run under conditions normally used for liquids, the resulting spectra have broad, poorly resolved peaks and yield little compositional information. This is mainly due to the effects of *magnetic dipolar interactions* between nuclei and *chemical shift anisotropy* which are manifested in solids [114, 181]. *Magnetic dipolar interactions* result from local dipolar magnetic field of the nuclei of interest being affected by the magnetic fields of surrounding nuclei. The motion of molecules in solids is limited and they remain rigidly fixed at particular angles. Thus, different magnetic fields are created, with different Larmor frequencies for each orientation, which results in broad peaks. In contrast, peaks are narrow in solution-state NMR due to rapid tumbling or rotational motion which averages interactions that are dependent on orientation. As mentioned earlier, chemical shifts are a result of the shielding of the nucleus from the external magnetic field by its surrounding electron cloud. This shielding may also depend on the anisotropic electron distribution around the nucleus and the orientation of the molecule in the magnetic field. This orientation dependence of chemical shifts is termed *chemical shift anisotropy.* Like magnetic dipolar interactions, chemical shift anisotropy also leads to a dispersion of peak positions and hence broader peaks. Chemical shift anisotropy arises from a non-spherical electron distribution around the nucleus. This effect is particularly important for functional groups in which the electron distribution is not the same in all directions, such as in aromatic and carbonyl carbons [180]. These structures have π orbital electrons which lie above and below the plane of the C-C or C=O bonds and the nuclei experience different levels of shielding depending on whether the bond axes are perpendicular or parallel to the field. In case of ^{13}C, line broadening results from ^{13}C-^{1}H dipolar coupling and ^{13}C chemical shift anisotropy.

2.2.1 Cross-Polarization Magic Angle Spinning

2.2.1.1 Magic Angle Spinning

Both chemical shift anisotropy and magnetic dipolar interaction have a $(3\cos^2\theta - 1)$ term in their mathematical expressions. When this term is equal to zero, one obtains conditions close to those found in the liquid state [39]. The angle at which this happens at is 57.4°, the 'magic angle'. Rapid spinning of a solid sample at an angle of 57.4° relative to the applied

magnetic field eliminates dipolar interactions and chemical shift anisotropy and is termed magic angle spinning (MAS). During MAS, all moieties are at an average angle of 57.4° with respect to B_0. A common problem associated with MAS is the presence of spinning side bands in the spectra. In a typical solid-state spectrum, a peak at a given position on the δ scale will have spinning sidebands, which are spaced symmetrically on each side of the peak at the frequency of rotation ω_r. These side bands are a manifestation of echoes which arise as a result of the refocussing of the magnetization due to the spinning of the sample [39]. Sidebands include peak signal and reduce the intensity and area of the primary peak. Thus the area of the associated sidebands must be added to that of the main signal to determine the total peak area. To test which peaks on a spectrum are representative of actual resonances, the sample can be run at two different spinning rates. Only the spinning sidebands shift positions in relation to spinning speed, whereas the real peaks do not. One way of reducing signal loss to spinning sidebands is to increase the spinning speed such that the side bands are further away from the main signal and lower in intensity and thus, do not interfere as much. They still however cause a reduction in signal intensity of the central peak. Specialized NMR pulse sequences such as cross polarization with total supression of spinning sidebands (CP-TOSS) are also sometimes employed for this purpose [39]. A lot of technological progress has been made over the past decade leading to the development of NMR probes which can achieve spinning rates of up to 30 kHz. An MAS spinning rate of 10 kHz was used on all the NMR experiments presented in this study. This value was chosen such that it is optimal for the functioning of standard cross-polarization (described below) techniques and is achievable for most samples, even with slight imperfections in rotor packing.

2.2.1.2 Cross-polarization

In solid-state NMR, the polarizations of low -γ nuclei such as ^{13}C are altered by exploiting their dipolar coupling to high- γ nuclei such as ^{1}H. The NMR pulse sequence used is called *cross-polarization* and involves an efficient transfer of net magnetization from very abundant proton spins to the less abundant ^{13}C and ^{31}P spins. This is accomplished in a dual-phase,

stepwise sequence as shown in Figure 4 and is briefly explained here. The $\pi/2$ pulse along x will generate a magnetization vector along the y axis. The phase shift of the ^{1}H rf field means that in the rotating frame, the magnetization becomes spin-locked and precesses about the the y axis at an angular frequency $(\omega_1)_H$:

$$(\omega_1)_H = (\gamma B_1)_H \tag{8}$$

A suitable rf field can also be applied so as to force the ^{13}C magnetization to precess in the rotating frame with a precession frequency given by

$$(\omega_1)_C = (\gamma B_1)_C \tag{9}$$

If $(\omega_1)_H$ equals $(\omega_1)_C$, then mutual spin-flips or mutual relaxation may occur, leading to what is referred to as the Hartmann-Hahn condition [139]. The ^{1}H magnetization is larger than that of ^{13}C, so cross relaxation from protons to carbon will cause the ^{13}C magnetization to increase. The magnitude of the ^{13}C signal is determined by the gyromagnetic ratio of ^{1}H producing a gain in signal amplitude of γ_H/γ_C. In case of ^{1}H-^{13}C cross polarization, a theoretical enhancement of the ^{13}C signal by a factor of 4 can be achieved because the gyromagnetic ratio of protons is 4 times that of the carbons (Table 1). Spectra can also be recorded in a shorter time because the ^{13}C or ^{31}P nuclei relax at the fast relaxation rates characteristic of protons. Also, since dipolar interactions between carbon and protons lead to line broadening, the ^{1}H transmitter is left on during acquisition (Figure 4), to provide *dipolar decoupling*. The combined cross-polarization - dipolar decoupling pulse sequence may be applied on a sample spinning rapidly at the magic angle to give a cross-polarization magic angle spinning (CP-MAS) experiment [139]. The increased resolution obtained has made CP based techniques standard for the NMR characterization of NOM [39].

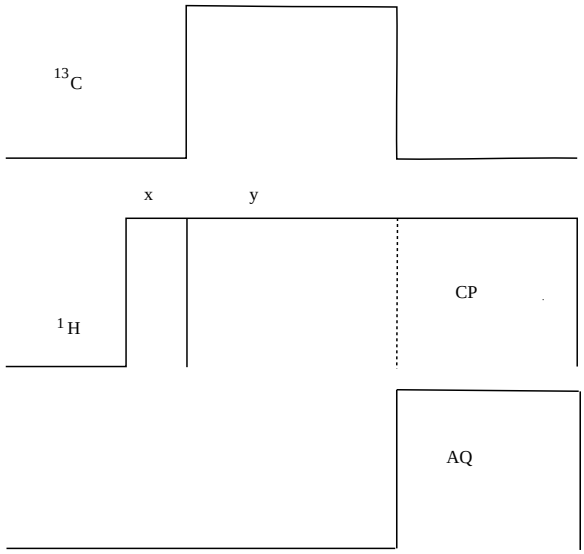

Figure 4: Cross-polarization pulse sequence; CP: Cross Polarization; AQ: Acquisition [139]

2.2.1.3 Optimization of CP-MAS Parameters

The dynamics of polarization transfer from protons to carbons is very complex and can be expressed mathematically (with some assumptions) as :

$$I(t) = \frac{I_0}{(1 - \frac{T_{IS}}{T_{1\rho}H})}[e^{(\frac{-t}{T_{1\rho}H})} - e^{(\frac{-t}{T_{1S}})}] \tag{10}$$

where I(t) is the observed intensity with a CP contact time t, I_0 is the ideal intensity, T_{IS} is the CP time constant whose reciprocal is the rate at which CP takes place, $T_{1\rho}H$ and $T_{1\rho}C$ are the spin-lattice relaxation rates in the rotating frame for H and C respectively. One of the assumptions used to obtain the above equation is that $T_{1\rho}H$/ $T_{1\rho}C \approx 0$. The double exponential nature of the CP intensity (I(t)) arises from the fact that it takes a finite amount of time for the polarization to be transferred from the protons to the carbon (T_{IS}) and that during this process, protons are also relaxing with a time constant $T_{1\rho}H$. If $T_{1\rho}H$ is much smaller than the time needed for the slowest carbons to cross-polarize, these carbons will not be observed. In complex mixtures such as NOM, a variety of $T_{1\rho}H$'s may exist, which make it necessary for the NMR experimental parameters to be optimized such that all the different functional groups are quantitatively detected [39, 114, 181].

To address this issue, a series of experiments were conducted on two marine ultrafiltered

dissolved organic matter (UDOM) samples. Both these samples were from Station Aloha in the Pacific Ocean, one of them was a surface sample from 20 m depth while the other was from a depth of 2500 m. These two samples were chosen to represent a range in organic C contents and are comparable to marine sediments and atmospheric aerosol WSOC as they had a similar diversity of C functional groups. A series of spectra were collected for both of these samples in which the contact time was varied from 0.5 to 5 msec. All other experimental parameters were identical for these runs. The NMR spectra obtained were processed and the areas under each peak region were integrated. Figure 5 plots the normalized NMR peak area versus the contact time for the 20 m UDOM . It can be seen that using a contact time of 1 msec consistently gives the largest signal intensity and peak area for all the C functional groups. The value of 1 msec for contact time determined during our optimization experiments has also been found to be optimal by other researchers for a wide variety of NOM samples. The NMR optimization experiments for ^{31}P were carried out by [34] and identical operating parameters to those have been used here.

The presence of paramagnetic species such as Fe^{2+} or Mn^{2+} can cause signal loss and greatly hamper acquisition of NMR spectra of natural samples [180]. The loss of signal can result from loss of field homogeneity and direct interactions with ^{13}C or coupled ^{1}H nuclei, causing line broadening and/or shifting of the ^{13}C NMR resonance. Paramagnetic species have a strong influence on the T_1 relaxation and can drastically shorten it. Since T_2 cannot be larger than T_1, an extremely shortened T_1 may shorten T_2 such that relaxation is faster than detection. This is especially the case for sites where carbons bind to metal ions. At low concentrations: paramagnetic impurities may be of advantage by shortening T_1 and therefore allowing faster data accumulation. NOM samples such as soils and sediments are routinely treated using various extraction methods such as those utilizing citrate-dithionate bicarbonate [89]; NaOH-EDTA [25, 131] and HCl/HF [66, 140] to remove paramagnetic material prior to NMR analyses. Removal of paramagnetics was not necessary for the UDOM, ultrafiltered particulate organic matter (UPOM) and WSOC samples, but an HCl/HF treatment was applied to the Effingham Inlet sediment samples in order to concentrate the organic fraction. Details of this treatment procedure are presented in

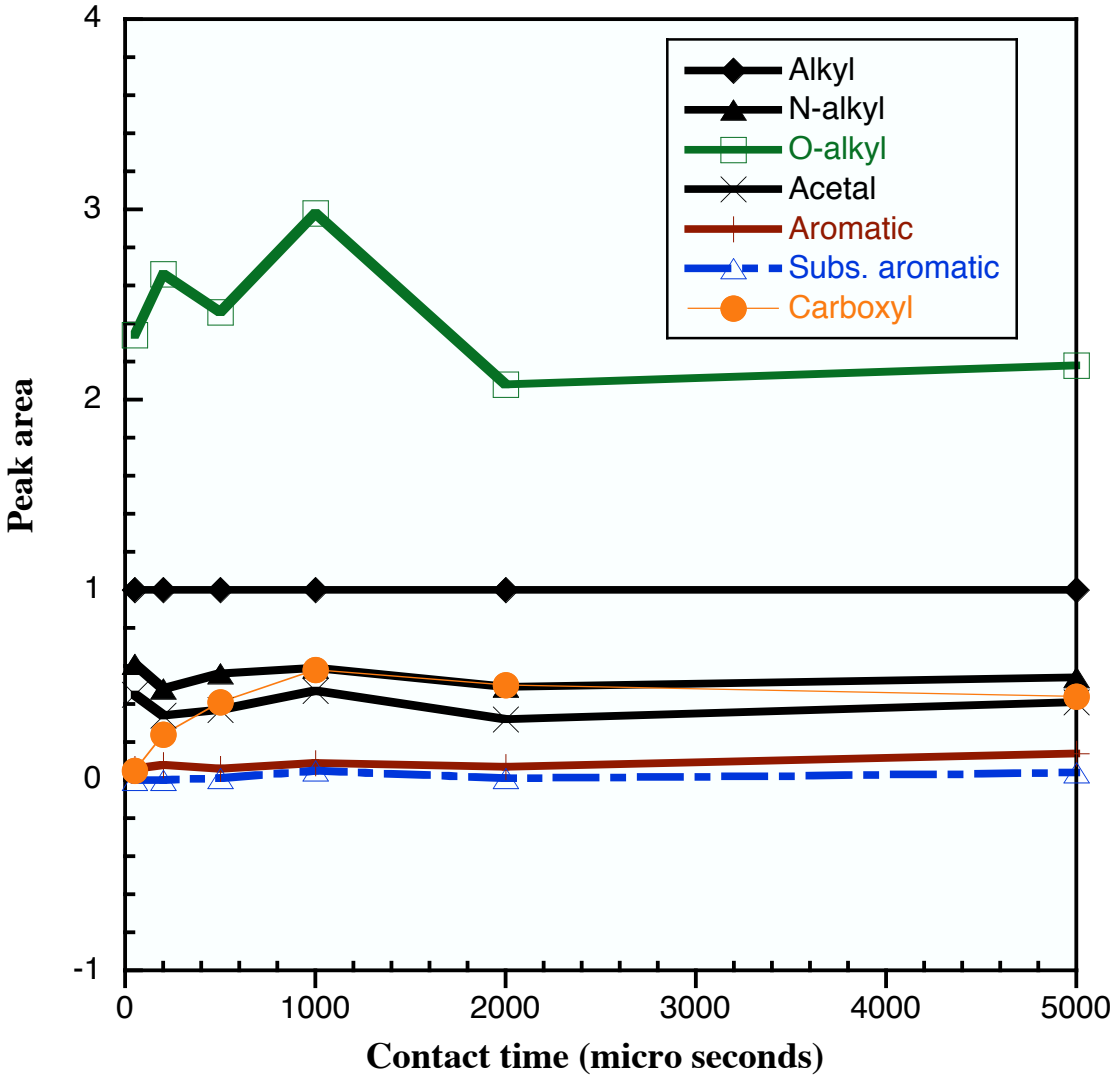

Figure 5: Integrated ^{13}C NMR peak areas under each spectral region for marine organic matter sample with varying contact times

Chapter 6.

2.3 NMR Studies on NOM

Samples for NMR spectroscopy of natural samples are often plagued by low concentrations of nuclei of interest resulting in poor spectral resolution. Despite these problems, a wealth of information on the composition of NOM has been obtained using this technique. In case of marine organic matter, this problem can be remediated by using concentration techniques such as tangential flow ultrafiltration. The coupling of ultrafiltration and NMR has been applied to solid-state ^{13}C [15, 118, 141], ^{31}P [35, 36, 102], and ^{15}N NMR [121] studies on marine dissolved and particulate organic matter. Solution and solid-state NMR has also been used to analyze marine and lacustrine sediments [81,89,140], soils [25,171], freshwater humic and fulvic acids ([181] and references therein), and marine particle/sediment trap material [70,71]. In case of aerosol water-soluble organic carbon (WSOC), NMR is beginning to advance as an analytical technique. ^{13}C NMR analyses of WSOC have been hindered by concentration problems, but several studies have used solution ^{1}H NMR to investigate this material [45, 47, 67, 69]. Very recently solid-state ^{13}C NMR spectroscopy has been applied to analyze WSOC composition [52, 142].

All the NMR spectra presented in this dissertation were acquired at on a Bruker DSX 400 spectrometer located in the School of Chemistry and Biochemistry at Georgia Institute of Technology. This spectrometer operates at a magnetic field strength of 9.4 Tesla and ^{13}C and ^{31}P frequencies of 100 MHz and 161 MHz respectively. Data processing was carried out off-line using the MestreC software package (MestreLab Research). The raw data obtained from the NMR spectrometer is first apodized using exponential line-broadening of 30-100 Hz, depending on the type of sample, and then Fourier transformed using MestreC. The resulting frequency domain spectrum is then phase corrected such that it is symmetric relative to the largest peak. If necessary, the spectrum baseline can also be adjusted using different mathematical fitting routines available in MestreC. The exact location of peaks and their signal-to-noise ratios can be determined using MestreC. Identification of peaks is done by comparing their position on the ppm scale to chemical shift tables in the literature.

Using the integration tool in the MestreC software package, peak areas between selected ppm ranges corresponding to different functional groups (Figures 2 and 3)can be integrated. The software returns absolute peak areas relative to a reference peak, whose area is set as 1. Percentage peak areas of individual peaks are then calculated by dividing their areas by the total spectral peak area of the sample. Using the software rather than manual integration, ensures that the spectral limits are chosen precisely for all spectra.

The following texts and internet resources were consulted during preparation of this chapter and are recommended for information on basic NMR theory : *Solid state NMR for Chemists* (Fyfe, 1983 [64]); *Modern NMR spectroscopy: A guide for chemists* (Sanders and Hunter, 1993 [139]); *Introduction to solid-state NMR spectroscopy*(Duer, 2005 [53]); *The basics of NMR*(Hornak, http://www.cis.rit.edu/htbooks/nmr). The following textbooks and review articles provide information on the applications of NMR spectroscopy to natural organic matter: *NMR techniques and applications in Geochemistry and Soil Chemistry* (Wilson, 1987 [180]); *Nuclear magnetic resonance spectroscopy in environmental chemistry* (Nanny et al. 1997 [127]); [24, 39, 114, 181].

CHAPTER 3

CYCLING OF DISSOLVED AND PARTICULATE ORGANIC MATTER AT STATION ALOHA: INSIGHTS FROM ^{13}C NMR SPECTROSCOPY COUPLED WITH ELEMENTAL, ISOTOPIC AND MOLECULAR ANALYSES

3.1 Abstract

Compositions of ultrafiltered dissolved organic matter (UDOM) and ultrafiltered particulate organic matter (UPOM) were characterized in samples collected from a depth profile (20 m to 4000 m) in the North Pacific at Station Aloha. ^{13}C Nuclear Magnetic Resonance (NMR) analyses together with (^{13}C values, C/N ratios and molecular characterizations of UDOM and UPOM indicate different bulk chemical compositions and sources for these two size fractions. Carbohydrates and amino acids are the major biomolecules present in UDOM and UPOM. At all depths, UPOM had higher amino acid and lower carbohydrate contents compared to UDOM. UDOM and UPOM samples showed a decrease in the relative contribution of carbohydrates to the total organic carbon with increasing depth, whereas the contributions of lipids increased. Amino acids did not show any clear depth trends for UDOM, but decreased in UPOM. The compositional trends with depth indicate that selective degradation processes, which preferentially remineralize reactive biomolecules such as carbohydrates, affect UDOM and UPOM compositions in the water column.

Molecular analyses of carbohydrates and amino acids characterized ∼9% of the C in UDOM and ∼28% of the C in UPOM. Although a relatively small proportion of the total C was characterizable with molecular analyses, the depth trends and the ratio of amino

Sannigrahi, P., Ingall, E.D. and Benner, R. Deep-Sea Research I 52(2005) 1429-1444.

acid to carbohydrates in UPOM and UDOM were similar to those determined by ^{13}C NMR. This suggests that the organic matter fraction characterized by molecular analyses is representative of the molecularly uncharacterized fraction of organic matter. It is postulated that the molecularly uncharacterized fraction is encapsulated or shielded by a hydrolysis-resistant matrix or the individual amino acid and sugar units have been altered to form a chemical entity unrecognizable by the molecular analyses.

3.2 Introduction

Organic matter (OM) in the oceans is one of the largest dynamic reservoirs of organic carbon (C) on Earth. The marine OM reservoir contains approximately 730Gt of C, which is comparable in size to the atmospheric CO_2 (750Gt) and land biota (570Gt) reservoirs [73]. The sizes of these reservoirs relative to the fluxes between them indicate that changes in marine OM cycling in the water column can significantly influence the global C cycle on relatively short time scales [73]. While, there has been considerable progress in our understanding of the origin, composition and cycling of marine OM, a large fraction still remains compositionally uncharacterized.

It has been recognized for some time that OM in seawater exists in a continuum of sizes [153]. This size-based separation of OM is practical and various kinds of analytical techniques have been employed to extract and analyze marine OM. To obtain a representative fraction, recent studies in this field have analyzed marine OM using bulk chemical and molecular level methods on materials extracted using size based extraction techniques. These size fractions have been collected using particle traps, in-situ filtration and tangential flow ultrafiltration [15, 70, 175].

Dissolved organic matter (DOM) is commonly divided into high molecular weight (HMW) and low molecular weight (LMW) size classes based on passage through an ultrafiltration membrane with a $\sim$1nm pore size and 1000 Dalton molecular weight cutoff. Recent studies have shown that percentages of total C accounted for as neutral sugars, amino sugars and amino acids in DOM and HMW-DOM, decrease with depth in the water column [12]. Higher yields of biomolecules in HMW-DOM relative to bulk DOM indicate that HMW-DOM is

less diagenetically altered and potentially more bioreactive than LMW-DOM. Direct comparisons of the bioreactivity of HMW and LMW DOM in a variety of marine environments also indicate that HMW-DOM is more bioreactive than LMW-DOM [6, 7, 12]. On the basis of these observations, Amon and Benner [6, 7] proposed a diagenetic continuum of organic matter reactivity and composition in the water column going from larger to smaller particle and dissolved phases (POM→ HMW-DOM→ LMW-DOM).

Studies focused on particulate organic matter (POM) have classified this material into two size classes based on the collection technique. Sinking POM (∼100-1000μm) is collected using particle traps or filters, and suspended POM (∼0.1-60μm), is collected using in situ filtration pumps or ultrafiltration. The relationship between the different size classes of POM (sinking and suspended) is not well established. The sources of suspended POM are also not very well understood. On the basis of elemental C/N and isotopic δ^{13}C ratios of suspended POM and DOM, Benner et al. [14] infer that POM dissolution to form DOM is feasible, but aggregation of DOM to form POM is probably not a significant process in the overall C dynamics. However, on the basis of radiocarbon measurements, a small fraction of DOM was postulated to be associated with POM. Druffel et al. [51] observed an 80‰ difference in Δ^{14}C values between surface water dissolved inorganic C (DIC) and suspended particulate organic C (POC) in the Panama basin. Assuming negligible resuspension of sediments at that site, these authors calculated that this difference could be accounted for by adding 13% DOC (with (Δ^{14}C = -525‰) by sorption on to the suspended POC pool.

Sinking POM has been extensively analyzed on the molecular level as a part of the USJGOFS Equatorial Pacific transect. The term molecular in these studies [72, 76, 108, 177] has been used to refer to the chromatographically separable parts of biomolecules such as individual amino acids, sugars and lipids. The same terminology has been used in this paper. Chromatographically separable suites of amino acids, carbohydrates and lipids have been analyzed in sinking POM and their compositional trends with depth and latitude documented [76, 108, 177]. However, analyses of sinking POM by ^{13}C NMR and molecular level techniques have yielded contrasting results [70, 71, 76, 108, 175–177]. Molecular-level carbohydrate, amino acid and fatty acid analyses show that with increasing depth in the

water column, the percent organic C that can be accounted for by these biomolecules decreases and, their relative proportions change. The relative contribution of amino acids and lipids to the total organic C decreases while that of carbohydrates increases. Within these biomolecule groups, the more labile compounds are preferentially degraded. For example, storage polysaccharides are degraded faster than structural polysaccharides [76]. However, relatively small compositional changes with depth were reported from ^{13}C NMR analyses of sinking POM from the same sites [70]. Based on the high inorganic content of sinking POM, this lack of variability has been attributed to the physical shielding of the organic matter by an inorganic matrix [70].

In spite of substantial research efforts and increasing analytical sophistication, more than half of the organic matter in seawater still remains uncharacterized at the molecular level [72]. The molecularly uncharacterized component (MUC) constitutes an increasing proportion of organic C in deeper waters. A similarly large uncharacterized fraction also exists in soils and sediments [72]. Identifying the composition and origin of the molecularly uncharacterized fraction is fundamental to understanding the sources and cycling of OM. From the similarities observed in the ^{13}C NMR spectra of plankton and sinking POM from different depths, Hedges et al. [70] inferred that the MUC was essentially same as the bulk OM. A recent study by Hwang and Druffel [84] explored the composition of the uncharacterized fraction in more detail than previously reported in literature. The acid - insoluble fraction remaining after extraction of lipids, hydrolysable amino acids and neutral carbohydrates was used as a proxy of the molecularly uncharacterized fraction. The results of their δ^{13}C and Δ^{14}C analyses suggest that the major portion of the acid-insoluble fraction of sinking POM is composed of lipid-like material that is biosynthesized by similar pathways to the extractable lipids, but is somehow resistant to organic solvents and acids.

In this study, DOM and POM isolated using tangential-flow ultrafiltration from station Aloha in the northwest Pacific Ocean have been characterized using solid-state ^{13}C Nuclear Magnetic Resonance (NMR) spectroscopy along with isotopic, elemental and molecular analyses. To the best of our knowledge, this is the first use of solid-state ^{13}C NMR to characterize suspended POM (as opposed to sinking POM) in the ocean and also the first

direct comparison of NMR results to molecular analyses on different size fractions from the same site. Direct comparison of the contribution of amino acids and carbohydrates to C in DOM and POM as obtained by ^{13}C NMR to molecular analyses allows approximation of the composition of the molecularly uncharacterized fraction. From our results, it appears that the molecularly uncharacterized fraction contains amino acids and carbohydrates in similar proportions as the fraction characterized by molecular analyses.

3.3 Materials and Methods

Water samples were collected from various depths (20 to 4000m) at station Aloha in the Pacific Ocean. The Hawaii Ocean Time Series Station Aloha (22.75°N, 158°W) is located in the oligotrophic waters of the north Pacific gyre, approximately 100 km north of Oahu, HI. The water depth at the sampling site is 4800 m. Further information on station Aloha and annual time series data reports can be accessed at http://hahana.soest.hawaii.edu/hot/hot_jgofs.html.

Samples were collected during a cruise to station Aloha in October 1999 aboard the R/V Ka'imikai-o-Kanaloa. Organic matter was isolated from seawater using tangential flow ultrafiltration [14, 15]. At each depth, ∼700 L of seawater was collected with four separate casts. From 600 L of this composite, the ultrafiltered POM (UPOM, 0.1- 60 μm) fraction was isolated aboard ship with an Amicon DC10L ultrafiltration system with a polysulfone hollow fiber filter. The filtrate from the DC10L system was fed directly into an Amicon DC30 ultrafiltration system with polysulfone membranes (S10N1; 1000Da cutoff) to isolate the ultrafiltered DOM (UDOM, 1 - 100nm), which is also referred to as high-molecular weight (HMW) DOM. The UDOM and UPOM concentrates were frozen for transportation to the laboratory, where they were dried under vacuum and stored for chemical analyses. Mass balances of dissolved organic C (DOC) ranged from 91% to 126% (107% average) with higher values at lower DOC concentrations. These values indicate that appreciable amounts of C were not lost or gained during ultrafiltration. Particulate organic C (POC) on an average represented 1.3% of total OC in the water column. Further details of these calculations can be found in Hernes and Benner [75].

Plankton samples were collected from surface waters (∼2m depth) using a 30 μm mesh

plankton net. Samples were washed with fresh water and frozen for storage and transportation to the laboratory. The frozen samples were freeze-dried and ground to a fine powder for analyses.

C and N contents and stable carbon isotope ratios were measured on dried UDOM and UPOM samples. C and N contents were measured after vapor phase acidification using a Carlo Erba CHN analyzer [74]. Stable C isotopes were measured in duplicate with a Finnegan Delta Plus system with in-line combustion and are presented as δ^{13}C (‰) relative to the Pee Dee Belemnite standard.

Solid-state ^{13}C NMR analyses of the UDOM and UPOM samples were carried out at the NMR center in the School of Chemistry and Biochemistry at the Georgia Institute of Technology. The ^{13}C NMR spectra were acquired on a Bruker DSX 400 spectrometer using Cross Polarization-Magic Angle Spinning (CP-MAS) at a ^{13}C frequency of 100 MHz. About 90 mg of powdered sample was packed into a 4 mm-diameter cylindrical zirconia rotor fitted with a Kel-F cap and spun at 10,000 $\pm$ 10 Hz in a Bruker magic - angle spinning probe. One limitation of NMR is gaining quantitative information on different C functional groups in a complex material such as natural OM. Direct polarization-Magic Angle spinning (DP-MAS) or Bloch Decay are the NMR techniques best suited for quantitative analyses, but very long spectrometer run times are required, which is often not practical. Cook [39], in a comprehensive review of NMR techniques available for the analyses of natural OM, suggested that presently cross polarization based methods appear to be best suited to obtain semi-quantitative data on C speciation. It has been reported that CP-MAS ^{13}C NMR spectroscopy overestimates the alkyl groups and underestimates the aromatic and carboxyl/carbonyl region [116, 132]. But, it has also been shown that through optimization of key NMR experimental parameters, such as contact time and recycle delay, reasonably quantitative estimates ($\pm$10%) of C bond distribution from NMR spectra are possible [70, 71, 180]. For all samples, an optimized cross polarization sequence was used with a 1.0 ms contact time and a recycle delay of 5 seconds. A total of 10,240 transients were collected for each UDOM sample and 34,000 transients for each UPOM sample. UDOM and UPOM spectra were processed with 30 Hz and 100 Hz exponential line broadening, respectively.

Data processing and calculation of integrated peak areas were carried out off-line using the Mestre-C software package.

The measured ^{13}C NMR spectral data were entered into a three end-member mixing model to estimate the biochemical composition of the UDOM and UPOM samples. The modeling results are semi-quantitative and are useful as a tool to further explore the NMR data from a biochemical perspective. The model involved "amino acid", "carbohydrate" and "lipid" end-members, which were used to represent the major biochemical types found in marine OM samples. The term 'lipid' here is being used to refer to lipid-like material, which may also comprise other biomolecules rich in aliphatic and carboxylic functionalities. Other biochemicals that are less abundant, and have not been taken in to account in this model, include pigments and nucleic acids [71, 108]. The modeling procedure was similar to that used by Hedges et al. [70, 71] and the reader is referred to these papers for a detailed discussion of the model and assumptions involved in it. The three end-members used were calculated from different literature sources to be representative of average amino acid ($C_{106}H_{168}O_{34}N_{28}S$), lipid ($C_{18}H_{36}O_2$), and carbohydrate ($C_6H_{10}O_5$) composition of typical marine organic matter. Average spectral characteristics were calculated for each of the end-members based on literature values for the relative abundances of carbon functional groups in their structures and are presented in Table 3. The choice of these end-member compositions assumes that all the nitrogen (N) resides in amine functional groups of amino acids. Acetylated amino sugars, such as those found in chitin and peptidoglycan [16, 120], also contribute to amide and amine functional groups in marine organic matter. As we will see from the results of the molecular level analyses presented in the next section, amino sugars are not a large fraction of the C and N in these samples, so this assumption does not affect the model output.

The NMR spectra were split into 7 spectral regions on the ppm scale (0 - 45, 45 - 60, 60 - 95, 95 - 110, 110 - 145, 145 - 165 and 165 - 215) and the integrated areas in each were determined. The three end-members were then numerically mixed in the model, using a MATLAB program (Appendix A) developed for this purpose, to determine the percentage of each biochemical that gave the best overall agreement between the calculated

and measured spectral abundances for each OM sample. This program was used to minimize the sum of the squared deviations between the calculated and measured peak areas to obtain the best fit. Thus, the results give most weight to close matching of major intensities. The model was constrained such that the sum of the percentages of the three biochemical end-members added to 100 and the predicted amino acid content did not exceed the amount possible given the N content of a sample. When the latter constraint was added, the model always returned the amino acid content as the maximum permissible value. Putting similar constraints on the other two end-members would have resulted in an over-constrained system of equations. The results obtained from the model were in the form of the relative abundances of amino acids, lipids and carbohydrates expressed as percentages of the total C in the sample. The percentage of total peak area under each spectral region as calculated by the model can be determined from the data in Table 3 using the formula: % peak area in spectral region= $\Sigma(\%biochemical\times$ % peak area in spectral region for that biochemical). The error/reproducibility for the entire procedure was estimated by analyzing two UDOM samples in triplicate and one UPOM sample in duplicate on the NMR and repeating the peak area integration and model calculations for each run. For the UDOM samples, the overall reproducibility (expressed as percent sample mean deviation) was $\pm$ 5.5% for the carbohydrate end member and $\pm$ 10.5% for lipids. The corresponding values for UPOM were $\pm$16% and $\pm$ 8%, respectively.

Total hydrolysable neutral sugars (THNS)in UDOM and UPOM samples were determined as described in Skoog and Benner [154]. Samples were hydrolyzed with 1.2M H_2SO_4, neutralized, and desalted by passage through cation exchange resins. Neutral sugars were separated and detected with a PA-1 column on a Dionex 500 ion chromatography system. The sum of seven neutral sugars (fucose, rhamnose, arabinose, galactose, glucose, mannose and xylose) is presented as the THNS yield. Total hydrolysable amino acids (THAA) were measured using high-performance liquid chromatography (HPLC) [40]. Samples were hydrolyzed with 6N HCl and analyzed on a Lichrospher 100 C18 column on an Agilent 1100 Liquid Chromatograph with fluorescence detection. The sum of sixteen amino acids is presented as the THAA yield. Total hydrolysable amino sugars (THAS) were determined as

described in Benner and Kaiser [16]. Samples were hydrolyzed with 3N HCl, neutralized, desalted and analyzed with a PA-1 column on a Dionex 500 ion chromatography system. The sum of glucosamine and galactosamine is presented as the THAS yield.

3.4 Results

3.4.1 C/N ratios and δ^{13}C of UDOM and UPOM

The organic C content of UDOM ranged from 13.1 to 19.3 wt. % and averaged 15 ± 1.7 wt. % (Table 2). The N content varied between 0.95 - 1.69 wt. %, with an average value of 1.2 ± 0.2. The corresponding values for UPOM are 0.71 to 2.53 wt. % C (average 1.9 ± 0.5) and, 0.08 to 0.32 wt. % N (average 0.2 ± 0.1). Depth trends were not clearly evident for C or N contents in UPOM and UDOM. The C/N atom ratios for UDOM ranged from 13.3 to 16.9 (average 15.3 ±1) and those for UPOM varied between 8.1 and 11.5 (average 9.4 ± 1.1).

Stable carbon isotopic ratios were also determined for UDOM and UPOM (Table 2). δ^{13}C values for UDOM varied between -21.2 to -21.7‰ (average -21.5 ± 0.2‰), and remained essentially constant throughout the water column. δ^{13}C values for UPOM ranged from -23.1 to -26.4‰ (average -25.1 ± 0.2‰), with isotopically heavier values in surface waters.

3.4.2 Results from ^{13}C NMR Spectroscopy

3.4.2.1 UDOM in the water column

Figure 6 shows a water column profile of UDOM ^{13}C NMR spectra. The major C functional groups identified in the UDOM spectra are alkyl (0 - 45 ppm), N-alkyl (45 -60 ppm), O-alkyl (60 - 95 ppm), acetal (95 - 110 ppm) and carboxyl/ester, amide (160-190 ppm). A weak unsaturated C signal (110 - 145 ppm) appears in the samples deeper than 500 m. Table 3 gives the relative abundance (as % of total peak area) of the C functional groups in UDOM as calculated from integrated peak areas. With increasing depth in the water column, the relative proportions of alkyl and N-alkyl groups increase, while that of O-alkyl and acetal decrease.

Using the modeling approach described in the materials and methods section, the contributions of carbohydrates, amino acids and lipids to UDOM and UPOM carbon were

Table 2: C, N contents; elemental C/N ratios and stable C isotope ratios of UDOM and UPOM from Station Aloha.

Depth (m)	wt% C	wt% N	Atomic C/N	δ^{13}C(‰)
UDOM				
20	13.1	1.0	15.9	-21.6
80	16.1	1.2	15.9	-21.7
110	14.3	1.1	15.3	-21.7
150	14.5	1.1	14.9	-21.7
200	15.1	1.2	15.2	-21.2
250	19.3	1.7	13.3	-21.9
300	15.4	1.2	14.5	-21.6
500	15.7	1.2	15.2	-21.4
750	14.3	1.1	14.9	-21.3
2500	14.1	1.0	16.9	-21.3
4000	13.3	1.0	16.3	-21.3
Average	15.0	1.2	15.3	-21.5
Std. Dev.	1.7	0.2	1.0	0.2
UPOM				
20	2.2	0.3	8.1	-23.1
80	2.0	0.3	8.4	-23.4
110	2.5	0.3	9.9	-25.6
150	2.1	0.3	8.5	-25.0
200	1.3	0.2	8.1	-24.3
250	1.8	0.2	10.0	-26.2
300	2.5	0.3	9.5	-26.5
500	2.5	0.3	9.4	-26.4
750	1.8	0.2	9.9	-24.5
2500	0.7	0.1	10.3	-25.5
4000	1.8	0.2	11.5	-25.7
Average	1.9	0.2	9.4	-25.1
Std. Dev.	0.5	0.1	1.1	1.2

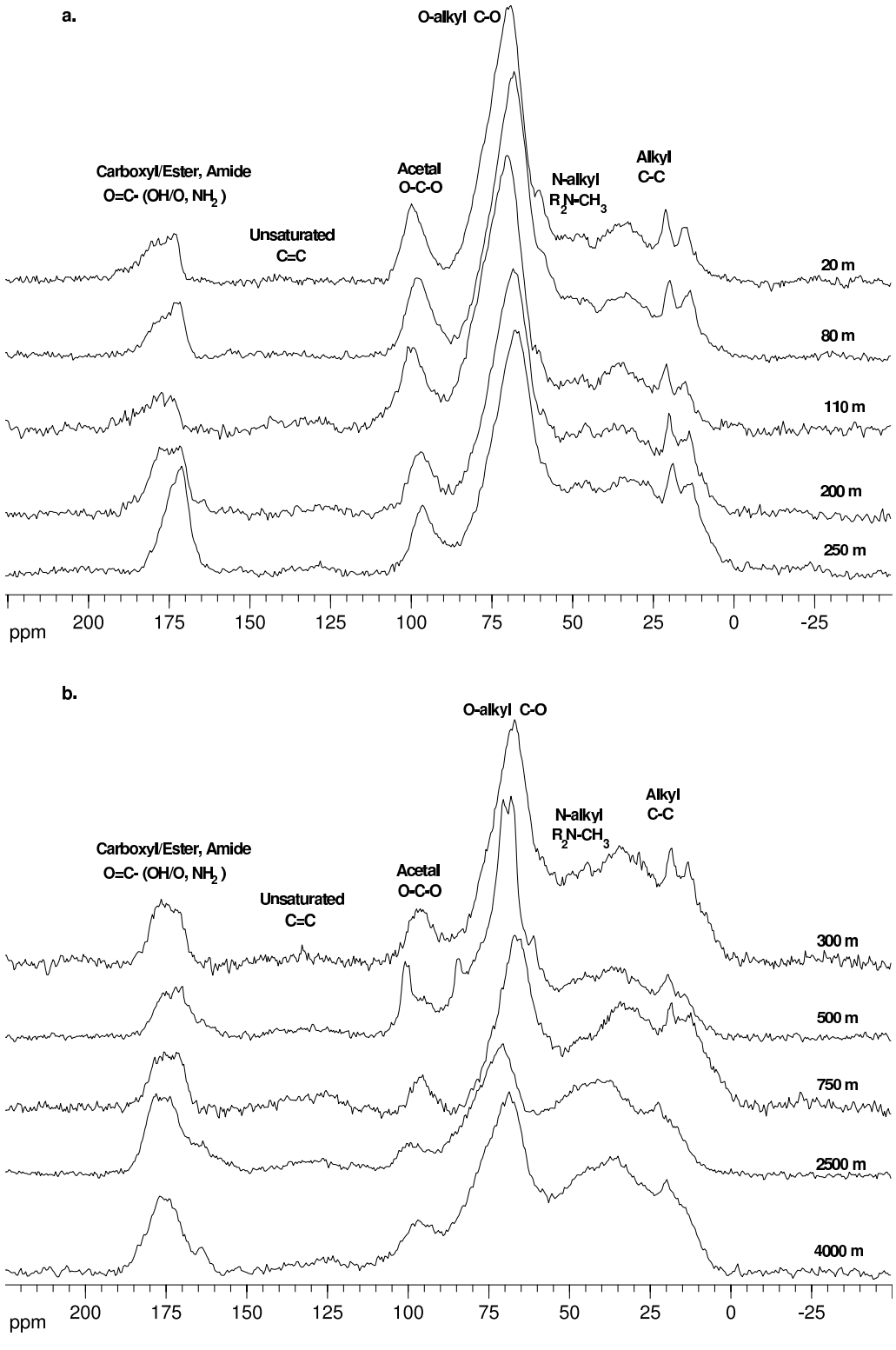

Figure 6: CP-MAS ^{13}C NMR spectra of UDOM from station Aloha stacked according to depth in the water column. Also indicated are the major peaks and the functional groups represented by them. NMR operating parameters: contact time 1ms; recycle delay 5s; 10240 transients. (a)^{13}C NMR spectra of UDOM from 20 to 250 m. (b)^{13}C NMR spectra of UDOM from 300 to 4000m.

estimated. The results reflect the major compositional trends observed in the NMR spectra (Table 3). In UDOM, the percentage of carbohydrate C decreases from 65 to 39% with depth, whereas percentages of lipid C (11- 37%) increase and amino acid C (24 - 29%) shows very little variation. Carbohydrates are the dominant biomolecules at most sampling depths. The relative abundance of lipids becomes comparable to carbohydrates in samples below 750m.

3.4.2.2 UPOM in the Water Column

Figure 7 shows the ^{13}C NMR spectra of UPOM from different depths in the water column. Alkyl, N-alkyl, O-alkyl, carboxyl/ester, amide and unsaturated C are the major functional groups present. Alkyl, N-alkyl and O-alkyl comprise a major part of the total spectral peak area at all depths. Some of the UPOM samples were not analyzed using ^{13}C NMR, as their C contents were too low to yield meaningful results with reasonable use of spectrometer time.

The proportions of the various functional groups in UPOM were also modeled to estimate the relative contributions of amino acids, lipids and carbohydrates. Amino acids and carbohydrates were the dominant biochemicals at all depths. Carbohydrates varied in relative abundance from 30 - 46%, amino acids from 33 - 47% and lipids ranged from 15 - 30%. There was an overall decrease in the relative proportion of amino acids and increase in lipids with depth, but no clear trend is discernible in carbohydrates.

3.4.3 Molecular-level Amino acid and Carbohydrate Analyses

The results of the molecular-level analyses of THAA, THNS and THAS on the UDOM and UPOM samples are presented as percentages of total C identifiable as a specific class of biomolecules (Table 4). In case of UDOM, THNS percentages range from 2.8 - 10.1 %C and decrease with depth. THAS contents vary from 0.6 - 1.9 %C and these too decrease with depth. The trend of decreasing carbohydrate content of UDOM with depth, which was observed in the ^{13}C NMR data and modeling results, is also reflected in the molecular-level analyses. THAA contributions range from 1.7 - 3.8 %C and do not show consistent trends with depth. The percentage of C in UPOM represented by THNS ranges from 4.6 - 12.5

Table 3: Percentage of total NMR peak area measured under each spectral region for UDOM, UPOM, plankton and calculated for the amino acid, lipid and carbohydrate end-members used in the model

Depth (m)	% Total peak area under each spectral region*							% Biomolecules		
	I	II	III	IV	V	VI	VII	%AA	%Lp	%CHO
UDOM										
20	19.2	7.2	56.8	8.8	0	0	8.4	24	11	65
80	21.7	8.7	54.3	8.7	0	0	6.5	24	14	63
110	19.2	7.7	53.8	11.5	1.9	0	5.8	25	11	64
150	23.2	9.3	48.8	9.3	0	0	9.3	26	16	58
200	28.6	11.4	46.0	6.0	0	0	8.6	26	21	53
250	22.7	11.4	32.0	4.5	0	0	6.8	29	23	48
300	34.5	10.3	41.4	7.0	0	0	7.0	26	26	47
500	25.6	10.3	46.1	7.7	2.6	0	7.7	25	19	56
750	43.5	9.0	34.8	4.3	0	0	9.0	26	36	39
2500	35.7	10.7	28.6	3.6	3.6	0	17.9	23	37	41
4000	35.7	10.7	35.7	7.1	0	0	10.7	23	32	45
UPOM										
20	27.0	13.5	29.7	5.4	10.8	0	13.5	47	15	38
80										
110	26.3	15.8	39.5	2.6	2.6	0	13.2	38	16	46
150	32.3	12.9	25.8	6.5	9.7	0	12.9	45	22	34
200										
250										
300	33.3	23.3	16.7	3.3	10.0	0	13.3	40	30	30
500										
750										
2500										
4000	31.3	31.3	19.0	6.2	9.4	0	3.1	33	22	45
Plankton	47.6	19	14.3	4.8	4.8	0	9.5	58	28	14
Model end-members										
Amino acid	36.3	21	7.4	0	7.8	1.5	2.6			
Lipid	94.4	0	0	0	0	0	5.6			
Carbohydrate	0	0	83.3	16.7	0	0	0			

I (0-45 ppm); II (45-60 ppm); III (60-95 ppm); IV (95-110 ppm); V (110-145 ppm); VI (145-160 ppm); VII (160-190 ppm)

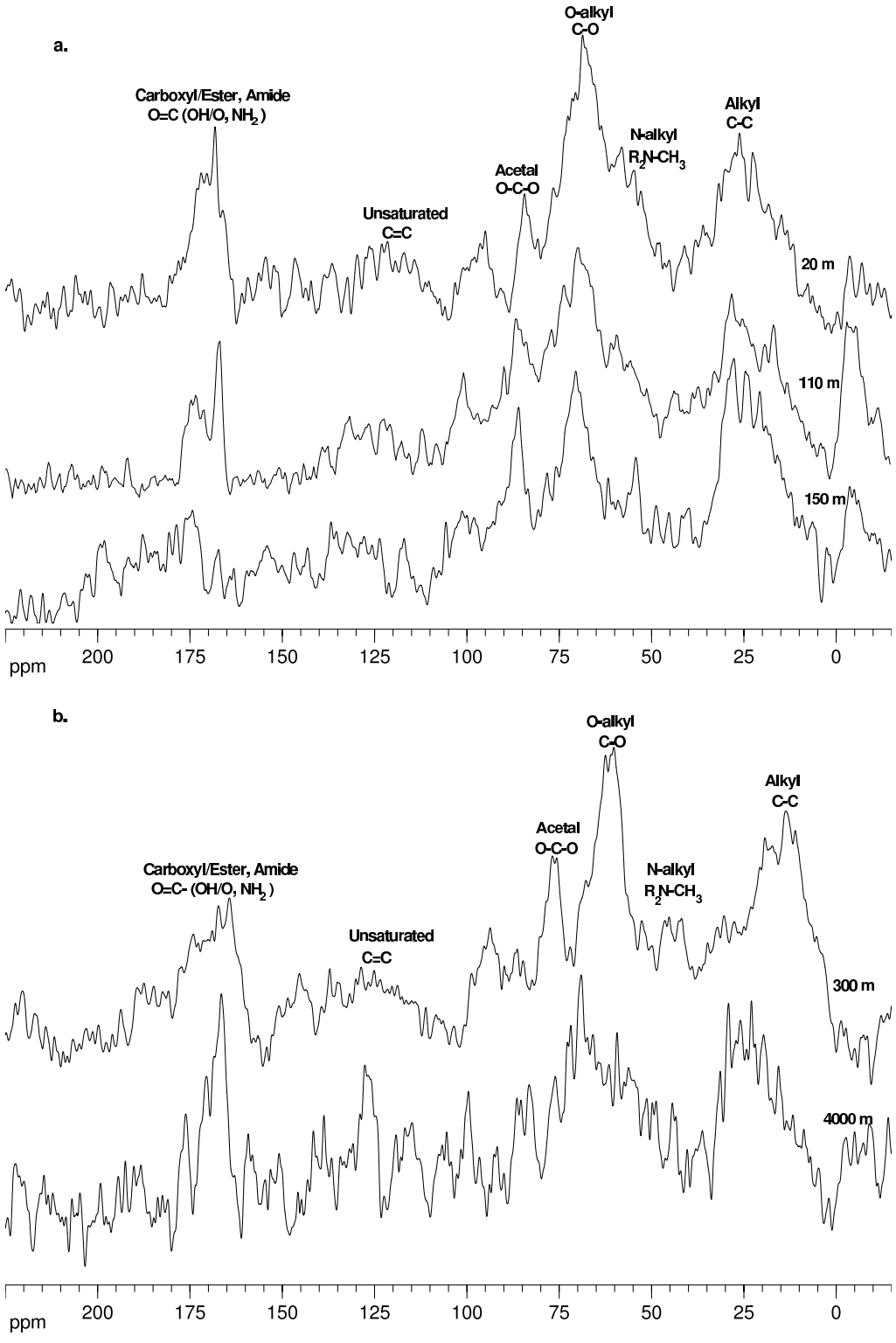

Figure 7: CP-MAS ^{13}C NMR spectra of UPOM from station Aloha stacked according to depth in the water column. Also indicated are the major peaks and the functional groups represented by them. NMR operating parameters: contact time 1ms; recycle delay 5s; 30720 transients. (a)^{13}C NMR spectra of UPOM from 20 to 150 m. (b)^{13}C NMR spectra of UPOM from 300 to 4000m.

%C, with an overall decreasing trend with depth. The UPOM sample from 4000 m does not follow this trend and appears to be an outlier (Table 4). Results from replicate analyses of this sample showed good precision and high sugar yields. The high THNS content could have resulted from the inclusion of fecal pellet fragments in the UPOM sample. THAS contents vary from 0.4 - 1.1 %C. While the contributions of THNS and THAS to C in UDOM and UPOM are comparable, THAA is a much larger fraction of the identifiable C in UPOM. THAA contents range from 11.8 - 24.6 %C with an overall decreasing trend with depth.

3.5 Discussion

3.5.1 C/N ratios and δ^{13}C of UDOM and UPOM

The C/N values of UDOM and UPOM were slightly higher in deep waters than in surface waters indicating a selective removal of N (Table 2). The higher C/N values of UDOM as compared to UPOM indicate a major difference in the bulk chemical composition of these two size fractions of marine organic matter. Benner et al. [14], have also reported large differences in C/N values between UDOM and UPOM and that this trend is geographically invariant.

The results of the δ^{13}C measurements are similar to those of Benner et al. [14] and indicate that UDOM is primarily of marine origin and its δ^{13}C composition is invariant with depth as well as geographic region. This predominantly marine source is also supported by lignin measurements from station Aloha, which indicate only a $\sim$1% contribution from terrigenous DOC [75]. The δ^{13}C values of UPOM are all depleted in δ^{13}C relative to UDOM. They are also depleted compared to suspended POM collected on 0.8 μm quartz fiber filters [50], which showed δ^{13}C values of -20.1 to -22.6 ‰ below depths of 100 m in the northeast Pacific Ocean. The differences between the δ^{13}C values in the two size fractions have been previously discussed in detail [14, 75]. One possible reason for the observed discrepancy in δ^{13}C values between UPOM and POM collected on quartz filters is that the difference is due to small sub-micron particles that pass through 0.8 μm filters but are retained by 0.1μm filters [14]. The 0.1- 0.7 μm fraction could account for as much as 40 to

Table 4: Results from molecular-level amino acid and carbohydrate analyses on UDOM and UPOM

Depth (m)	THNS (%C)	THAS (%C)	Sum CHO (%C)	THAA (%C)
UDOM				
20	10.1	1.8	11.9	2.5
80	8.8	1.9	10.7	1.9
110	6.9	1.7	8.6	2.0
150	5.3	1.9	7.2	1.7
200	4.3	1.1	5.4	2.6
250	3.8	1.2	5.0	3.8
300	3.2	1.1	4.3	3.1
500	2.7	0.9	3.6	3.1
750	3.5	0.8	4.3	3.4
2500	1.9	0.7	2.6	2.0
4000	2.8	0.6	3.4	2.4
UPOM				
20	10.9	0.9	11.8	20.9
80	10.5	0.9	11.4	17.9
110	11.1	1.0	12.1	16.8
150	8.5	0.8	9.3	21.8
200	6.3	0.7	7.0	24.6
250	4.6	0.5	5.1	21.9
300	5.5	0.7	6.2	23.3
500	7.6	0.9	8.5	16.8
750	7.7	0.6	8.3	17.4
2500	6.1	0.4	6.5	15.9
4000	12.5	1.1	13.6	11.8

- THAA: Total hydrolysable amino acids
- THAS: Total hydrolysable amino sugars
- THNS: Total hydrolysable neutral sugars
- Sum CHO = THNS + THAS

50% of suspended POC [2, 14]. Aerosol particles (having C in the 0.1 to 0.7 (m size range) over the Pacific and Atlantic Oceans have δ^{13}C values ranging from -26.5 to -26.7‰ and a terrestrial source [31]. Results from lignin phenol analyses by Hernes and Benner [75] also indicate that a substantial fraction of UPOM is of terrigenous origin. Carbon-normalized lignin phenol yields below 110 m at station Aloha were 1-2 orders of magnitude greater in UPOM than in the dissolved phase.

3.5.2 Comparison of UDOM and UPOM from Aloha

3.5.2.1 ^{13}C NMR Spectroscopy

The results from ^{13}C NMR spectroscopy of UDOM from Aloha are similar to earlier studies from this and other regions [15, 118]. The most notable difference between this study and that of earlier studies is in the unsaturated and aromatic region of the spectra. This region appears to have been overestimated in the early ^{13}C NMR studies of UDOM presumably due to baseline imperfections, typical of NMR instruments of that time.

Carbohydrates are the common biomolecules containing O-alkyl and acetal groups. The ratio of integrated areas of O-alkyl (60-95 ppm) to acetal (95-110 ppm) functional groups for UDOM varied from 5 to 8 and is consistent with a predominantly carbohydrate source for these functional groups. In typical carbohydrates, such as pentoses and hexoses, this ratio has values of 4 and 5, respectively, and can be used to roughly estimate the relative abundances of these carbohydrates. Earlier studies [3, 15] also reported combined carbohydrates as the major biopolymers in HMW-DOM. The large decrease in the fraction of combined carbohydrates between surface and deeper waters indicate that these polymers are highly reactive. These results agree with those of molecular-level carbohydrate studies [4,119,130,154]. Amino acids, as peptides and proteins, are the dominant form of organic N in organisms. They often comprise a major fraction of the C and N in biomass [177], and are useful indicators of the diagenetic state of organic matter [41]. Amino acids constitute a smaller fraction of organic C in UDOM than carbohydrates, and do not exhibit much variation with depth. The increasing fraction of alkyl functional groups with depth in the UDOM ^{13}C NMR spectra (Table 3) is primarily due to a relative increase in the fraction

of lipids. An increase in lipids as a percentage of C in UDOM, with depth has also been reported by [4].

The relative proportions of the different functional groups in UPOM do not change with depth as consistently as seen with UDOM (Table 3). There is a relative increase in N-alkyl groups, while O-alkyl groups show a decreasing trend with depth. Acetal and carboxyl/ester, amide functional groups do not show any appreciable changes with depth. The ratio of O-alkyl to acetal varies quite significantly and ranges from 2 - 15 for UPOM. This may be a result of a greater proportion of the O-alkyl functional groups being present in amino acids rather than carbohydrates.

The most significant difference between the ^{13}C NMR spectra of UDOM and UPOM from the same depth is the much higher unsaturated C content and lower O-alkyl content of UPOM (Table 3). The unsaturated C signal may be due in part to terrigenous components, which are relatively abundant in UPOM [75]. The relative proportions of the various functional groups also vary differently with depth in UDOM compared to UPOM. For example, alkyl (0 - 45ppm) functional groups increase significantly with depth in UDOM, but are almost invariant in UPOM (Table 3).

3.5.2.2 Modeled Biomolecule Contents

The modeled biochemical composition is an excellent tool to evaluate compositional variations directly from ^{13}C NMR spectral data. The relative compositions of surface UDOM (0 - 200m), subsurface UDOM (500 - 4000m), surface UPOM (0 - 200m), subsurface UPOM (300 - 4000m) and plankton are compared in Figure 8. The data for plankton were obtained by modeling the ^{13}C NMR spectrum presented in Figure 9. Comparing UDOM and UPOM spectra from the same depths, the modeling results indicate a much higher amino acid content and lower carbohydrate content in UPOM relative to UDOM. The fraction of C as amino acids decreases with depth in UPOM but remains fairly constant in UDOM. The fraction of C in carbohydrates decreases with depth in UDOM but remains fairly constant in UPOM. These analyses indicate that amino acids are the most reactive components

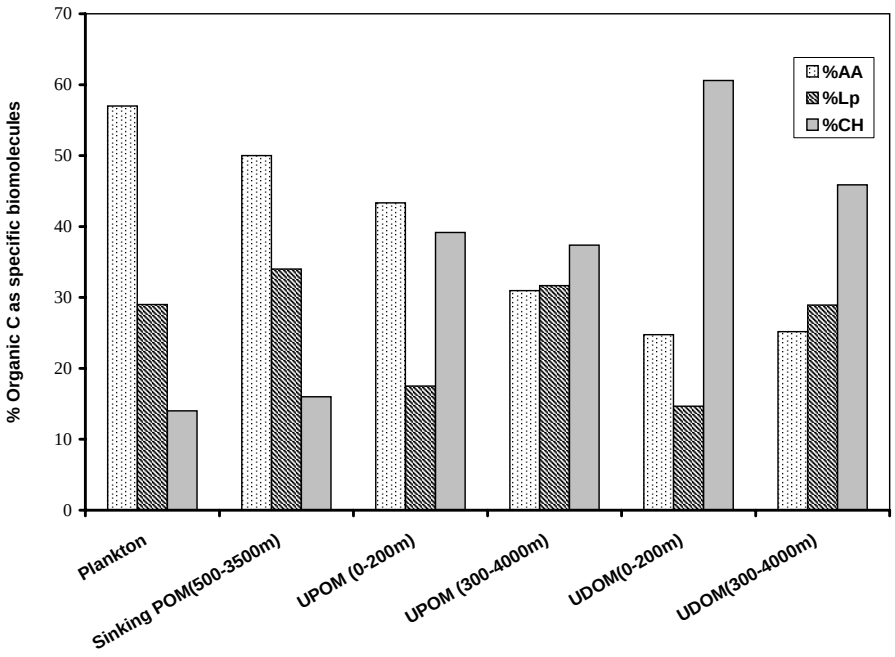

Figure 8: Modeled contributions made by amino acid, carbohydrate and lipid end-members to the total organic carbon in UDOM and UPOM at different depths. Also given for comparison are the values for plankton from station Aloha.

in UPOM, whereas carbohydrates are the most reactive components of UDOM. Lipids increase in relative proportion in both UPOM and UDOM and appear to be the least reactive fraction by this analysis. The modeling results indicate a higher amino acid and lower carbohydrate content in plankton as compared to UPOM from all depths. The deeper water UPOM samples have a slightly higher lipid content than plankton. Amino acids appear to be reactive components of plankton as well and are preferentially lost when UPOM is formed from plankton.

The δ^{13}C values and lignin yields [75] indicate that UPOM and UDOM have different sources. While UDOM is predominantly marine, UPOM appears to have a mixture of marine and terrestrial sources. The terrigenous component of UPOM is not a part of the diagenetic continuum of marine POM→ HMW-DOM→LMW-DOM. However both UDOM

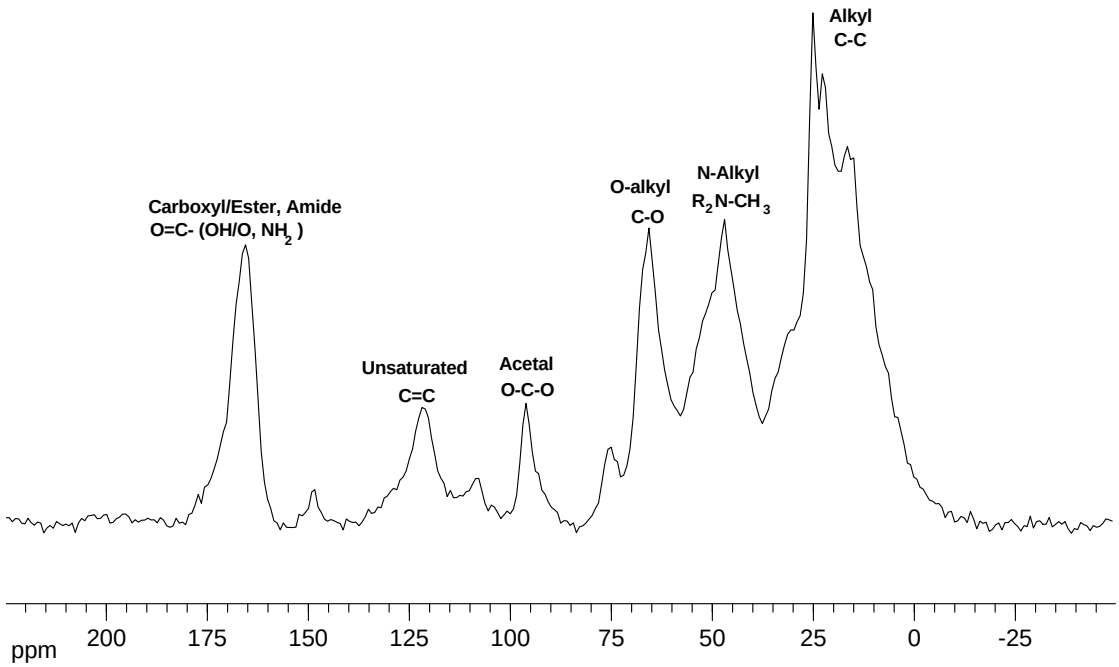

Figure 9: CP-MAS ^{13}C NMR spectra of net plankton from station Aloha. Also indicated are the major peaks and the functional groups represented by them. NMR operating parameters: contact time 1ms; recycle delay 5s; 10,240 transients.

and UPOM shows signs of increasing diagenetic alteration with depth in the water column and it appears that the marine component of UPOM is more reactive than the terrigenous component.

3.5.2.3 Molecular Amino acid and Carbohydrate Contents

One distinct advantage of molecular methods of analysis over the NMR modeling is that there is very little ambiguity about the biochemical identity of a molecule. Yields of recognizable biomolecules such as THAA, THAS and THNS are considered key indicators of the diagenetic state and bioreactivity of organic matter [12, 13]. In general, higher biochemical yields are indicative of relatively fresh and bioreactive organic matter, whereas lower yields are indicative of more diagenetically altered and less bioreactive material. The fraction of C accounted for by THAA, THAS and THNS is much greater in UPOM than in UDOM. This

suggests that UPOM is less diagenetically altered and of more recent origin than UDOM. The fraction of C in UDOM that can be accounted for as specific sugars and amino acids decreases with depth in the water column. These data clearly demonstrate that deep water UDOM is more diagenetically altered than surface water UDOM. Lower amino acid and higher carbohydrate contents of UDOM compared to UPOM revealed by ^{13}C NMR, are also clearly reflected in the molecular-level analyses.

Although the compositional variations with depth revealed by molecular-level analyses are similar to those revealed by ^{13}C NMR, the percentages of C indicated as amino acids and carbohydrates by ^{13}C NMR are consistently higher (Table 5). The proportion of carbohydrates identifiable as specific sugars and proportion of proteins/peptides recognizable as specific amino acids can be calculated from the ratios of the molecular to NMR results for each biomolecule class. In UDOM, up to 18.2 % of the carbohydrate content and 13.3 % of the amino acid content estimated by NMR is measured by the molecular level analyses. A greater fraction of the biomolecules (up to 31% of carbohydrates and 58% of the amino acids) in UPOM is measured by molecular-level analyses. This further indicates that UPOM is less diagenetically altered than UDOM, a finding consistent with the size-reactivity continuum model presented by Amon and Benner [7].

3.5.3 Composition of the Molecularly Uncharacterized Component of Marine Organic Matter

NMR spectral analyses are useful in providing information about the broad structural features of complex mixtures such as marine OM. More specific information is difficult to obtain from NMR data, as it is not often possible to assign the peaks/resonances unambiguously to particular biochemicals. On the other hand, molecular-level analyses of specific biochemical classes such as amino acids, sugars and lipids provide specific structural information, but a relatively small fraction of the C is identified. Comparison of biomolecule proportions (carbohydrate to amino acid ratio) as determined independently from NMR and molecular analyses provides clues about the composition of the molecularly uncharacterized component. For most samples, the biomolecule proportions as calculated from the ^{13}C NMR results and molecular-level analyses (Table 5) are in reasonably good agreement

Table 5: Comparison of the relative amino acid and carbohydrate contents of UDOM and UPOM as measured by molecular analyses and calculated from ^{13}C NMR peak areas

Depth (m)	% Carbohydrates as specific sugars	% Peptides as specific amino acids	NMR CHO/AA	Molec. CHO/AA
UDOM				
20	18.2	10.5	2.7	4.8
80	17.1	7.9	2.6	5.6
110	13.5	8.1	2.6	4.3
150	12.4	6.7	2.3	4.2
200	10.2	10.1	2.1	2.1
250	10.4	13.3	1.7	1.3
300	9.1	11.8	1.8	1.4
500	6.5	12.4	2.2	1.2
750	11.1	13.3	1.5	1.3
2500	6.4	8.9	1.8	1.3
4000	7.6	10.3	1.9	1.4
UPOM				
20	31.2	44.6	0.8	0.6
80			0.6	
110	26.3	43.8	1.2	0.7
150	27.7	48.8	0.8	0.4
200			0.3	
250			0.2	
300	20.8	58.4	0.7	0.3
500			0.5	
750			0.5	
2500			0.4	
4000	30.2	35.8	1.4	1.2

- AA: Amino acid; CHO: Carbohydrates; Molec. : Molecular analyses

(±30%) considering the limitations of the model and the molecular analyses. This agreement suggests that the molecularly uncharacterized fraction is similar in composition to the characterized fraction but is somehow shielded or altered rendering it unrecognizable by the molecular analyses. The only exception to the correspondence in biomolecule proportions is seen in the four surface UDOM samples (20 - 150m), where the molecular carbohydrate to amino acid ratio is almost twice that obtained from NMR. This deviation would be expected because surface UDOM samples are enriched in polymers containing THNS and THAS and are less altered relative to deeper samples. The carbohydrates in surface samples are more readily analyzed by molecular methods.

Another hypothesis regarding the composition of the molecularly uncharacterized component has been proposed by Hwang and Druffel [84], who suggest that this fraction is composed primarily of lipid-like materials in sinking POM. The NMR results of Hedges et al. [70] also indicate a significant (up to 32%) lipid fraction in sinking POM. In contrast, our NMR results (Table 3) indicate that lipid-like material is less abundant in UDOM and UPOM (average ∼22% of the C) than in sinking POM. Thus, lipids do not appear to be the dominant component of the molecularly uncharacterized fraction of UDOM or UPOM.

3.6 Conclusions

Results from ^{13}C NMR analyses together with δ^{13}C clearly illustrate the differences in the composition and sources of UDOM and UPOM. Modeling of ^{13}C NMR spectral peak areas indicate that carbohydrates are the major biochemical class in UDOM, followed by amino acids and lipids. UPOM is compositionally different with amino acids as the dominant biochemical class followed by carbohydrates and lipids. In both UDOM and UPOM, carbohydrates and amino acids decrease and lipids increase with depth in the water column reflecting the action of selective decomposition. These compositional trends are also reflected by molecular-level amino acid and carbohydrate analyses of UDOM and UPOM. A larger fraction of the C in UPOM can be accounted for by the molecular analyses as compared to UDOM, indicating that UPOM is diagenetically less altered. The similarities observed in the carbohydrate to amino acid ratio in most samples as determined by NMR

and molecular analyses indicate that the molecularly uncharacterized fraction is compositionally similar to the characterized fraction.

CHAPTER 4

ORGANIC PHOSPHORUS COMPOSITION AND CYCLING AT STATION ALOHA: INSIGHTS FROM ^{31}P NMR SPECTROSCOPY AND ELEMENTAL ANALYSES

4.1 Abstract

Compositions of ultrafiltered dissolved organic matter (UDOM; 1-100 nm size fraction) and ultrafiltered particulate organic matter (UPOM; 0.1-60 μm size fraction) were characterized in samples collected from a depth profile (20-4000m) at Station Aloha in the North Pacific subtropical gyre, using solid-state ^{31}P nuclear magnetic resonance (NMR) spectroscopy and elemental analysis. ^{31}P NMR spectra from UDOM reveal that P esters (75%) and phosphonates (25%) are the major P functional groups present, with their relative proportions unvarying with depth in the water column. However, P esters were the only P bond type observed in the NMR spectra of UPOM. The C:N:P atom ratios of UDOM and UPOM show little variation with depth in the water column, averaging 211:14:1 and 130:13:1, respectively. The differences in UDOM and UPOM compositions with respect to both C and P suggest that UDOM does not originate from simple solubilization of UPOM, and the aggregation of UDOM is not the primary source of UPOM. Regression analyses indicated that P in UDOM and UPOM is likely present as altered biopolymers of RNA, DNA, sugar phosphates and phosphoamino acids. P is also likely present as phospholipids and lipopolysaccharides in UPOM. Further, it appears that the P functional groups are balanced in their distribution among molecular classes, because they remain in relatively constant proportion throughout the ocean.

4.2 Introduction

Phosphorus (P) is an essential nutrient required by all living organisms, and it occurs in organic form in the four major classes of biomolecules (nucleic acids, carbohydrates, lipids and amino acids). Recent studies have suggested that P may play a significant role in limiting primary productivity and nitrogen fixation in oligotrophic ocean regions (for example, [143]). In one such oligotrophic region, the North Pacific subtropical gyre (NPSG), the concentration of dissolved inorganic P (DIP), which is considered the most readily available form of P for microorganisms, has been decreasing in the upper water column for at least the last several years [95, 96]. However, levels of primary productivity are being maintained and may even be increasing in this region, indicating that either DIP recycling and utilization has greatly increased in efficiency or, other sources of P are being exploited. In oligotrophic regions such as the NPSG, dissolved organic P (DOP) often comprises a major fraction of the total dissolved P (TDP) pool especially in surface waters [19, 90, 99]. The DOP pool at station Aloha located in the NPSG, constitutes ∼75 - 80% of the TDP pool and is frequently 5-10 times larger than the measured DIP pool [98]. Thus, DOP is an important potential P source for the ecosystem at this site and obtaining new insights into its composition is an important step for understanding the dynamics of P cycling.

^{31}P nuclear magnetic resonance (NMR) spectroscopy has been shown to be an excellent tool for determining P composition of marine organic matter. Using ^{31}P NMR the major P functional groups present in marine organic matter (OM) have been identified for several sites in the world oceans [11, 35, 36, 102, 131]. Solid-state ^{31}P NMR spectroscopy has been used to study marine high-molecular weight (HMW) ultrafiltered dissolved OM (UDOM; 1-100 nm), ultrafiltered particulate OM (UPOM; 0.1-60 μm), sinking particles and sediments [11,35,36,89,102,140]. Solution ^{31}P NMR has also been applied to elucidate the composition of marine sinking particles from various locations [131]. These NMR studies have shown that P esters and phosphonates are the dominant forms of organic P observed in marine organic matter [11, 35, 36, 102, 131]. Other studies have indicated that compounds such as polyphosphates and pyrophosphates are present as minor constituents in marine sediments

and sinking particulate matter [131, 140, 161].

Recently, results of DOP bioavailability, hydrophobic P distribution, oxygen isotopic ratios of DIP and multi-year OM inventory studies, have provided new insights into P cycling at station Aloha [21,33,37,166]. Some of these studies have indicated possible changes in the P cycle dynamics in this region. Results from Church et al. [33] indicate that over a 10-year time period from 1989 to 1999, the dissolved organic carbon (DOC) and dissolved organic nitrogen (DON) inventories at station Aloha increased without a corresponding increase in the DOP pool. These changes resulted in increases in C:P and N:P ratios on the order of 17%, which indicate changes in the OM cycling in this ecosystem resulting from reorganization of the phytoplankton community. In particular, the phytoplankton community once dominated by eukaryotes, appears to have shifted to a phototrophic community dominated by smaller prokaryotic cells such as Prochlorococcus and Synechococus [94]. As a result of this ecological reorganization, a doubling of the chlorophyll a inventory and rate of primary production has also been reported [94,95]. In this paper, we present results from solid-state ^{31}P NMR spectroscopy along with atomic C:P and N:P ratios and P contents of UDOM and UPOM samples from a detailed depth profile at station Aloha. The compositional information gained from elemental analyses and solid-state ^{31}P NMR spectroscopy from the two size fractions of OM have been interpreted in light of the developments presented in recent literature.

4.3 Materials and Methods

4.3.1 Site Location and Sample Collection

Water samples were collected from various depths (20 to 4000m) at station Aloha in the Pacific Ocean. Station Aloha (22.75°N, 158°W), located approximately 100 km north of Oahu, Hawaii, has been the subject of intensive study for many years as part of the Hawaii Ocean Time Series program. The water depth at the sampling site is 4800 m. Further information on station Aloha and annual time series data reports can be accessed at http://hanana.soest.hawaii.edu/hot/hot_jgofs.html.

Samples were collected during a cruise to station Aloha in October 1999 aboard the R/V

Ka'imikai-o-Kanaloa. Organic matter was isolated from seawater using tangential flow ultrafiltration [14,15]. At each depth, ∼700 L of seawater was collected with four separate casts of a Niskin bottle rosette. From 600 L of this composite, the ultrafiltered POM (UPOM, 0.1- 60 μm) fraction was isolated aboard ship with an Amicon DC10L ultrafiltration system with a polysulfone hollow fiber filter. The filtrate from the DC10L system was fed directly into an Amicon DC30 ultrafiltration system with polysulfone membranes (S10N1; 1000Da cutoff) to isolate the ultrafiltered DOM (UDOM, 1 - 100nm), which is also referred to as high-molecular weight (HMW) DOM. The UDOM and UPOM concentrates were frozen for transportation to the laboratory, where they were dried under vacuum and stored for chemical analyses. A mass balance of organic C was performed for each ultrafiltered sample, details of which can be found in Benner et al [14], and Hernes and Benner [75]. The results indicate that appreciable amounts of C were not gained or lost during ultrafiltration.

The percentage recovery of DOP was determined by dividing the measured P concentration of UDOM (Table6) by the DOP concentration of seawater at that depth. The seawater DOP concentrations used were the average values for the week immediately preceding and following our sampling cruise, obtained from the Hawaii Ocean Time series data set. These calculations indicate that on average 32% of the total dissolved organic phosphorus present was recovered during ultrafiltration. This recovery is comparable to that of DOC [14]. Potential problems that may be encountered during ultrafiltration include contamination by P leaching from surfaces within the ultrafiltration system; scavenging of inorganic P during concentration of trace metals and, artifactual production of colloidal organic P via the association of inorganic P with organic molecules [10]. Evidence presented in Kolowith et al. [102] shows that using our sampling protocol, these processes are not significant factors affecting the isolation of ultrafiltered organic matter.

4.3.2 Elemental C, N, P Measurements

C, N and P contents were measured on dried UDOM and UPOM samples. C and N contents were measured after vapor phase acidification using a Carlo Erba CHN analyzer [74]. Total P contents were determined by a modification of the combustion method of Aspila et al. [9].

5 mg of each sample were ashed at 550°C for 2 hours and treated with 15 ml of 1 N HCl overnight. The HCl extracts were filtered through a 0.45 μm puradisc polypropylene filter and the P content measured using standard spectrophotometric techniques [125].

4.3.3 ^{31}P NMR Experiments

Solid-state ^{31}P NMR analyses of the UDOM and UPOM samples were carried out at the NMR center in the School of Chemistry and Biochemistry at the Georgia Institute of Technology. The ^{31}P NMR spectra were acquired on a Bruker DSX 400 spectrometer using Cross Polarization-Magic Angle Spinning (CP-MAS) at a ^{31}P frequency of 161 MHz. Approximately 90 mg of powdered sample was packed into a 4 mm-diameter cylindrical zirconia rotor fitted with a Kel-F cap and spun at 10,000 $\pm$ 10 Hz in a Bruker magic - angle spinning probe. The presence of spinning sidebands is an artifact of MAS, but at fast enough spinning rates such as the one used here, they do not interfere with the peak resonances. For all samples, a cross polarization sequence, optimized to obtain semi-quantitative data, was used with a 1.0 msec contact time and a pulse delay of 4 seconds. In order to obtain semi-quantitative data using CP-MAS techniques, the time delay between two consecutive NMR pulses (referred to as the pulse delay), used should be much greater than the spin-lattice relaxation times ($T_{1\rho}$H's) of all the different functional groups present [180]. In complex material such as natural organic matter, where a range of $T_{1\rho}$H's are present, NMR optimization experiments have to be performed to determine an optimal value of pulse delay that satisfies the above condition. In a series of experiments performed on marine dissolved organic matter samples, Clark [34] found that varying the pulse delay from 1 second to 20 seconds did not appear to alter the relative peak areas of the P-ester and phosphonate peaks, suggesting that 4 seconds was a sufficient pulse delay for these peaks to relax in the natural organic matter sample matrix. A contact time of 1msec, commonly used for natural organic matter samples, was found to be optimal in this case as well. A total of 8000 transients were collected for each UDOM sample and 32,000 transients for each UPOM sample. UDOM and UPOM spectra were processed with 30 Hz and 100 Hz exponential line broadening respectively. Data processing was carried out off-line using the Mestre-C software

package (Mestrelab Research, Santiago de Compostela, Spain). Identification of functional groups by ^{31}P NMR is based on their chemical shift relative to an external phosphoric acid standard. Chemical shift values are used to represent differences in resonance frequency of different P compound classes. These values are dimensionless and are expressed in parts per million (ppm) relative to the phosphoric acid standard set at 0 ppm. The chemical shift ranges (in ppm) of some naturally occurring P functional groups are: polyphosphates (-18 to -30); pyrophosphates (-5 to -10); phosphate diesters (-5 to 0); orthophosphate (0 to 5); phosphate monoesters (0 to 10) and phosphonates (15 to 30). Chemical structures of P functional groups present in UDOM and UPOM are indicated on Figures 10 and 11.

4.4 Results

4.4.1 P and N:P ratios of UDOM and UPOM

The concentrations of P and C: P, C:N and N : P atom ratios of UDOM and UPOM are presented in Table 6. The C : N ratios presented in Table 6 have been previously presented in [75, 141]. The concentrations of P in UDOm decreased with depth and ranged from 98.2 nM in the surface waters to 27 nM in deep water. The concentrations of P in UPOM decreased with depth and ranged from 18.5 nM in surface waters to 2.8 nM below the euphotic zone. The C:N ratios for UDOM ranged from 13.3 to 16.9 (average 15.3 $\pm$ 1) and those for UPOM varied between 8.1 and 11.5 (average 9.4 $\pm$ 1.1). The C : P ratio of UDOM ranged from 169 to 268 (average 211 $\pm$ 28). The corresponding values for UPOM ranged from 92 to 149 (average 118.8 $\pm$ 20.2). The average N : P ratio for UDOM was 13.9 $\pm$ 2.1, whereas it was 13.1 $\pm$ 3.1 for UPOM.

4.4.2 ^{31}P NMR Spectroscopy

Figure10 shows a water column profile of UDOM ^{31}P spectra. Spectra from all depths show a prominent peak at -3 ppm and a smaller peak at $\sim$ 20 ppm. The peak at -3 ppm can be attributed to phosphate monoesters and diesters. Phosphonates, a group of compounds containing a direct C-P bond, are also present in UDOM as revealed by the peak at approximately 20 ppm in the UDOM spectra (Figure 10). P-esters and phosphonates comprise 75% and 25% respectively of the organic P in terms of relative proportions. This

Table 6: P contents and atomic C:P, N:P and C:N ratios of UDOM and UPOM from station Aloha. The C:N ratios are from [141].

Depth (m)	P (nM)	Atomic C/P	Atomic N/P	Atomic C/N
UDOM				
20	98.2	169	10.7	15.9
80	83.6	213	13.3	15.9
110	73.1	241	15.8	15.3
150	64.5	210	14.1	14.9
200	55.0	172	11.6	15.2
250	36.2	200	15.0	13.3
300	39.3	213	14.7	14.5
500	33.5	220	14.5	15.2
750	28.9	268	18.0	14.9
2500	27.0	219	12.9	16.9
4000	29.3	198	12.2	16.3
Average		211.2	13.9	15.3
Std. Dev.		28.1	2.1	1.0
UPOM				
20	6.7	142	17.5	8.1
80	10.0	109	13.0	8.4
110	18.5	129	13.1	9.9
150	5.3	134	15.7	8.5
200	3.3	106	14.0	8.1
250	3.5	110	11.0	10.0
300	2.8	149	15.7	9.5
500				9.4
750				9.9
2500	3.0	92	8.9	10.4
4000	6.7	98	8.6	11.5
Average		118.8	13.1	9.4
Std. Dev.		20.2	3.1	1.1

ratio remains constant for UDOM throughout the water column. Essentially identical trends with depth have been observed in other oceanographic regions [36, 102].

Results from ^{31}P NMR spectroscopy of UPOM from station Aloha are presented in Figure11. These spectra exhibit only a single peak at -3 ppm, attributable to P-esters. This peak is located in the same region as the P-ester peak observed in UDOM and does not change in intensity with depth in the water column. UPOM from other geographic locations also show only a single solid-state ^{31}P NMR peak due to P-esters [35, 36, 102].

4.5 Discussion

4.5.1 C:N:P ratios of UDOM and UPOM

The atomic C:P and N:P values (Table 6), together with atomic C:N ratios [75, 141] clearly indicate differences in the bulk chemical composition of UDOM and UPOM. UDOM from all depths deviate substantially from the Redfield C:N:P ratio of 106:16:1 (Redfield, 1958), especially in terms of the C:P ratios. It is not known whether UDOM is produced in non-Redfield stoichiometry or if the observed ratios are a result of preferential remineralization of P relative to C. Various studies have reported C:N:P ratios of bulk DOM from station Aloha to be much higher than Redfield ratios, especially in deeper waters, indicating preferential remineralization of P over C and N [33, 168]. At station Aloha's 1000 m reference depth, the estimated 9 year average C:N:P ratio of bulk DOM is 2,600:129:1 [168]. The C:N:P ratios of bulk DOM are, in general, higher than those for UDOM, which represents the high molecular weight (> 1000 Da) fraction [33, 80, 102, 168].

One possible explanation for the differences between C:N:P ratios in UDOM and those reported for bulk DOM above is that the low molecular weight (LMW; <1000 Da) fraction of DOM is extremely depleted in P. Another explanation could be related to the potentially large errors and uncertainties in sub-euphotic zone DOP measurements. DOP concentrations are estimated as the difference between TDP and DIP measurements [98]. Because DOP concentration is typically less than 10% of TDP concentration in the sub-euphotic zone, determining DOP as the difference between two relatively large values (TDP and DIP) can lead to large errors in calculated DOP values and C:P ratios [5, 98]. In addition,

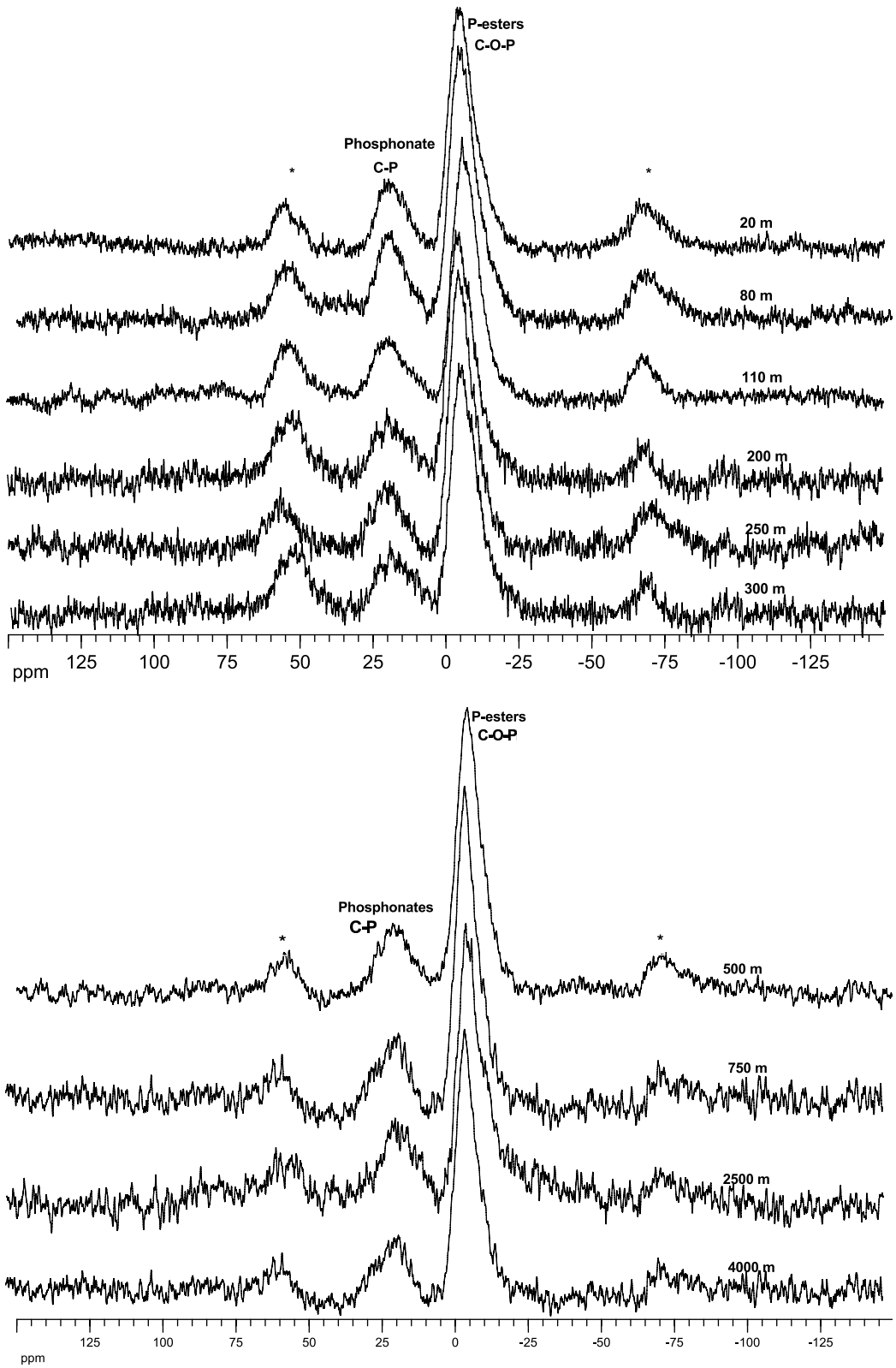

Figure 10: CP-MAS ^{31}P NMR spectra of UDOM from station Aloha stacked according to depth. Asterisks denote spinning sidebands. Also indicated are the major peaks and the functional groups represented by them. NMR operating parameters: contact time 1ms; recycle delay 4s; 8000 transients.

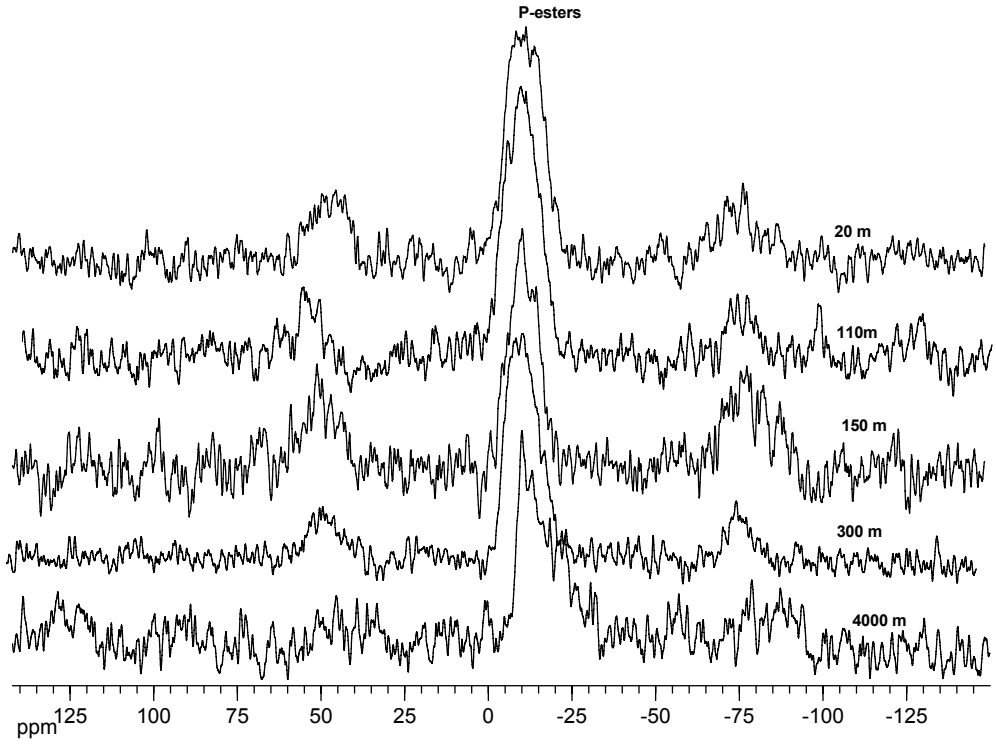

Figure 11: CP-MAS ^{31}P NMR spectra of UPOM from station Aloha. Also indicated are the major peaks and the functional groups represented by them. NMR operating parameters: contact time 1ms; recycle delay 4s; 32000 transients.

some organic P is hydrolyzed during the standard molybdenum blue assay for phosphate, leading to an overestimation of phosphate and DIP concentrations [98]. In contrast, organic P concentrations inf UDOM and UPOM are measured directly and the problems inherent in determining concentrations by difference can be avoided.

DOP measurements and associated C:P ratios in the deep ocean show no consistent pattern which is likely a reflection of measurement errors. Reported deep water DOP concentrations (below 800 m) range from 10 nM in the middle Atlantic Bight [79] to 170nM in the Southern Ocean [112]. The variations in reported values of C:P ratios of DOM are even greater. While, C:P ratios as high as 3100:1, 4400:1 and 4768:1 have been reported from the N-E Atlantic Ocean, middle Atlantic Bight and the north Pacific Ocean, respectively [5, 79,80], such high values were not observed in detailed depth profiles from the eastern North Pacific or Southern Ocean [112]. In contrast to the extremely high C:P values mentioned above, the highest deep water DOM C:P ratio reported by Loh and Bauer [112] was 688 in the Southern Ocean.

The average C:P and N:P values of UPOM were closer to Redfield stoichiometry than UDOM suggesting a planktonic source. Similar results from other locations in the Pacific Ocean, have been reported by [102]. A substantial contribution of terrestrial OM to UPOM at Station Aloha has been inferred from δ^{13}C and lignin measurements [14,75,141]. Depending on the type of vegetation, such as plants with soft tissues vs. woody tissues, terrestrial OM show a wide range of C:P and N:P values. In general, terrestrial plants are relatively poor in P and N with C:P ratios ranging from 300 to 1300 and N:P from 10 to 100 for soft tissues [138]. C:P ratios for woody tissues can be greater than 1300, while their N:P values range from 100 to 1000 [138]. Given the large range in C:P and N:P ratios of terrestrial plants and soil organic matter, it is not clear how the terrestrial component of UPOM is reflected in the observed C:P and N:P values.

4.5.2 P Composition and Cycling of UDOM and UPOM

P esters are the dominant P functional group observed in the solid-state ^{31}P NMR spectra of both UDOM as well as UPOM. Phosphate monoesters are present in biomolecules

such as mononucleotides and sugar phosphates, whereas diesters occur in phospholipids and nucleic acids [131]. The abundance of P esters in natural organic matter is undoubtedly related to the synthesis of these compounds by all living organisms. P-esters are typically the most abundant functional group observed in both marine and terrestrial environments. Phosphonates occur widely among biogenic and anthropogenic compounds in the form of phosphonolipids and as side groups on polysaccharides and glycoproteins. The strong covalent C-P bonds in phosphonates make them resistant to chemical, thermal and photolytic degradation [103, 167]. Though their presence in marine DOP had been proposed earlier [29, 101] phosphonates have only recently been recognized as a significant component of marine UDOM [35, 36, 102]. ^{31}P NMR results from sinking particles and sediments from the Cariaco Basin show up to 23% phosphonates in sediments and up to 18% in sinking particulate material [11]. Solution NMR spectra of sinking particulate material have shown phosphonates to comprise a much smaller percentage of the P (up to 6 %) in sinking POM [131]. ^{31}P NMR analyses of UDOM and UPOM isolated from laboratory cultures of several marine primary producers detected P-esters as the only organic P compound [36]. Phosphonates were also not detected in ^{31}P NMR spectra of bulk plankton tow samples from the coastal Pacific Ocean and Cariaco basin [11, 131]. The sources of phosphonates in the ocean are yet to be ascertained and the dynamics by which they become a major fraction of UDOM is not known. The widespread distribution of phosphonates in UDOM seen here and in other locations in the Pacific and Atlantic Oceans [102] suggests that phosphonates originate from a widely distributed group of marine organisms such as bacteria.

There are clear differences in the ^{31}P NMR spectra (Figures 10 and 11) and C:N:P ratios (Table 6) for UDOM and UPOM from station Aloha. A ^{13}C NMR study of the same materials also revealed clear differences with respect to carbon in the overall composition of UDOM and UPOM [141]. Solid-state ^{13}C NMR spectroscopy indicated, UPOM had a greater abundance of amino acids and lower relative abundance of carbohydrates than UDOM. The differences in UDOM and UPOM composition with respect to both C and P suggest that UDOM does not originate from simple solubilization of UPOM, and the aggregation of UDOM is not the primary source of UPOM.

Depth-related compositional variations are quite distinct for C and P. Both UDOM and UPOM show little compositional variation with respect to organic P with depth (Figures 10 and 11). In contrast, solid-state ^{13}C NMR and molecular level analyses indicate clear compositional variations in organic C with depth [141]. The percentages of carbohydrate-C in UDOM and UPOM decreased with increasing depth, whereas the percentages of lipid-C increased with depth. The percentage of amino acid-C in UDOM remained fairly constant with depth but decreased in UPOM. These depth-related compositional trends were also reflected by the molecular level carbohydrate and amino acid analyses. Decreases in the relative abundance of carbohydrates relative to other compound classes with depth are indicative of selective degradation processes.

The selective decomposition of certain organic carbon compound classes with depth in the ocean may be indirectly related to the abundance of DIP in the deep ocean. In the deep ocean, growth of heterotrophic organisms is likely limited by the availability of suitable carbon substrates rather than nutrients such as P. Hence, there is selective remineralization of certain carbon compounds like carbohydrates, which are presumably better substrates for heterotrophic microorganisms. This idea is supported by isotopic studies of oxygen (δ^{18}O) associated with DIP at station Aloha [37]. Profiles of these oxygen isotopic ratios with depth suggest that DIP remineralization in the deep ocean is incidental to the microbial consumption of OM as an energy and C source, rather than to fulfill cellular DIP requirements.

4.5.3 Association of P with Biomolecules in UDOM and UPOM

In order to explore possible biomolecular associations of P, relationships between the concentrations of C in carbohydrates, lipids and amino acids (estimated from ^{13}C NMR results [141]) and P concentrations in UDOM and UPOM were examined. Results of linear regression analyses for UDOM show a strong positive correlation ($R^2 > 0.80$) between P contents and carbohydrate and amino acid C contents (Figure 12). These results indicate that a large fraction of the P in UDOM is associated with carbohydrates and amino acids. As seen in the ^{31}P NMR results above, P-esters and phosphonates are the two organic P

functional groups present in UDOM. The association of P with carbohydrates is not unexpected given that they constitute a major fraction of the C in UDOM [4, 14, 141], and P-esters can be associated with carbohydrates in a variety of biomolecules such as nucleic acids (DNA and RNA), nucleotides (eg. ATP), and sugar phosphates. The association of P with amino acids may be in the form of a class of biomolecules known as phosphoamino acids.

At station Aloha, P in dissolved nucleic acids (DNA plus RNA) was estimated to account for 10 to 12% of the DOP in the euphotic zone [98]. P is in the form of diesters in DNA and RNA. RNA is more abundant than DNA in organisms and the dissolved as well as particulate fractions at Station Aloha, with RNA to DNA ratios ranging from 3 to 10 in the dissolved fraction [97]. Thus, a fraction of the P in UDOM is likely associated with carbohydrates (ribose and deoxyribose) in RNA and to a lesser extent DNA. Among the other possible P-ester containing biomolecules, ATP has been measured in the water column at Aloha in trace amounts [20]. However, the contributions of the other P bearing carbohydrate biomolecules have not yet been quantified.

Phosphoamino acids are formed by the addition of phosphate groups to amino acids via a P-ester linkage by phosphate donors such as ATP. This modification of amino acids is regulated by the protein kinase group of enzymes and is a ubiquitous regulatory mechanism in prokaryotes as well as eukaryotes [78]. Intracellular phosphorylation of amino acids by protein kinases, to form phosphoproteins provides a mechanism for the cell to switch on or off many processes including cell signaling, growth, metabolic pathways, membrane transport and gene transcription [78]. In bacteria, the amino acids histidine, aspartic acid and glutamic acid, are usually favored for phosphorylation [182]. It is possible that the P associated with amino acids is also linked with carbohydrates via the phosphoenolpyruvate:sugar phosphotransferase system (PTS). This mechanism of phosphoprotein regulation is used for sugar transport, phosphorylation and chemoreception and its presence has been detected in marine bacteria [77]. The coordination and regulation of cellular metabolism are key ecological processes and large portions of the bacterial and archaeal genomes appear to be used for regulation. Therefore it is possible that regulatory compounds such as

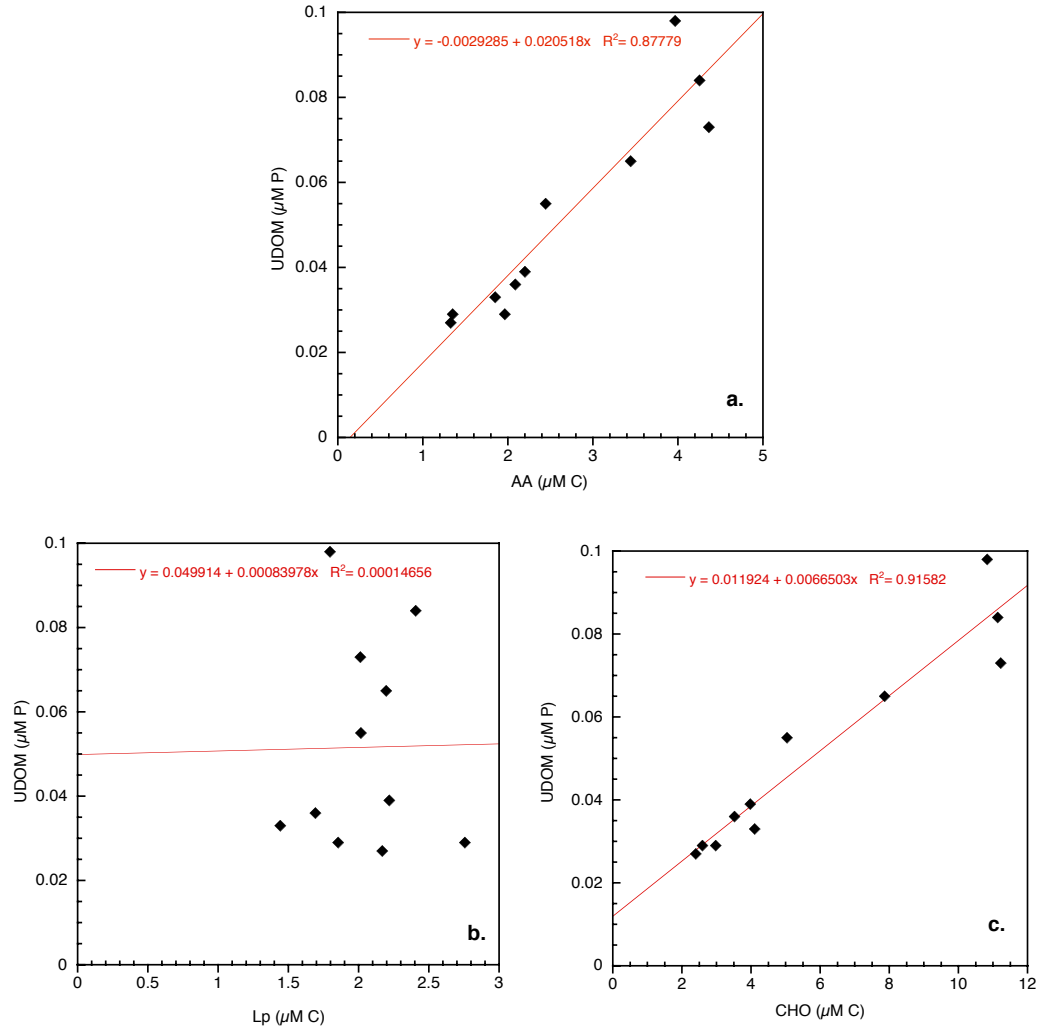

Figure 12: P contents of UDOM (μM) plotted against the concentration of C (μM) present in amino acids (AA); lipids (Lp) and carbohydrates (CHO). Biomolecule contents were obtained from ^{13}C NMR results [141].

phosphoamino acids are constantly produced and used by marine microorganisms and these compounds could, in theory, be selectively retained in the DOM pool following exudation or cell death [98].

Phosphonates, the other P functional group in UDOM can also be associated with carbohydrates and amino acids in the form of phosphonosugars and phosphonoproteins, but little information is available on the composition and abundance of these compounds especially in the marine environment. P concentrations in UDOM do not exhibit a significant correlation with lipid C (Figure 12). The lack of a strong relationship between lipid-C and P in UDOM suggests phospholipids and phosphonolipids are minor components of UDOM. This is somewhat surprising given the presence of phospholipids and lipopolysaccharides in marine DOM [98].

All three biomolecule classes in UPOM show strong relationships ($R^2 > 0.92$) with P concentrations in UPOM (Figure 13). The dataset is smaller for UPOM, because the low C and P contents of certain samples, did not allow NMR spectra to be acquired in a reasonable amount of time. However, the data available are representative of the entire range of sampling depths. The main distinction between UDOM and UPOM in terms of biomolecule versus P correlations is the additional association of P with lipids in UPOM. P associated with lipids can be present in the form of phospholipids, which are widely present in Bacteria and Eukarya and are important structural components of biological membranes [98]. P-esters in UPOM can also be associated with lipopolysaccharides, which contain both aminosugars as well as fatty acids, and are components of the cell wall of Gram negative bacteria [98]. The presence of lipopolysaccharides relates to the correlation observed between P and lipids as well as carbohydrates and amino acids. The strong positive correlation between P and lipid-C concentrations in UPOM corroborates our earlier observation that UDOM and UPOM are compositionally distinct.

4.6 Conclusions

Results from ^{31}P NMR analyses together with atomic C:N:P ratios clearly indicate differences in the bulk chemical composition of UDOM and UPOM. These results also suggest

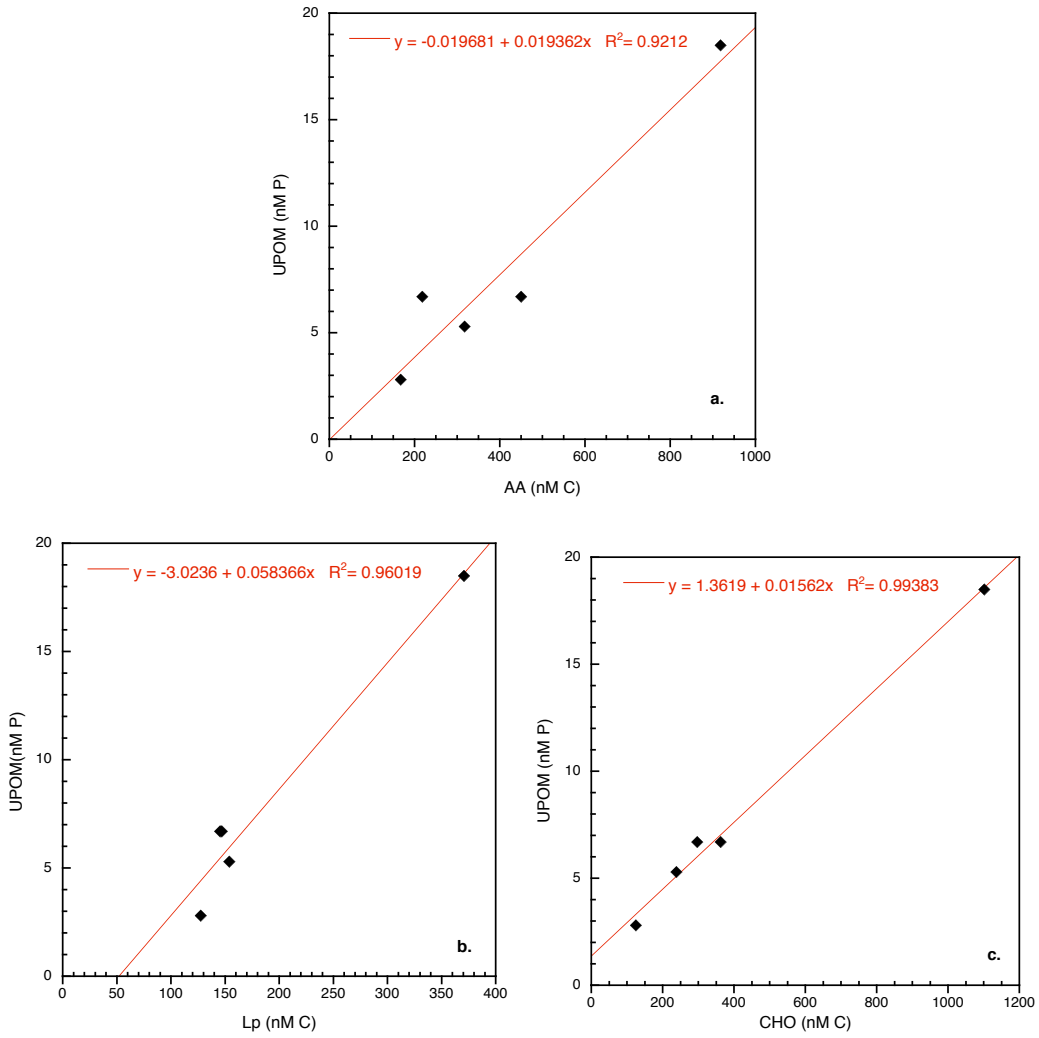

Figure 13: P contents of UPOM (nM) plotted against the concentration of C (nM) present in amino acids (AA); lipids (Lp) and carbohydrates (CHO). Biomolecule contents were obtained from ^{13}C NMR results [141].

that aggregation of UDOM does not result in the production of UDOM and conversely UDOM is not produced simply by the solubilization of UPOM. UDOM is composed of P-esters (75%) and phosphonates (25%), whereas UPOM is composed predominantly of P-esters. Regression analyses indicated a large fraction of the P in UDOM is associated with carbohydrates and amino acids, but not with lipids. Similar analyses for UPOM indicated that P is associated with carbohydrates, amino acids and lipids. P in UDOM and UPOM is likely present as altered biopolymers of RNA, DNA, sugar phosphates and phosphoamino acids. P is also likely present as phospholipids and lipopolysaccharides.

CHAPTER 5

COMPOSITION AND CYCLING OF DISSOLVED AND PARTICULATE ORGANIC MATTER AT THE BERMUDA ATLANTIC TIME-SERIES STUDY (BATS) STATION

5.1 Abstract

Ultrafiltered dissolved and particulate organic matter (UDOM and UPOM) and suspended particulate organic matter (SPOM) collected using pressure filtration were characterized in samples from a depth profile in the Atlantic Ocean. Results from elemental C/N ratios and δ^{13}C ratios reveal differences in the bulk composition and sources of UDOM and suspended POM. Suspended POM collected using two different techniques (ultrafiltration and pressure filtration) were found to have similar isotopic and elemental composition. Results from ^{13}C Nuclear Magnetic Resonance (NMR) spectroscopy on UDOM indicates that carbohydrates are the major biomolecular group present, followed by lipids and amino acids. With increasing depth in the water column, the contribution of carbohydrates to the organic C decreases and that of lipids increases in UDOM. These changes reflect the action of selective degradation processes acting on UDOM during its transit through the water column. Lipids appear to be more resistant to degradation than carbohydrates and amino acids, thus accounting for their increased abundance with depth.

5.2 Introduction

Organic matter in the oceans is a part of a size continuum that includes dissolved and colloidal molecules as well as suspended and sinking particles [107, 153]. Dissolved organic matter (DOM) is the largest reservoir of exchangeable carbon (C) in the ocean, comparable in quantity to atmospheric carbon dioxide. The sinking of particulate matter from surface

to deeper waters is also a major pathway for the transport of carbon and other biologically associated elements. A variety of biological, physical and chemical processes alter the composition of organic matter during its cycling in the ocean. High molecular weight (HMW; > 1000 Da) DOM as isolated using tangential-flow ultrafiltration comprises about one third of the dissolved organic C (DOC) in the ocean [14, 119, 136]. It has been shown that HMW-DOM is more biochemically reactive than the overall DOC pool in the ocean [6] and thus plays an important role in in carbon and nutrient cycling.

DOM is classified as high molecular weight and low molecular weight (LMW) based on passage through an ultrafiltration membrane with a ∼1 nm pore size and 1000 Da molecular weight cutoff. Particulate organic matter (POM) is divided into two size classes based on the collection technique. Sinking POM (∼100 - 1000 μm) is collected with particle traps and suspended POM is collected with in-situ filtration or by ultrafiltration.

Analyses of chromatographically separable fractions of dissolved and particulate organic matter in the oceans have revealed that it consists of analytically identifiable biomolecules such as carbohydrates, lipids and amino acids [12, 72, 76, 108, 177]. However, results of these molecular level analyses typically account for only a small fraction of the C in this material [72]. For example, molecular level carbohydrate and amino acid analyses characterized ∼9% of the C in HMW DOM and ∼28% of the C in suspended POM in the north Pacific Ocean [141]. The results of ^{13}C NMR and molecular level studies infer that the molecularly uncharacterized fraction is similar in composition to the characterized fraction [70, 141]. However, on the basis of stable carbon isotopic ratios (δ^{13}C) of chromatographically separated biomolecule fractions, the molecularly uncharacterized fraction in HMW-DOM, has been found to be similar to the amino acid and carbohydrate fraction [113], while that in sinking particulate organic matter has been reported to resemble lipids [84].

The chromatographically separated fractions of marine organic matter have also been found to have distinct $\delta^{13}C$ signatures and $\Delta^{14}C$ ages [84,113,179]. These differences reflect differences in organic C sources, microbial utilization and decomposition as well as isotopic fractionation during biosynthesis of organic compounds [179].

In this study, DOM and POM isolated using tangential-flow ultrafiltration and suspended POM collected using pressure filtration have been characterized using isotopic and elemental analyses. The δ^{13}C and elemental C/N ratios of DOM have been compared to those from suspended POM collected using two different techniques. DOM has also been characterized using solid-state ^{13}C NMR spectroscopy and results have been modeled to estimate the contributions of carbohydrate, lipids and amino acids to the organic C in this material. The results indicate different bulk chemical and isotopic composition for DOM and suspended POM and selective degradation of reactive biomolecules such as carbohydrates in DOM.

5.3 Materials and Methods

Water samples were collected from various depths (20 to 4300m) at the BATS site in the Atlantic Ocean. The Bermuda Atlantic Time-series Study site (BATS) (31° 40′N, 64°10′W) is located in the oligotrophic waters of the Sargasso Sea, approximately 85 km southeast of Bermuda. The water depth at the sampling site is 4800 m. Further information on the BATS site and annual time series data reports can be accessed at http://www.bbsr.edu/cintoo/bats/bats.html.

Samples were collected during a cruise to BATS in June-July 2001 aboard the R/V Cape Hatteras. Organic matter was isolated from sea water using tangential flow ultrafiltration [14,15]. At each depth, ∼700 L of seawater was collected with four separate casts. From 600 L of this composite, the ultrafiltered POM (UPOM, 0.1- 60 μm) fraction was isolated aboard ship with an Amicon DC10L ultrafiltration system with a polysulfone hollow fiber filter. The filtrate from the DC10L system was fed directly into an Amicon DC30 ultrafiltration system with polysulfone membranes (S10N1; 1000Da cutoff) to isolate the ultrafiltered DOM (UDOM, 1 - 100nm), which is also referred to as high-molecular weight (HMW) DOM. The UDOM and UPOM concentrates were frozen for transportation to the laboratory, where they were dried under vacuum and stored for chemical analyses.

Suspended particulate organic matter of a different size compared to UPOM was collected by pressure filtration using GF/F (Whatman) filters with a nominal cutoff of 0.7

μm. Suspended POM collected using pressure filtration is referred to as SPOM for the rest of this chapter. Approximately 20 L water from the Niskin bottles were transferred directly to pressurized stainless steel cans. The water from the cans was passed through the GF/F filters under pressure. The filters with collected SPOM were wrapped in pre-muffled aluminum foil and stored frozen. The frozen filters were freeze-dried prior to analyses in the laboratory.

C and N contents and stable carbon isotope ratios were measured on dried UDOM, UPOM and freeze dried filter samples. C and N contents were measured after vapor phase acidification using a Carlo Erba CHN analyzer [74]. Stable C isotopes were measured in duplicate with a Finnegan Delta Plus system with in-line combustion and are presented as δ^{13}C (‰) relative to the Pee Dee Belemnite standard.

Solid-state ^{13}C NMR analyses of the UDOM samples were carried out at the NMR center in the School of Chemistry and Biochemistry at the Georgia Institute of Technology. The ^{13}C NMR spectra were acquired on a Bruker DSX 400 spectrometer using Cross Polarization-Magic Angle Spinning (CP-MAS) at a ^{13}C frequency of 100 MHz. About 90 mg of powdered sample was packed into a 4 mm-diameter cylindrical zirconia rotor fitted with a Kel-F cap and spun at 10,000 $\pm$ 10 Hz in a Bruker magic - angle spinning probe. For all samples, an optimized cross polarization sequence was used with a 1.0 ms contact time and a recycle delay of 5 seconds. A total of 10,240 transients were collected for each UDOM sample. The UDOM ^{13}C spectra were processed with 30 Hz exponential line broadening. Data processing and calculation of integrated peak areas were carried out off-line using the Mestre-C software package (www.mestreC.com).

The measured ^{13}C NMR spectral data were entered into a three end-member mixing model to estimate the biochemical composition of the UDOM samples. The model involved "amino acid", "carbohydrate" and "lipid" end-members, which were used to represent the major biochemical types found in marine OM samples. The term 'lipid' here is being used to refer to lipid-like material, which may also comprise other biomolecules rich in aliphatic and carboxylic functionalities. Other biochemicals that are less abundant, and have not been taken in to account in this model, include pigments and nucleic acids [71, 108]. The

modeling procedure was similar to that used by [70, 71] and has been described in more detail in Chapter 3. The three end-members used were calculated from different literature sources to be representative of average amino acid ($C_{106}H_{168}O_{34}N_{28}S$), lipid ($C_{18}H_{36}O_2$), and carbohydrate ($C_6H_{10}O_5$) composition of typical marine organic matter. Average spectral characteristics were calculated for each of the end-members based on literature values for the relative abundances of carbon functional groups in their structures and are presented in Table 8. The choice of these end-member compositions assumes that all the nitrogen (N) resides in amine functional groups of amino acids. Acetylated amino sugars, such as those found in chitin and peptidoglycan [16, 120], also contribute to amide and amine functional groups in marine organic matter. However, as seen in the molecular level data presented in Sannigrahi et al. [141] and Chapter 3 of this dissertation, amino sugars are a very small fraction of the C in these samples and are not expected to have a significant contribution.

5.4 Results

5.4.1 C/N ratios and δ^{13}C of UDOM and POM

The organic C content of UDOM ranged from 10.8 to 23.3 wt. % (average 17.3 ± 3.8; Table 7). The N content varied between 0.71 - 1.52 wt. % (average 1.13 ± 0.2). The organic C content of UPOM ranged from 0.8 to 2.2 wt. % (average 1.48 ± 0.6; Table 7). The N content varied between 0.09 - 0.22 wt. % (average 0.16 ± 0.05). The organic C and N contents of SPOM are reported as μM C and μM N respectively (Table 7). They ranged from 0.75 to 5.69 μM C (average 1.87 ± 1.59) and, 0.07 to 0.66 μM N (average 0.22 ± 0.19). Depth trends were not clearly evident for C or N contents in UDOM and UPOM, but there was an overall decreasing trend for both C and N in case of SPOM. The C/N atom ratios for UDOM ranged from 17.1 to 18.5 (average 17.9 ± 0.45) and those for UPOM varied between 7.8 and 15 (average 10.8 ± 2.5). The C/N ratios for SPOM were lower than UDOM or UPOM and ranged from 7.3 to 11(average 8.7 ± 1.2)

Stable carbon isotopic ratios were also determined for UDOM and UPOM (Table 7). δ^{13}C values for UDOM varied between -20.9 to -21.2‰ (average -21 ± 0.2‰), and remained essentially constant throughout the water column. δ^{13}C values for UPOM ranged from

-23.4 to -26.7 ‰ (average -25.6 ± 1.4‰) and those for SPOM ranged from -24.3 to -27.0 ‰ (average -25.5 ± 0.2‰), with no distinct depth trends.

5.4.2 Results from ^{13}C NMR Spectroscopy

Figure 14 shows a water column profile of UDOM ^{13}C NMR spectra from BATS. THe major C functional groups identified in these spectra are alkyl (0-45 ppm), N-alkyl (45-60 ppm), O-alkyl (60-95 ppm), acetal (95-110 ppm) and carboxyl/ester, amide (160-190 ppm). Small peaks attributed to unsaturated/aromatic C bonded to O or N (145-160) can be seen in the UDOM spectra from below 100 m. Table 8 gives the relative abundance (as % of total peak area) of the C functional groups present in UDOM as calculated from the integrated peak areas. The relative contributions of the different functional groups to the organic C composition of UDOM change with depth in the water column (Table 8). The relative proportions of alkyl and N-alkyl increase with increasing depth in the water column while those of O-alkyl, acetal and carboxyl/ester, amide decrease.

The contributions of carbohydrates, amino acids and lipids to UDOM C was estimated using the modeling approach described in the materials and methods section. The results reflect the major compositional trends observed in the NMR spectra (Table 8). The percentage of carbohydrate C decreased from 42 to 29 % with depth, whereas percentages of lipids C (37 to 50 %) increase and amino acids (21 to 22 %) show almost no variation. Carbohydrates are the dominant biomolecule class in the surface UDOM samples, but the relative abundance of lipids becomes becomes greater than that of carbohydrates below 1000 m.

5.5 Discussion

5.5.1 C/N Ratios and δ^{13}C of UDOM, UPOM and SPOM

The C/N ratios of UDOM did not exhibit much variation throughout the water column, indicating stoichiometric release of C and N during remineralization. These C/N ratios are higher than those for UPOM and SPOM and largely reflect differences in the bulk chemical composition of the different size fractions. These values are within range of those reported in the literature on similar material from this and other geographical locations [14,112,141].

Table 7: C, N contents; elemental C/N ratios and stable C isotope ratios of UDOM and UPOM from BATS

Depth (m)	δ^{13}C(‰)	wt% C	wt% N	Atomic C/N
UDOM				
20	-21.17	23.34	1.52	17.85
100	-21.17	17.73	1.21	17.1
350	-20.93	18.99	1.26	17.64
1363	-20.91	10.79	0.71	17.71
2010	-21.02	16.53	1.04	18.48
3253	-20.83	15.47	0.99	18.16
4302	-20.91	18.07	1.16	18.18
Average	-20.99	17.27	1.13	17.87
Std. Dev.	0.13	3.80	0.25	0.45
UPOM				
20	-23.38	2.14	0.21	11.88
100	-23.75	1.55	0.22	8.21
350	-25.01	1.13	0.17	7.75
500	-26.77	0.81	0.09	10.49
1363	-25.39	2.22	0.19	13.62
2010	-26.97	1.78	0.21	9.82
3253	-26.71	0.81	0.1	9.44
4302	-26.62	1.41	0.11	14.94
Average	-25.58	1.48	0.16	10.77
Std. Dev.	1.43	0.55	0.05	2.54
SPOM				
		μM C	μM N	
20	-24.29	5.69	0.66	8.60
150	-25.42	3.70	0.46	8.10
250	-24.77	1.63	0.19	8.48
350	-25.17	075	0.07	11.09
500	-26.83	1.63	0.22	7.35
900	-26.99	0.95	0.10	9.86
1360	-25.57	1.09	0.12	8.76
2000	-25.63	1.21	0.12	9.80
3301	-25.33	1.27	0.12	7.28
4302	-24.75	0.78	0.10	7.96
Average	-25.48	1.87	0.22	8.73
Std. Dev.	0.86	1.59	0.19	1.20

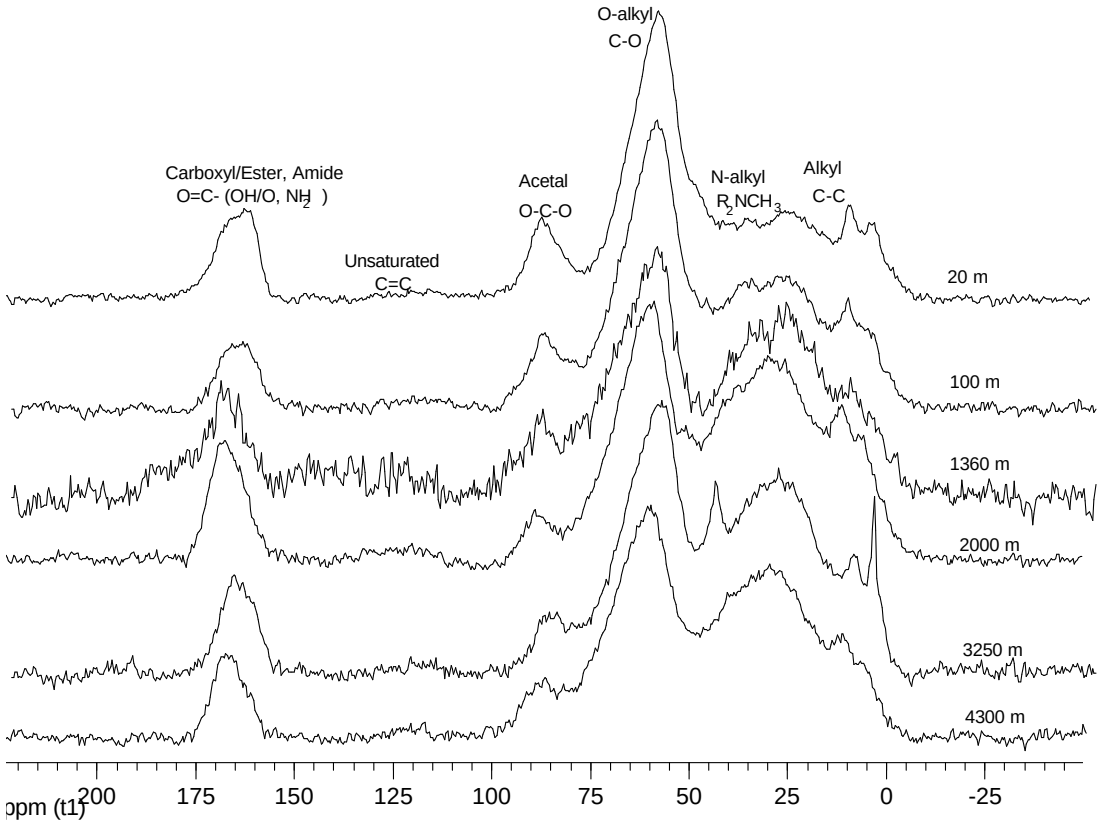

Figure 14: CP-MAS ^{13}C NMR spectra of UDOM from BATS stacked according to depth in the water column. Also indicated are the major peaks and the functional groups represented by them. NMR operating parameters: contact time 1ms; recycle delay 5s; 10240 transients

.

Table 8: Percentage of total NMR peak area measured under each spectral region for UDOM and plankton and calculated for the amino acid, lipid and carbohydrate end-members used in the model

Depth (m)	% Total peak area under each spectral region							% Biomolecules		
	I	II	III	IV	V	VI	VII	%AA	% Lp	%CHO
UDOM										
20	33.1	21.9	25.5	8.0	0.7	0.0	10.9	21	37	42
100	38.3	20.7	25.7	6.5	1.5	0.8	6.5	22	39	39
1360	30.2	11.2	18.7	4.8	2.4	24.2	8.5	21	40	40
2000	49.3	18.7	19.7	2.0	1.0	0.5	8.9	21	50	29
3250	44.8	19.3	24.2	3.6	0.9	0.0	7.2	21	45	34
4300	45.3	17.0	26.0	4.5	0.5	0.0	6.7	21	44	35
Model end-members										
Amino acid	36.3	21	7.4	0	7.8	1.5	2.6			
Lipid	94.4	0	0	0	0	0	5.6			
Carbohydrate	0	0	83.3	16.7	0	0	0			

I (0-45 ppm); II (45-60 ppm); III (60-95 ppm); IV (95-110 ppm); V (110-145 ppm); VI (145-160 ppm); VII (160-190 ppm)

The C/N ratios of SPOM are closest to the Redfield ratio (C/N = 6.63) for marine plankton, whereas UDOM shows the largest deviation from the Redfield ratio.

The results of the δ^{13}C measurements on UDOM are similar to those of [14,75,141] and indicate that UDOM is primarily of marine origin and its δ^{13}C composition is invariant with depth as well as geographic region. The δ^{13}C values of UPOM and SPOM agree well with each other and are all depleted in δ^{13}C relative to UDOM. They are also depleted compared to suspended POM collected on 0.8 μm quartz fiber filters [50], which showed δ^{13}C values of -20.1 to -22.6 ‰ below depths of 100 m in the northeast Pacific Ocean. The differences between the δ^{13}C values between UPOM and suspended POM collected on quartz fiber filters have been previously discussed in detail [14, 75]. One possible reason for the observed discrepancy in δ^{13}C values between UPOM and POM collected on quartz filters is that the difference is due to small sub-micron particles that pass through 0.8 μm filters but are retained by 0.1μm filters [14]. The 0.1- 0.7 μm fraction could account for as much as 40 to 50% of suspended POC [2, 14]. Aerosol particles (having C in the 0.1 to 0.7 μm size range) over the Pacific and Atlantic Oceans have δ^{13}C values ranging from -26.5 to -26.7‰ and a terrestrial source [31]. Our results however, indicate almost identical δ^{13}C values for UPOM and SPOM. Thus, differences in δ^{13} C values of POM between different studies could simply reflect differences in particle sizes sampled, When using glass and quartz fiber filters, particle retention is dependent upon sample loading. When a filter starts to get loaded, its cutoff usually decreases in size. It is likely that the SPOM fraction collected using pressure filtration in this study contained some of the smaller (0.1- 0.7 μm) size fraction depleted in ^{13}C.

5.5.2 Biomolecular Composition of UDOM

The results from ^{13}C NMR spectroscopy of UDOM from BATS are similar to earlier studies from this and other regions [15, 118, 141]. Carbohydrates are the the common biomolecule groups containing O-alkyl and acetal groups. A decrease in the sum of their integrated peak areas (Table 8) is reflected by the decreasing carbohydrate content seen in the modeling

results. Earlier studies [3, 15] also reported combined carbohydrates as the major biopolymers in HMW-DOM. The large decrease in the fraction of combined carbohydrates between surface and deeper waters indicate that these polymers are highly reactive. These results agree with those of molecular-level carbohydrate studies [4, 119, 130, 154]. The increasing fraction of alkyl functional groups with depth in the UDOM ^{13}C NMR spectra (Table 8) is primarily due to a relative increase in the fraction of lipids. An increase in lipids as a percentage of C in UDOM, with depth has also been reported by Aluwihare et al. [4]. The larger lipid fraction obtained in the NMR modeling results from BATS as compared to those from Station Aloha, suggests that it includes other carboxylic acid-rich aliphatic material, which is similar in composition to lipids.

In a recent study, Loh et al. [113] found that the carbohydrate and amino acid fractions extracted using chromatographic separations had relatively younger Δ^{14}C ages compared to the lipid fraction in HMW-DOM from the same region as BATS. The solvent extracted lipid fraction was on average 13 -14 kyr older than the carbohydrate and amino acid fraction. The increase in lipid contents and decrease in carbohydrate contents with depth observed in UDOM from BATS are consistent with older ages of the lipids. This biomolecular group appears to be more resistant to remineralization, hence persisting longer in the water column. The three fractions also have distinct δ^{13}C ratios, with the lipid fraction being significantly depleted in ^{13}C compared to the other two [84, 113, 179].

5.5.3 Comparison to Results from Station Aloha

BATS and Station Aloha are both located in oligotrophic oceanic regions. The primary difference between these two open-ocean sites is that while the waters at Station Aloha are stratified throughout the year, those at BATS are only seasonally stratified [28]. The water column at BATS undergoes an annual cycle, which is characterized by a period of deep mixing in the winter and highly stratified conditions from late spring through fall [28]. As a result, the phytoplankton community structure also varies seasonally at BATS [28] and different species dominate at the two sites. The abundances of *Prochlorococcus* and *Synechococcus* exhibit an oscillating pattern at BATS, with one being high while the other

is low [54]. On the other hand, *Proclorococcus* dominates year-round at Aloha [26]. UDOM and UPOM from BATS have similar δ^{13}C values as those from Station Aloha [141]. Both OM size fractions have slightly higher C/N ratios in the Atlantic Ocean. However, the most prominent difference in OM composition between these two oligotrophic sites is seen in the biochemical compositions derived from modeling of the ^{13}C NMR spectra of UDOM. The UDOM samples from Station Aloha have higher carbohydrate contents compared to those from BATS (Tables 3 and 8). The relative proportion of amino acids is also slightly lower in case of UDOM from BATS. However, these samples have a higher lipid content compared to those from Station Aloha. These compositional differences are especially pronounced in the surface UDOM samples. Thus, UDOM at BATS appears to be relatively depleted in the reactive biomolecules classes such as carbohydrates and amino acids and enriched in the less reactive lipids. This may be due to rapid degradation of UDOM somehow triggered by the winter time deep-mixing of the water column at BATS. The lower reactive biomolecule contents may also be attributed to older, more degraded UDOM being brought to the surface by this seasonal mixing. Differences in the phytoplankton community structure may also contribute to the observed compositional differences between the two sites.

5.6 Conclusions

Results from elemental C/N ratios and δ^{13}C ratios reveal differences in the bulk composition and sources of UDOM and suspended POM. Suspended POM collected using two different techniques (ultrafiltration and pressure filtration) were found to have similar isotopic and elemental composition. Modeling of ^{13}C NMR spectral peak areas indicates carbohydrates are the major biomolecular group present, followed by lipids and amino acids. With increasing depth in the water column, the contribution of carbohydrates to the organic C decreases and that of lipids increases in UDOM. These changes reflect the action of selective degradation processes acting on UDOM. Lipids appear to be more resistant to degradation than carbohydrates and amino acids, thus accounting for their increased abundance with depth.

CHAPTER 6

POLYPHOSPHATES AS A SOURCE OF ENHANCED P FLUXES IN MARINE SEDIMENTS OVERLAIN BY ANOXIC WATERS: EVIDENCE FROM ^{31}P NMR

6.1 Abstract

Sedimentary phosphorus (P) composition was investigated in Effingham Inlet, a fjord located on the west coast of Vancouver Island in Barkley Sound. Solid-state ^{31}P nuclear magnetic resonance (NMR) spectroscopy was applied to demineralized sediment samples from sites overlain by oxic and anoxic bottom waters. The two sites were similar in terms of key diagenetic parameters including mass accumulation rate, integrated sulfate reduction rate and bulk sediment organic carbon content. In contrast, P benthic fluxes were much higher at the anoxic site. ^{31}P NMR results show that P-esters and phosphonates are the major organic P species present at the surface and at depth in sediments at both sites. Polyphosphates were only found in the surface sediment of the site overlain by oxic waters. Varying stability of polyphosphates in microorganisms under different redox conditions may in part explain their distribution as well as differences in P flux between the two sites.

6.2 Introduction

Phosphorus (P) is an essential and in many cases limiting nutrient sustaining marine primary productivity. Burial of P compounds resistant to remineralization during diagenesis is a significant sink in the global marine P budget [57, 58, 63, 87, 137, 163]. The global biogeochemical cycle of P may be affected by shifts in the extent of oxic/anoxic regions within ocean models [109, 110, 173, 174, 178]. Release and benthic flux of P from sediments relative to carbon (C) and nitrogen (N) remineralization may change significantly as a function of

Sannigrahi, P and Ingall, E.D. Geochemical Transactions 6(2005) 52-59

bottom-water oxygen availability. Evidence from direct measurement of benthic fluxes or fluxes calculated from pore water profiles suggests that the presence of anoxic bottom waters enhances the release of P (as compared to N and C) from organic matter [38, 85, 122]. Preferential regeneration of P from sediments overlain by anoxic bottom waters has also been suggested from studies of solid phase P distribution [86,88,123,124,133,155]. However, this hypothesis remains controversial, as other studies propose that the net effect of anoxia on P release is not as significant [8,11,49,58,137]. This controversy may be resolved in part with a better understanding of redox sensitive mechanisms involved in P cycling.

The sensitivity of P flux and burial in sediments to bottom water oxygen levels has commonly been explained by cycling of P associated with reducible ferric oxyhydroxide phases [23, 63, 122, 163]. Reduction of ferric oxyhydroxide phases in sediments in response to decreasing redox potential results in the release of dissolved ferrous iron and P to sediment pore waters and ultimately to overlying waters. However, it is also possible that a large fraction of the P released in response to decreasing redox potential originates directly from benthic microorganisms rather than ferric hydroxides [44]. The storage and release of P (in the form of intracellular polyphosphate granules) by certain bacteria and protozoan genera has been suggested as an explanation [44, 65, 82, 86, 162], but direct evidence for this process in marine sediments has been limited [150]. In addition to redox sensitive P cycling mechanisms, very little is known about organic P speciation as a function of redox conditions [11, 27].

In this study, we present results from solid-state ^{31}P NMR spectroscopic characterization of organic matter in demineralized sediments from sites overlain by anoxic and oxic waters in the Effingham inlet, British Columbia (Figure 15). The sites in Effingham Inlet are separated by only 1km and were similar in terms of key diagenetic parameters including mass accumulation rate and bulk sediment organic carbon content [88] (Figure 16). The similarities in these key parameters allow a focus on diagenetic effects attributable to depositional oxygen availability. These diagenetic effects include differences in P benthic flux, total and organic P concentration and elemental C: P ratio of the sediments (Figure 16; [88]). NMR data as well as simple calculations suggest that storage and release of biogenic inorganic

P in the form of polyphosphate by certain microorganisms under oscillating oxic anoxic conditions can account for some of the differences in P fluxes and sediment characteristics between the two sites.

6.3 Materials and Methods

6.3.1 Study Site

Effingham Inlet is a fjord on the southwestern coast of Vancouver Island, British Columbia, which opens in to the Imperial Eagle Channel in eastern Barkley Sound. It is approximately 17 km long and 1 km in width along its entire length. Depth profiles for Effingham Inlet indicate the presence of two sills. The outer basin, which reaches a depth of approximately 210 m, is located behind the outer sill, which is at 70 m water depth (Figure 15). The inner sill is located at approximately 149°03′N and 40 m water depth. The inner basin, which reaches a depth of about 120 m, is located behind this sill. The shallow sills, low wind mixing rates and cool dense saline waters of the deep portions of the inner and outer basins collectively inhibit ventilation of basin subsurface waters. The reduced subsurface water replacement rates probably lead to long deep-water residence times, which are consistent with measurements of water column anoxia in the inner and outer basins [88].

Sediments from two sites at approximately 120 m water depth in the Effingham Inlet were collected during a cruise aboard the R/V Barnes during May and June of 1997 (Figure 15). Site 1 is located in the deepest part of the inner basin. The sediments at this site were black, fine-grained microlaminated muds. The black coloration of sediments record anomalous enrichments in acid-volatile sulfide [83]. The oxygen concentration in the water column at site 1 decreases to 0 at a depth of 65 m (Figure 17). Sediment characteristics such as laminations coupled with measured accumulation rates (using the ^{210}Pb and ^{137}Cs techniques) suggest that bottom waters at this site have remained anoxic for at least the last 60 years [88]. Site 2 is located at the southern edge of the outer basin. The Site 2 water column was also characterized by decreasing oxygen concentrations with depth (Figure 17). However in contrast to Site 1, bottom waters at Site 2 remained oxic with oxygen concentrations of approximately 8 μM at the sediment-water interface (Figure 17). Cores

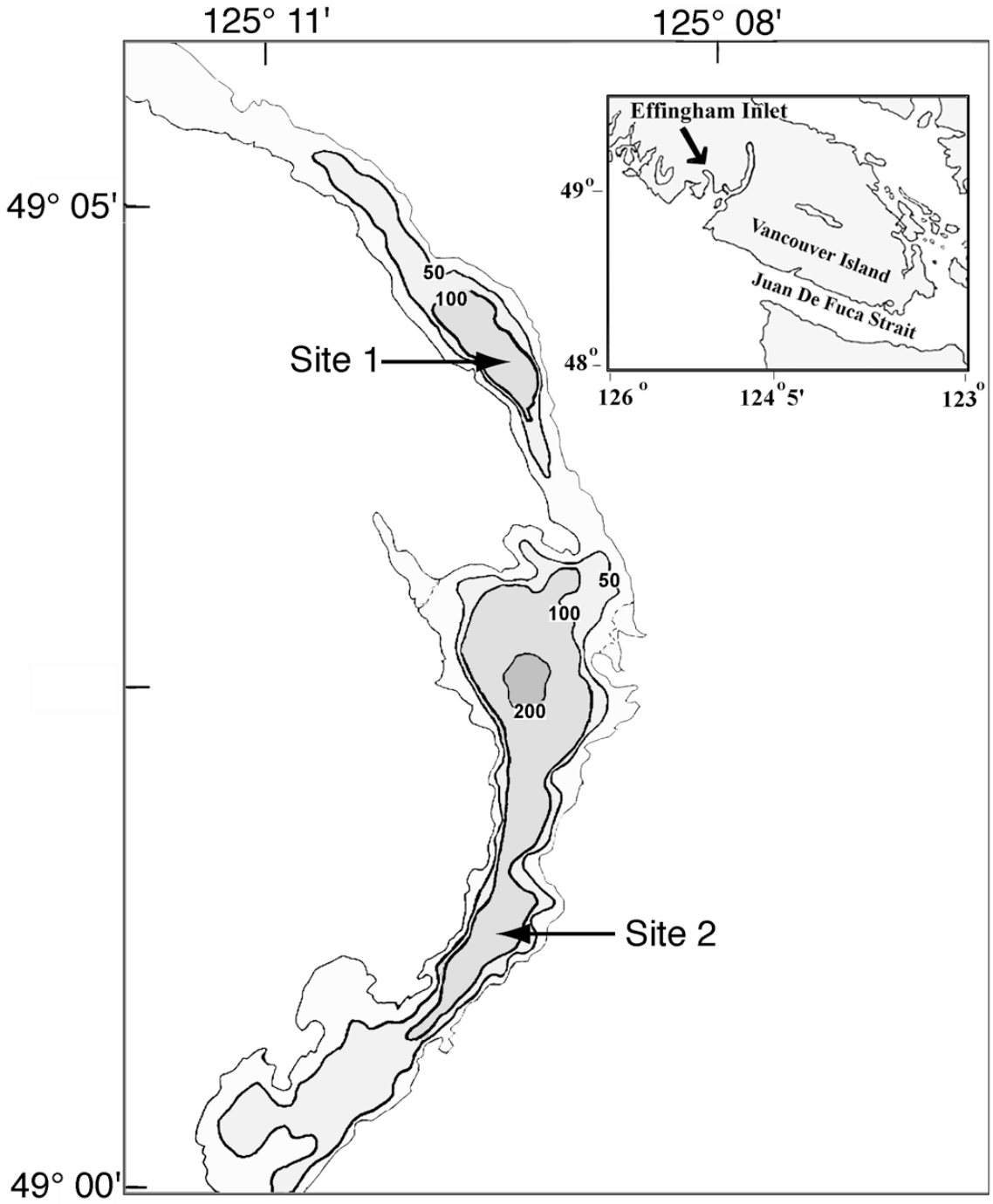

Figure 15: Map of Effingham Inlet displaying sampling sites 1 and 2. The water column at sampling Site 1 (called the anoxic site in the text) is anoxic below of a depth of 65 m. Waters at Site 2 (referred to as the oxic site in the text) contain oxygen at the sediment-water interface. Inset map shows the relation of Effingham Inlet to Barkley Sound on the west coast of Vancouver Island.

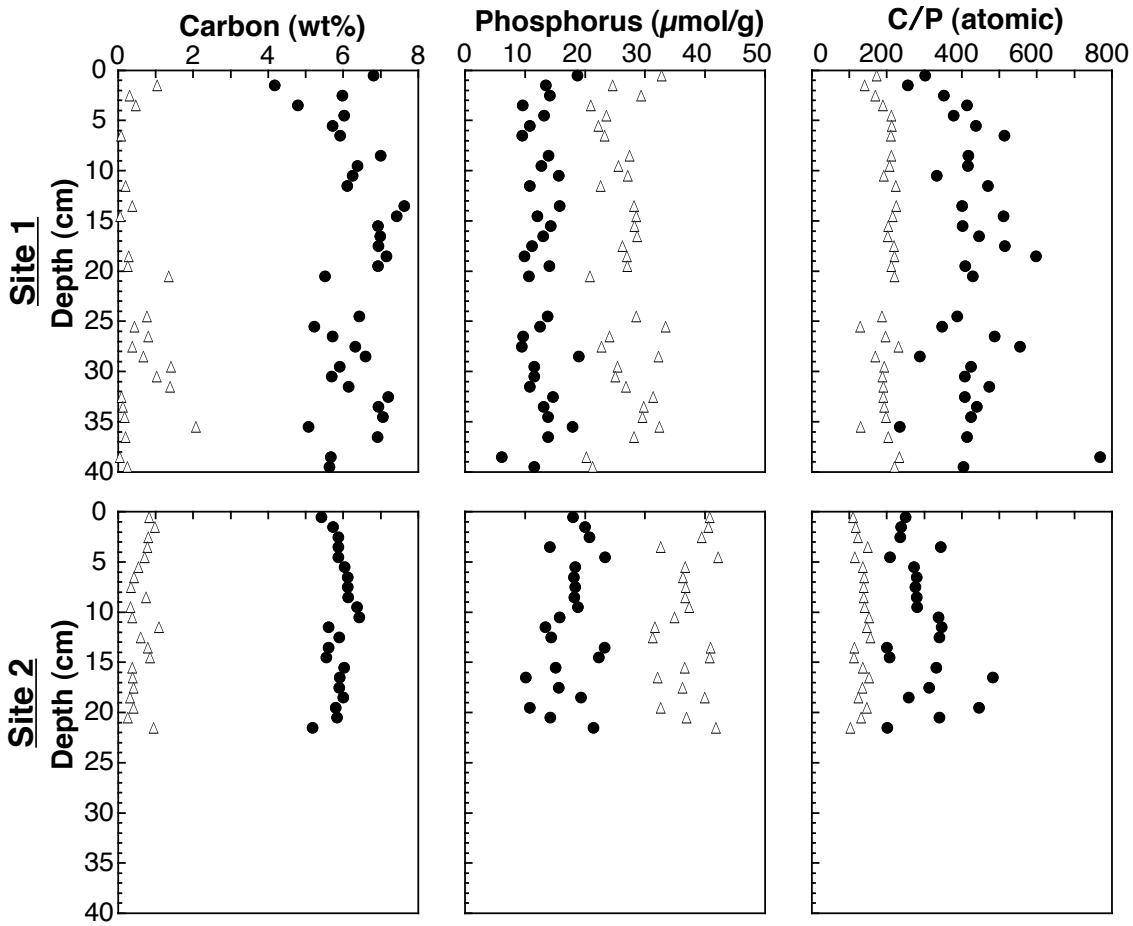

Figure 16: Sediment solid phase inorganic carbon (triangles), organic carbon (circles); organic phosphorus (circles), total phosphorus (triangles); organic C/total P (triangles) and organic C/organic P (circles) atomic ratio distributions for sites 1 and 2 in Effingham Inlet. Data presented are from natural sediments and are taken from [88]

taken at Site 2 consist of homogenized, grey-brown, fine-grained muds. Consistent with the presence of bottom water oxygen, small infauna and mm-scale burrows were observed in Site 2 cores, and these cores had no visible evidence of lamination. Additional description of sediments from both sites can be found in Hurtgen et al. [83] and Ingall et al. [88]. Site1 is referred to as the anoxic site and Site 2 as the oxic site hereafter in the text.

6.3.2 Sample Collection and Processing Procedures

All sediment cores were collected using a gravity corer and sliced at 1 cm intervals under a N2 atmosphere at $\sim$ 8 °C, the ambient bottom-water temperature. These samples were placed in plastic dishes and frozen for later analyses. Prior to chemical analyses, sediment samples were freeze-dried and then ground using an agate mortar and pestle. Samples from 2 depths from each site, one from the surface and one deeper in the sediment column, were chosen to evaluate the effect of diagenesis on P speciation. The samples taken at depth at each site had organic C and P concentrations close to the average values for each core (Figure 16).

Low organic C concentrations coupled with potentially high concentrations of paramagnetic metals in soils and sediments often lead to poor quality NMR spectra [66]. In order to obtain NMR spectra using reasonable amounts of spectrometer time, a demineralization procedure developed by Gelinas et al. [66] was adopted to remove paramagnetic metals and mineral phases (carbonates and silicates) and concentrate the organic fraction. Between 0.7 to 0.9 g of dried sediment was weighed directly into 50 ml polystyrene centrifuge tubes with screw caps. In order to dissolve salt, carbonate and sesquioxide coatings, 30 ml of 1N HCl were added, and the samples were agitated for 1 h at room temperature. Residues were recovered by centrifugation and rinsed three times with a total of 20ml of deionized water. The sediment fraction remaining after HCl treatment was treated with a 1 N HCl and 10 % (v/v) HF solution to dissolve the silicates. A 20 ml aliquot of the HCl/HF solution was added to the sediment, and the mixture was shaken for 12 h at room temperature. The supernatant was removed by centrifugation, and the same treatment was repeated a second time. After removing the second supernatant, the residue was washed

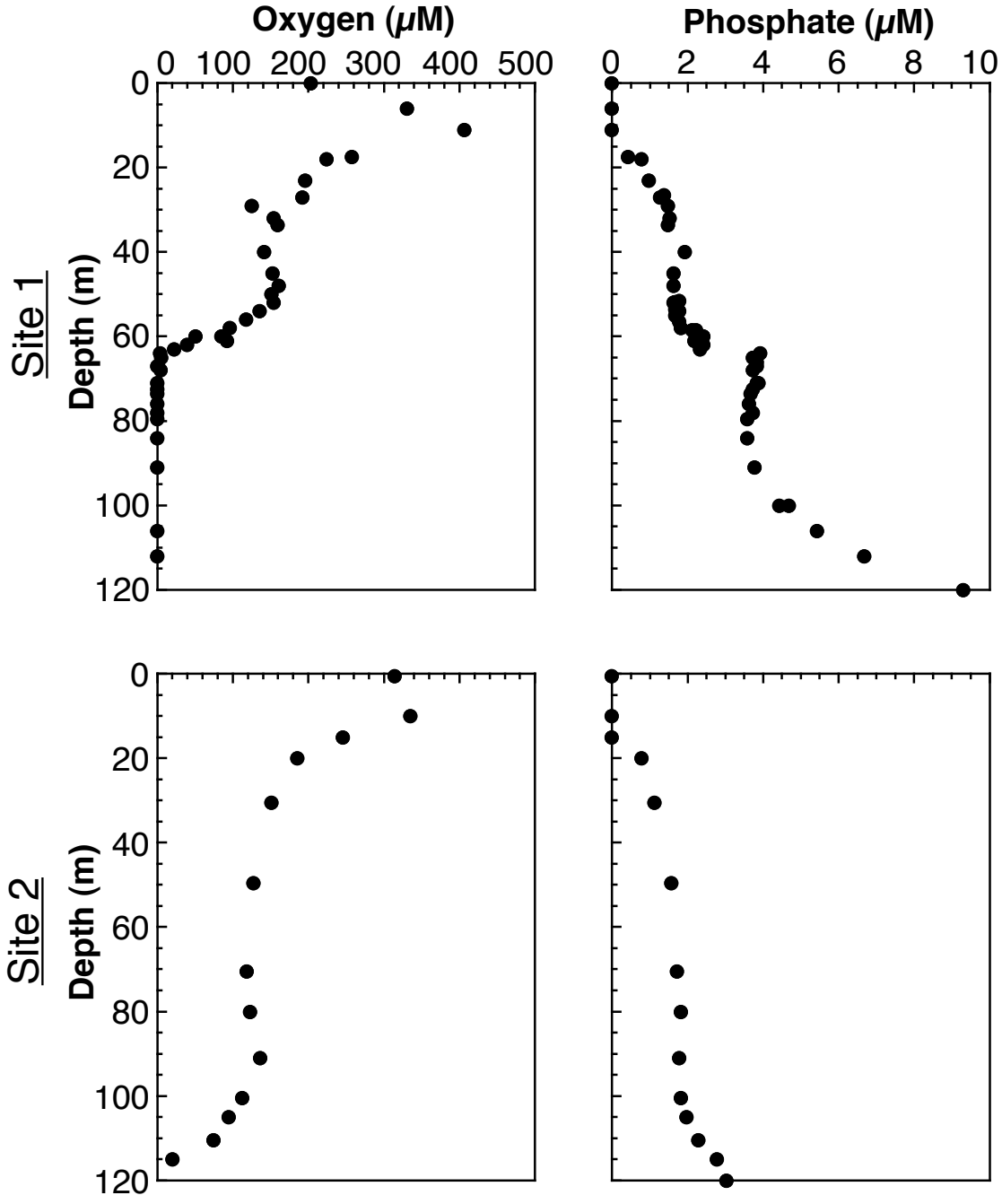

Figure 17: Water column distributions of dissolved oxygen, and phosphate for sites 1 and 2 in Effingham Inlet. Data presented are from Ingall et al. [88].

three times with a total of 10 ml of deionized water. The sediment fraction remaining after the treatment was freeze-dried and ground with an agate mortar and pestle. Given the high organic carbon content of the Effingham sediments (ca. 6 weight percent), the protocols for samples with high organic carbon contents (greater than 1%) specified by Gelinas et al. [66], where the supernatants from the HCl and HCl/HF treatments are not recombined with the final organic fraction, were followed. The organic C, N and P contents of the demineralized sediments were measured [9, 74]. The results indicate that the molecular composition of the organic fraction, as represented by the organic C/N atomic ratios, is not appreciably altered during the demineralization procedure. The organic C/N atomic ratios of the demineralized samples were only 1-5 % higher than the natural sediments. These results agree with those of Gelinas et al. [66]. However, the organic P contents and organic C/P atomic ratios show that there is a preferential loss of organic P from these samples following demineralization. The organic C/P atomic ratios of the demineralized sediments are 20-45% higher than the unprocessed samples. Thus, it appears that despite the relatively high organic C contents of these sediments, the supernatants from the HCl and HCl/HF treatments should be combined with the final organic fraction for future studies. Although P is lost relative to C during demineralization, this procedure is very unlikely to create or hydrolyze polyphosphates and phosphonates, which are resistant to acid hydrolysis [25, 157, 168]. These compound classes are usually extracted using alkaline treatments [25, 168] or high-temperature acid treatments [43]. However, it is likely that the labile P compounds such as P-esters [98] are preferentially remineralized and more resistant compounds such as polyphosphates and phosphonates may be concentrated relative to them in the demineralized samples.

Solid-state ^{31}P NMR analyses of the sediment samples were carried out at the NMR center in the School of Chemistry and Biochemistry at the Georgia Institute of Technology. The ^{31}P NMR spectra were acquired on a Bruker DSX 400 spectrometer using Cross Polarization-Magic Angle Spinning (CP-MAS) at a ^{31}P frequency of 161 MHz. Approximately 90 mg of powdered sample was packed into a 4 mm-diameter cylindrical zirconia rotor fitted with a Kel-F cap and spun at 10,000 10 Hz in a Bruker magic - angle spinning

probe. The presence of spinning sidebands is an artifact of MAS, but at fast enough spinning rates such as the one used here, they do not interfere with the peak resonances. For all samples, a cross polarization sequence, optimized to obtain semi-quantitative data, was used with a 1.0 msec contact time and a pulse delay of 4 seconds. In order to obtain semi-quantitative data using CP-MAS techniques, the time delay between two consecutive NMR pulses (referred to as the pulse delay), used should be much greater than the spin-lattice relaxation times ($T_{1\rho}$H's) of all the different functional groups present [180]. In complex material such as natural organic matter, where a range of $T_{1\rho}$H's are present, NMR optimization experiments have to be performed to determine an optimal value of pulse delay that satisfies the above condition. The presence of paramagnetic material in natural samples usually helps lower the relaxation times and thus more scans can be acquired in a given amount of time. In a series of experiments performed on marine dissolved organic matter samples, Clark [34] found that varying the pulse delay from 1 second to 20 seconds did not appear to alter the relative peak areas of the P-ester and phosphonate peaks, suggesting that 4 seconds was a sufficient pulse delay for these peaks to relax in the sample matrix. A contact time of 1msec, commonly used for natural organic matter samples, was found to be optimal in this case as well. A total of 32,000 transients were collected for each sample and the spectra were processed with 100 Hz line broadening. Data processing and calculation of integrated peak areas were carried out off-line using the Mestre-C software package (Mestrelab Research, Santiago de Compostela, Spain). The peaks present in the solid-state ^{31}P NMR spectra were accepted for further analyses only if their signal to noise ratios (as determined using the Mestre-C software) were greater than 4. Identification of functional groups by ^{31}P NMR is based on their chemical shift relative to an external phosphoric acid standard. Chemical shift values are used to represent differences in resonance frequency of different P compound classes. These values are dimensionless and are expressed in parts per million (ppm) relative to the phosphoric acid standard set at 0 ppm. Figure 3 illustrates the chemical structures and ^{31}P NMR chemical shift ranges of common P functional groups in both natural and standard materials as compiled from the literature [82, 127, 131, 171].

Using the Mestre-C software package, peak areas between selected ppm ranges corresponding to different P functional groups (Figure 3) can be integrated. The software returns absolute peak areas relative to a reference peak (whose area is set as 1). Percentage peak areas of individual peaks are then calculated by dividing their areas by the total spectral peak area of the sample. Using the Mestre-C software rather than manual integration, ensures that the spectral limits are chosen precisely for all spectra. The errors associated with solid-state ^{13}C CP-MAS NMR measurements and peak area determinations are on the order of 10% [71, 141]. Given that NMR parameters such as contact time and recycle delay were optimized using a similar procedure to the ^{13}C measurements, and the analyses were carried out on the same instrument, it is expected that errors in ^{31}P will be of similar magnitude.

6.4 Results and Discussion

6.4.1 ^{31}P NMR Results

Solid-state ^{31}P NMR spectra of demineralized sediment samples from Effingham inlet are presented in Figures 18 and 19. The most prominent feature observed in all the spectra is the peak centered at around -3 ppm. Peaks in the chemical shift range (10 to -10 ppm) are primarily attributed to P esters. Resonances on the right (up-field) side of this central peak are attributed to P diesters, pyrophosphates and end-groups of polyphosphates (Figure 3). Peak area integrations (Table 9) indicate that P esters comprise the major percentage of P in the demineralized sediments. Phosphate monoesters are present in biomolecules such as mononucleotides, sugar phosphates and inositol phosphate, whereas diesters occur in phospholipids and nucleic acids [131]. The abundance of P esters in natural organic matter is undoubtedly related to the synthesis of these compounds by all living organisms and they are typically the most abundant compound class seen in studies from both marine and terrestrial environments [25, 89, 171].

Comparison of the prominent P-ester peak for the sediments from the oxic and anoxic sites indicates that it is broader in the up-field region of the spectrum for the oxic sediments. Small peaks on the right shoulder of the central peak can also be seen in the spectra of the

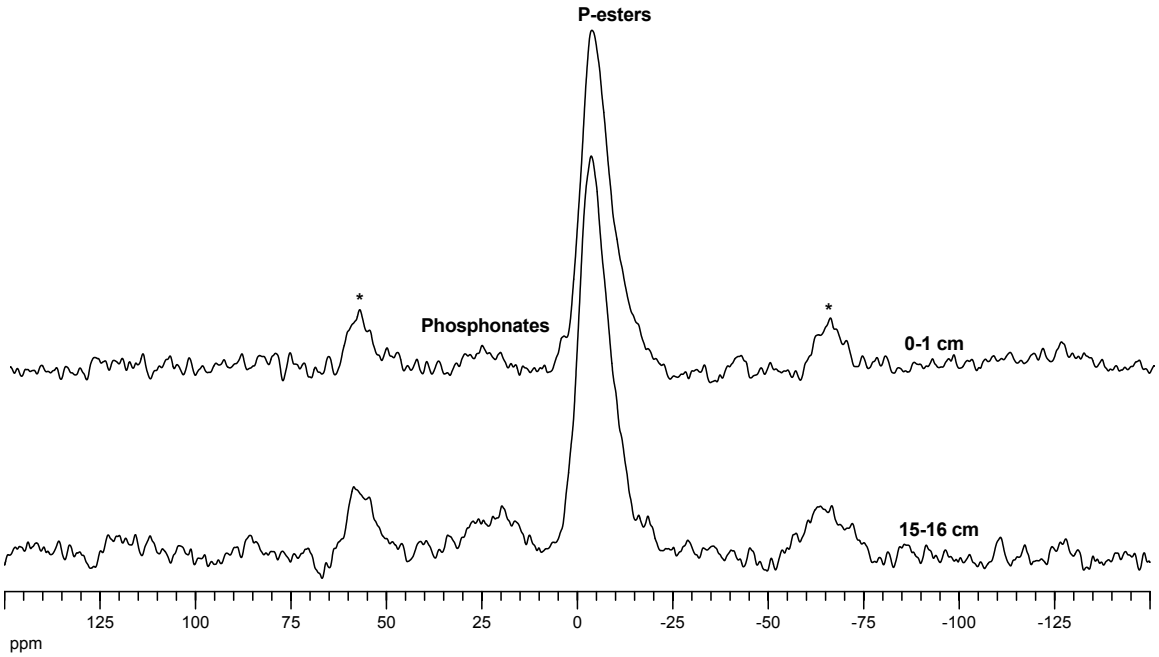

Figure 18: Solid-state CP-MAS ^{31}P NMR spectra of demineralized sediments from Site 1 stacked according to depth. Asterisks denote spinning sidebands. NMR operating parameters: Contact time 1ms; recycle delay 4s; 32,780 transients

Table 9: Relative percentages of total ^{31}P NMR peak area represented by different P functional groups in samples from different depths in sites 1 and 2.

Site 1	**P-esters**	**Phosphonate**	**Polyphosphate**
0-1 cm	94	6	0
15-16 cm	86.6	13.4	0
Site 2			
1-2 cm	82	10	8
13-14 cm	85	15	0

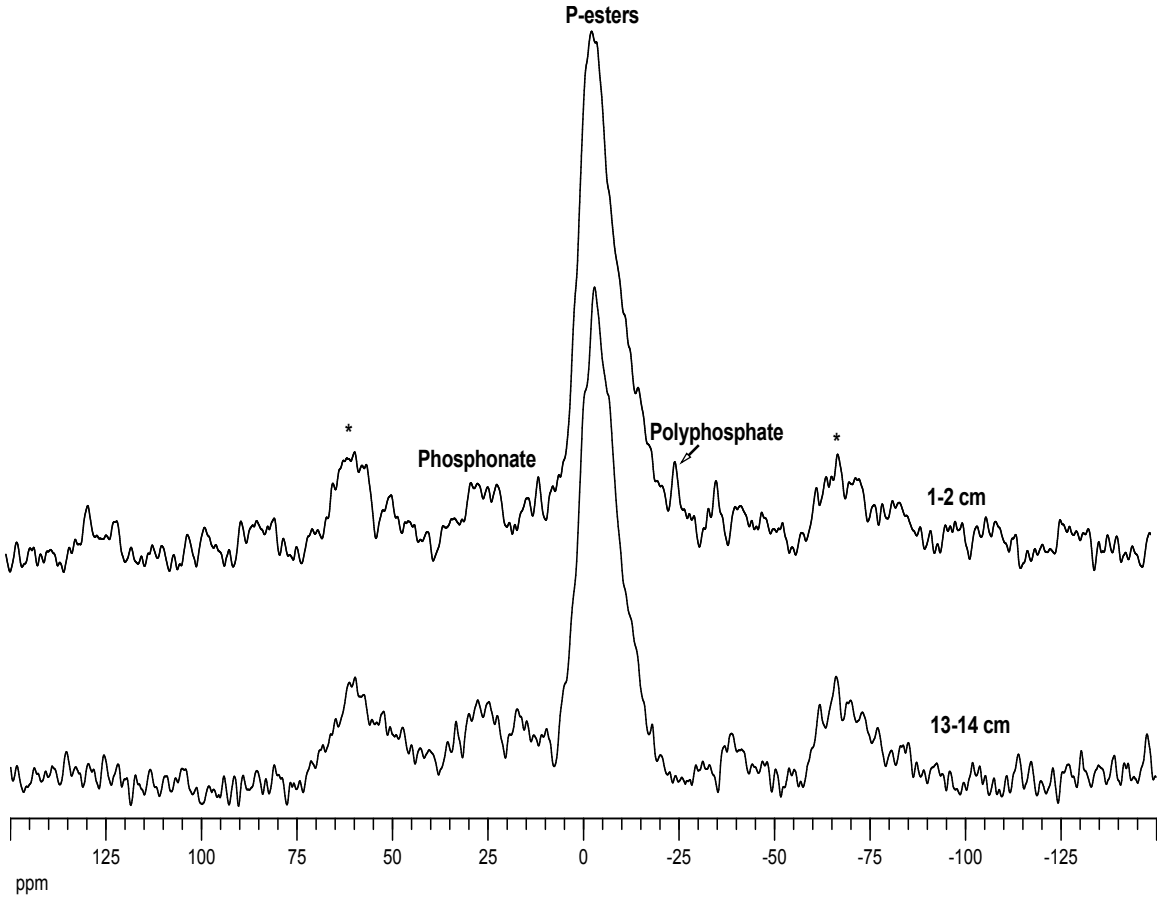

Figure 19: Solid-state CP-MAS ^{31}P NMR spectra of demineralized sediments from Site 2 stacked according to depth. Asterisks denote spinning sidebands. NMR operating parameters: Contact time 1ms; recycle delay 4s; 32,780 transients

oxic site sediments. The asymmetric shape of the P-ester peak and the presence of these smaller peaks suggest that phosphate diesters, pyrophosphates and polyphosphates (end groups) may be more abundant in sediments from the oxic site. Pyrophosphates have been observed in zooplankton and phytoplankton samples [17]. Small pyrophosphate peaks have also been seen in ^{31}P NMR spectra of marine sinking particulate material [131, 161]. In a comparative study of sediments from oxic and anoxic sites in the Baltic Sea by Carman et al. [27], pyrophosphates were only present in sediments from oxic sites. The results of Carman et al. [27] and this study are consistent and suggest that presence of pyrophosphates may be sensitive to redox conditions.

Phosphonates, a group of compounds containing a direct C-P bond, are also present in the Effingham Inlet sediments as revealed by the peak at approximately 25 ppm in all spectra (Figures 18 and 19). The strong covalent C-P bonds in phosphonates make them resistant to chemical, thermal and photolytic degradation [103, 167]. They occur widely among biogenic and anthropogenic compounds in the form of phosphonolipids and as side groups on polysaccharides and glycoproteins. Phosphonates comprise 6 - 15 % of the P in the sediments from both sites in the Effingham Inlet (Table 9).

In both sites in the Effingham Inlet, the percentage of phosphonates shows a small increase with depth suggesting no preferential removal relative to P-esters (Table 9). This is in contrast to the results of Benitez-Nelson et al. [11] who reported a decrease in the proportion of phosphonates relative to P-esters in sinking particles as these particles sedimented from the oxic to anoxic portions of the Cariaco Basin water column. Carman et al. [27] also observed a small phosphonate signal (4% of P) in sediments from an oxic site in the Baltic Sea, but none from the anoxic site. Experiments studying the uptake of dissolved P suggest that P-esters should be more bioavailable than phosphonates [98]. In marine waters, P-esters can be utilized by algae as well as bacteria, but only bacteria have demonstrated the capability of cleaving C-P bonds. The most common enzymatic pathway of bacterial phosphonate degradation involves the enzyme C-P lyase that catalyzes the direct cleavage of the C-P bond to produce the corresponding alkane and phosphate. Only special strains, rather than certain groups of prokaryotic microorganisms, are able to cleave

the C-P bond [103]. The ability to degrade phosphonates by the C-P lyase mechanism is more prevalent among Gram-negative bacteria than Gram-positive bacteria [103]. Thus, the conflicting observations over the stability of phosphonates under anaerobic conditions may be a reflection of differences in the microorganisms present at different locations.

The solid-state ^{31}P NMR spectrum from the surface sediments at the oxic site in Effingham Inlet shows the presence of inorganic phosphates in the form of a distinct polyphosphate peak signal at -25 ppm (Figure 19). This peak is not observed in any of the other spectra (Figures 18 and 19) and is attributed to polyphosphate middle groups [82]. The end groups of polyphosphate chains occur at around the same region in the NMR spectra as pyrophosphates ($\sim$ -10 ppm) and cannot be resolved from the latter using solid-state NMR spectroscopy. The presence of polyphosphate has also been reported in marine sinking particles and sediments [105, 131] and lacustrine sediments [27, 82]. In our samples, polyphosphate comprised 8% of the P in the 1-2 cm sediment from the oxic site, but was not detected in the deeper sample (Table 9). Similar trends have also been seen in lake sediments, where polyphosphate accounted for up to 11% of the total P in the top 0.5 cm, but were not observed in deeper sediments [82]. The middle groups of polyphosphate chains are more susceptible to degradation than the end groups, which could explain their rapid disappearance from deeper sediments [82].

6.4.2 Polyphosphate Synthesis and Diagenesis

Some microorganisms such as certain bacteria and yeast are able to store and accumulate P as intracellular polyphosphate granules. Polyphosphates have been reported to account for 30% of the cellular phosphate of two different plankton species *Skeletonema costatum* and *Amphidinium carteri* [157]. Polyphosphate chains in certain bacteria such as E.coli can have a length of up to 1000 phosphate groups [128]. Accumulation of polyphosphate occurs under aerobic conditions when excess dissolved P is available. If these microorganisms are exposed to an anaerobic environment, the stored P is utilized as an energy source and is eventually released in dissolved form to the surrounding waters [65, 82, 150]. Polyphosphate accumulating organisms are dominant under oscillating redox conditions in

wastewater treatment plants involving biological P removal [82]. The presence of higher amounts (6.6%) of polyphosphate has also been documented in marine sediments deposited under fluctuating redox conditions in the Santa Monica basin [105]. Several bacterial genera (e.g., *Escherecia, Bacillus, Flavobacterium* and *Pseudomonas*) and protozoans (e.g., *Vorticella, Opercularia* and *Epistylis*) have the ability to take up P and form intracellular polyphosphate under appropriate conditions of external P and oxygen availability.

Polyphosphates can be used as an energy source, a phosphate donor for sugars and a chelator for divalent cations. Polyphosphate kinase and 1.3-diphosphoglycerol-polyphosphate phosphotransferase are two known polyphosphate synthesizing enzymes. Polyphosphatase and tripolyphosphatase are enzymes of polyphosphate degradation (see review by Nesmeyanova [128]. In laboratory experiments with lake sediments and benthic microorganisms, an increase in the polyphosphate content and chain lengths was observed under aerobic conditions [82]. Both polyphosphate content and chain length decreased under anaerobic conditions. A recent study by Schulz and Schulz [150] provided comprehensive evidence for large benthic P fluxes resulting from polyphosphate utilization by the sulfide oxidizing bacterium Thiomargarita namibiensis in shelf sediments. Large amounts of polyphosphate inclusions were found in these bacteria under oxic conditions. Very high pore water phosphate concentrations (of up to 300 μM) were reported in a narrow region of sediments densely populated by *T. namibiensis*. Phosphate concentrations measured during an anaerobic incubation experiment confirmed that *T. namibiensis* alone could account for the observed pore water phosphate peak and resulting hydroxyapatite precipitation in the Namibian coast sediments [150].

In Effingham Inlet, high phosphate concentrations coupled with the availability of oxygen at the water column redox transition zone (at approximately 65 meters; Figure 17) would provide an ideal environment for polyphosphate accumulation by microorganisms. Presence of polyphosphates in sediments from the oxic site suggests that polyphosphate accumulating microorganisms are transported and sedimented from the water column redox transition zone. Rapid and complete utilization of the sedimented polyphosphates at the

sediment-water interface in the anoxic site may explain their absence at this site. Complete utilization at the sediment-water interface would be consistent with extremely high sulfate reduction rates indicating high levels of microbial activity in this region [88]. At the oxic site, conditions at the sediment-water interface are not conducive for the utilization of polyphosphates. However, anoxic sediment conditions below a few cm at the oxic site would likely induce the utilization and subsequent disappearance of polyphosphates at depth.

In the sediments at the oxic site, P released during organic matter decomposition, polyphosphate metabolism and reduction of ferric oxides may be permanently sequestered via a number of mechanisms. One commonly described mechanism is related to the large sorption capacity of ferric oxyhydroxide particles for phosphate [23,63,122,163]. When these iron oxyhydroxides are reduced, the associated phosphate is released. In sediments overlain by anoxic bottom waters the released iron and phosphate can diffuse out of the sediments. In contrast, the transition between oxidizing and reducing conditions is located within the sediments rather than in the water column, at the site overlain by oxic bottom waters. Oxic conditions in the upper few centimeters of the sediments prevent the reduction of ferric oxyhydroxides and subsequent release of associated P. Additionally, in this situation, ferrous ions diffusing from the deeper anoxic regions of the sediment column can precipitate as ferric oxyhydroxides in the oxic upper sediment layers. These newly precipitated ferric oxyhydroxides can absorb and trap phosphate released during early diagenesis. Another potential mechanism for P trapping in oxic site sediments would be related to polyphosphate metabolism by organisms living at the oxic-anoxic transition in the sediments. Polyphosphate metabolism occurs along a redox potential range that overlaps microbially mediated iron reduction [42]. Thus, in a similar fashion to the cycling of iron and phosphate around the sediment oxic-anoxic transition, phosphate from polyphosphates remineralized in the deeper anoxic portions of the sediment could be sequestered by polyphosphate formation at the transition. Sequestration of phosphate by the above mechanisms would be consistent with the much lower pore water phosphate concentrations measured in the oxic site sediments as compared to those from the anoxic site [88].

Ultimately, it is unlikely that either the iron cycling or polyphosphate metabolism mechanisms will permanently trap pore water phosphates in sediment columns overlain by oxic waters. Any phosphate trapped in ferric oxyhydroxides or polyphosphates in the oxic region of the sediments will be released upon burial in the anoxic region. Thus, a steady-state situation can develop where the amount of trapped P is related to the concentration of iron undergoing redox cycling and the activity of polyphosphate producing organisms. However, permanent sequestration of P in sediments may be indirectly related to the intense cycling of P around the sediment redox transition. Cycling around the sediment redox transition can lead to extremely high pore water phosphate concentrations. When fluoride ions are readily available, such as under typical marine conditions, these high pore water phosphate concentrations can result in the precipitation of authigenic phosphate minerals such as apatite [137, 149, 172].

The sequestration of P through authigenic mineral formation is consistent with the large difference in total phosphorus concentrations and C/P ratios observed at the oxic and anoxic sites (Figure 16). Average total phosphorus concentrations for the natural sediments are 37.1± 3.5 (μmol/g) at the oxic site and 26.7± 3.7 (μmol/g) at the anoxic site (Figure 16; [88]). Sediments from the two sampling sites in the Effingham Inlet differ in terms of their organic C to total P ratios. The molar ratios of average organic C to average total P (C/P tot) are 197 for the anoxic site and 133 for the oxic site, indicating higher levels of P sequestration relative to C under oxic conditions (Figure 16; [88]).

6.4.3 Relation between Polyphosphate Cycling and Benthic P flux

The two sites have widely contrasting benthic P fluxes. Direct measurement of benthic P flux (using a benthic chamber) was successful only at the anoxic site and yielded a value of 0.69 mol/m^2/y [88]. At the oxic site, a benthic P flux of 0.032 mol/m^2/y was modeled from pore water phosphate measurements [88]. The molar ratio of carbon oxidation to the benthic P flux at the anoxic site is 39, which is well below the Redfield ratio for average marine organic matter and the observed solid phase organic C to organic P ratio of 410 in these sediments [88]. These observations support the idea of preferential remineralization

of P relative to organic C during diagenesis in sediments overlain by anoxic bottom waters.

Calculations indicate that P release associated with the reduction of ferric oxyhydroxide particles and organic matter remineralization is insufficient to account for the observed P fluxes at the anoxic site [88]. Total reactive iron concentrations, which are a measure of the total sulfidized iron, have values of 1.51 and 2.35 wt. % at the sediment-water interface at the anoxic and oxic sites respectively [83]. Assuming the iron in these sulfides ultimately originates from ferric oxyhydroxide reduction and dissolution, the difference in total reactive iron contents at the sediment-water interface represents the total amount of iron that is liberated during reduction and then sequestered as sulfides at the site overlain by anoxic bottom waters. The difference in total reactive iron concentrations between the two sites is 0.84 wt. %. This value, together with an average sedimentation rate of 32.5 $mg/cm^2/y$ for the anoxic site, yields a reducible iron production rate of 0.05 $mol/m^2/y$ for the sediments at this site. Although poorly constrained, an average ratio of iron to P in reducible ferric oxyhydroxide particles of 10.8 has been previously reported [86]. Using this value, the benthic P flux resulting solely from the release of P from ferric oxyhydroxide particles is estimated to be 4.6 x 10^{-3} $mol/m^2/y$, which accounted for only 0.7% of the total P flux for the anoxic site.

P released during the oxidation of organic matter can also contribute to the benthic P fluxes. Using the average C oxidation rate of 27.3 $mol/m^2/y$, the benthic P flux from the oxidation of Redfield organic matter (C:P = 106:1) is calculated to be 0.25 $mol/m^2/y$. This amounts to 36% of the P flux. These calculations suggest that either organic matter with a C:P ratio significantly lower than Redfield (<40) is being remineralized, or P is preferentially released relative to C during diagenesis, or other redox-sensitive P remineralization mechanisms must be acting in the Effingham Inlet in order to account for the P fluxes at the anoxic site. The explanation of a large contribution of low C/P ratio organic matter is unlikely for Effingham Inlet where the water column microfauna is dominated by diatoms [30]. An average molar C:P ratio of 129 has been reported for marine diatoms [135]. Thus it appears that oxidation of this diatom-rich organic matter alone cannot account for the measured benthic P flux.

Earlier studies have invoked the release of P from the degradation of polyphosphates as a potential source of P to explain the enhanced benthic P fluxes commonly observed under anoxic conditions [65,82,86,88,162]. The availability of information on sedimentation rates and carbon fluxes for the Effingham Inlet site makes it possible to calculate the potential contribution of polyphosphate remineralization to the observed benthic P flux. It should be noted here that even though these calculations are not entirely quantitative, they are useful in estimating the relative significance of the different processes in explaining the observed P fluxes. The depositional flux of C to the sediments can be estimated from the sum of the C oxidation and C burial rates. Using measured sulfate reduction rates, Ingal et al. [88] calculated an average C oxidation rate of 27.2 mol/m^2/y. The C burial rate can be calculated using the measured mass accumulation rate (32.5 mg/cm^2/y) and sediment organic C content (6.3 wt. %) to be 1.7 mol/m^2/y. The sum of the C oxidation and C burial rates results in a C depositional flux of 28.9 mol/m^2/y or 346.8 g/m^2/y. Deinema et al. [48] have reported that polyphosphates can account for up to 20% of the dry weight of a bacterial cell. Conservatively assuming that bacteria and diatoms at Effingham Inlet contain 2% polyphosphates, an order of magnitude less than that reported by Deinema et al. [48], and assuming that most of the dry weight of a cell is C, we can estimate that 6.9g polyphosphate P/m^2/y are being deposited to the sediments. Considering a 3-unit polyphosphate chain, the polyphosphate flux translates to a P flux of 0.08 molesP/m^2/y, which is 12% of the measured benthic P flux at the anoxic site. This simple calculation shows that the release of P under anoxic conditions by polyphosphate accumulating benthic microorganisms can account for a part of the enhanced P fluxes observed at the anoxic site.

6.5 Conclusions

Results from solid-state ^{31}P NMR spectroscopy of demineralized sediments from two sites overlain by oxic and anoxic bottom waters in the Effingham Inlet reveal that P-esters and phosphonates are the major organic P species present. However, there was no evidence of preferential remineralization of either organic P species with depth in these sediments. Biogenic inorganic P in the form of polyphosphates was seen only in the surface sediments from

the oxic site. Ratios of C oxidation rates to benthic P fluxes strongly indicate preferential remineralization of P relative to C at the anoxic site. This study provides evidence that P release during the utilization of polyphosphates by benthic microorganisms can account for a part of the enhanced P fluxes observed in sediments overlain by anoxic bottom waters.

CHAPTER 7

CHARACTERIZATION OF WATER-SOLUBLE ORGANIC CARBON IN URBAN ATMOSPHERIC AEROSOLS USING SOLID-STATE ^{13}C NMR SPECTROSCOPY

7.1 Abstract

Solid-state ^{13}C nuclear magnetic resonance (NMR) spectroscopy has been used to investigate the distribution of carbon functional groups in urban Atlanta aerosol fine (PM2.5) particles. Carbonaceous aerosol particles comprise a significant fraction of the ambient particle mass and are environmentally significant as they may influence radiative and cloud nucleating properties and can also produce adverse health effects upon inhalation. The water-soluble organic carbon (WSOC) fraction was extracted from multiple 24-hour integrated high-volume quartz filter samples and further separated into recovered hydrophobic and hydrophilic fractions using an approach similar to that used to extract humic and fulvic acids from aqueous samples. ^{13}C NMR results indicate that WSOC in urban atmospheric aerosol particles is mostly aliphatic in nature ($\sim$ 95% by C mass) with major contributions from alkyl and oxygenated alkyls ($\sim$80%), carboxylic acid ($\sim$10%) and aromatic functional groups ($\sim$4%). The aromatic C is associated with the recovered hydrophobic fraction of WSOC. These spectra have been compared to the ^{13}C NMR results obtained from Suwannee River Humic Acid and a fractionated biomass burning sample. WSOC, and more importantly, its recovered hydrophobic fraction, is found to be only qualitatively similar to aqueous humic material. The biomass burning sample, is significantly different from urban Atlanta WSOC, and is composed of substantial amounts of sugar derivatives and

Sannigrahi, P., Sullivan, A.P., Weber, R.J. and Ingall, E.D. Environmental Science and Technology (in press)

phenolic compounds, as expected. The NMR results demonstrate the potential of this technique to investigate aerosol WSOC composition and to study its variations with changes in parameters such as aerosol sources.

7.2 Introduction

The ambient carbonaceous aerosol is composed of primary emissions including both elemental and organic, and secondary organic compounds formed in the atmosphere. Organic carbon (OC) compounds are major constituents of fine atmospheric particles [32, 146], and several studies have investigated its composition [60, 91, 152]. A major sub-fraction of these compounds are soluble in water [111]. Like OC, these water-soluble OC (WSOC) compounds have both primary and secondary sources. Because secondary organic aerosol (SOA) formation leads to the formation of water soluble compounds, the study of WSOC is one route to investigate SOA. WSOC is also of interest because it may possess important physical properties. For example, these compounds could produce unique adverse health responses when inhaled. The soluble organic fraction can also influence how ambient particles interact with water vapor. Particle hygroscopicity plays a major role in aerosol radiative properties by altering particle light absorption and scattering characteristics, and also affects cloud nucleating properties [115, 145]. These properties have implications for regional air quality and global climate.

WSOC often contains the bulk of the organic mass and has been reported to account for up to ∼80% of OC in aerosols during the day and 40% at night in samples from an urban site during the summer [158], yet it is one of the least well chemically characterized components of ambient aerosol. It is a complex mixture likely composed of oxygenated C functional groups such as COOH, COH, COC, $CONO_2$, CNO_2 and CNH_2 ([144] and references therein). Chemical characterization of aerosol OC is usually performed using an individual compound approach. While detailed information on a wide range of specific compounds can be obtained with techniques such as gas chromatography coupled with mass spectrometry (GC-MS), only a small fraction of aerosol OC has been identified in the form of specific compounds [45, 68]. One reason for this is that a substantial fraction of

the polar oxygenated organic compounds present in WSOC, cannot be put in a form that is readily analyzable by GC-MS. Recently, Hamilton et al. [68] used thermal desorption coupled with gas chromatography and time of flight-mass spectrometry to isolate about 10,000 individual species with a range of chemical functionalities from $PM_{2.5}$ (particles with aerodynamic diameters less than 2.5 μm) urban aerosol. A fraction of these compounds could be identified, but quantification was not attempted.

A large fraction of organic aerosols can be chemically characterized with spectroscopic techniques such as Fourier transform infrared (FTIR), UV, and nuclear magnetic resonance (NMR), which are capable of functional group analyses [1, 22, 45, 52, 67, 69, 100, 164]. Some limitations of FTIR include low sensitivity and having to mix the sample with KBr. UV spectroscopy also has limited scope because it is sensitive only to functional groups with conjugated bonds and inorganic ions such as nitrate may cause interferences. A detailed discussion of NMR spectroscopy is presented later in this section. For aqueous samples such as WSOC, fog, and cloud water, solid-phase extractions can be used to separate compounds based on their retention characteristics relative to a solid phase, usually a chemical resin. Sample chemistry can be inferred by comparing retention/elution behavior of samples relative to standard compounds. The advantages of solid-phase extractions are that they are relatively easy to perform, they provide a means of simplifying the sample chemical complexity, and isolated fractions can be further analyzed for properties of interest (e.g. [1, 22, 45, 52, 67, 69, 100, 164]. However, a disadvantage of using solid-phase extractions is that sample composition is inferred based on the premise that standard compounds adequately reflect the structure and behavior of complex natural material such as the WSOC component of ambient aerosol particles. Spectroscopic techniques such as IR or NMR, when used in conjunction with these extractions, provide an independent measure of the sample composition and an overview of the different C functional groups and compound classes present. Previous work involving solid-phase extractions coupled with spectroscopic techniques reveal that WSOC is mainly comprised of highly polyconjugated acidic compounds, or slightly polyconjugated, neutral, very hydrophilic compounds [100,104]. Functional group

analyses also suggest that these organic polyacidic compounds are similar to naturally occurring humic substances. The sources of these humic-like compounds are of current interest in part because they are a significant fraction of the ambient aerosol [46], and they exhibit unique properties, e.g., aqueous solutions containing humic-like compounds have reduced surface tension [55]. Among the various spectroscopic techniques available, solid-state ^{13}C NMR spectroscopy has many advantages. First, no sample processing is required other than freeze drying, and second, it is a non-destructive technique, leaving the sample available for other complementary chemical analyses. Although another technique, solution NMR, generally provides greater resolution relative to solid state NMR, solid-state NMR spectroscopy does not have some of the problems encountered during solution NMR analyses of natural organic matter samples including solvent effects on the chemical shifts of the sample and potential obscuring of certain sample chemical shifts by the solvent chemical shifts. One limitation of solid-state NMR is gaining quantitative information on different C functional groups in complex natural samples. Direct polarization-magic angle spinning (DP-MAS) or Bloch decay are the NMR techniques best suited for quantitative analyses, but very long spectrometer times are required, which are often not practical [39]. Cook [39] in a comprehensive review of NMR techniques suitable for the analyses of natural organic material, suggested that presently cross-polarization based methods appear to be best suited to obtain semi-quantitative data on C speciation. It has been shown that through optimization of key NMR parameters, such as contact time and recycle delay, reasonably quantitative estimates ($\pm$10%) of C bond distribution from NMR spectra are possible [71, 141, 180].

Solution ^{1}H NMR has recently been applied in a number of studies to characterize WSOC in aerosols, fog, and cloud water [45, 47, 67, 69, 165]. These studies have shown that WSOC in these samples is a complex mixture of aliphatic oxygenated compounds with a small aromatic content. The presence of polyacidic organic compounds or humic-like substances (HULIS) has also been inferred from ^{1}H NMR spectra [45, 69].

Low C contents of WSOC have probably hindered efforts to use ^{13}C NMR spectroscopy, which is a more suitable tool than ^{1}H NMR for investigating the distribution of C functional groups. For example, a significant fraction of WSOC is in the form of carboxylic acids

[46], which cannot be detected using solution ^{1}H NMR due to the presence of rapidly exchangeable protons. Recently, Duarte et al. [52] used solid-state ^{13}C NMR along with other spectroscopic techniques to compare WSOC collected from an agricultural site in summer and late autumn. Their NMR results clearly demonstrated the differences between aerosol OC sources in the two seasons. The autumn sample showed resonances attributable to phenol and aldehyde/ketone functional groups, which are usually associated with lignin and its degradation products, released during wood combustion.

In this paper, we present results of solid-state ^{13}C NMR analyses on WSOC samples from Atlanta, GA, collected from multiple high-volume quartz filter samples. To further simplify the aerosol particle chemical complexity and help identify sources and relationships between specific chemical fractions and observed physical properties, XAD-8 resins were used to separate WSOC into recovered hydrophobic and hydrophilic fractions, following the approach of [159]. This technique was adapted from methods developed to separate humic and fulvic acids in aqueous samples [170]. As a contrast to the WSOC of urban aerosols, the ^{13}C NMR results have been compared to those obtained from WSOC produced during biomass burning, a known source for humic-like aerosols [117], and a humic acid standard.

7.3 Materials and Methods

7.3.1 Aerosol WSOC Sampling

The Atlanta aerosol samples were collected during June-August 2004 from a rooftop laboratory in the Environmental Science and Technology building on the Georgia Tech campus, which is located very near downtown Atlanta. Twenty-four hour integrated PM2.5 samples starting at midnight were collected using a Thermo Anderson High Volume (Hi-Vol) Sampler. Pre-baked quartz filters were used, and the filter holder was cleaned with isopropanol prior to loading. Typically the entire or three quarters of the PM2.5 filter was extracted in 125 ml of deionized water in a Nalgene Amber HDPE bottle, sonicated with heat at 35°C for 1.25 hours, and then filtered using a disposable 0.45 μm PTFE syringe filter to remove quartz filter fibers. A total of 8 Hi-Vol samples were extracted separately, and the extracts were batched together to obtain sufficient mass for the NMR analyses. Since the ambient

conditions were qualitatively similar on all the sampling days, it is reasonable to combine samples to yield one representative of the entire sampling period.

Aerosol WSOC produced during the combustion of biomass was collected next to fires during routine prescribed burns at Fort Gordon, Augusta, GA, and Fort Benning, Columbus, GA, using the Thermo Anderson Sampler described above. Due to the much higher OC content of these samples compared to Atlanta WSOC, 2-hour integrated samples were collected. A quarter of 4 different Hi-Vol samples were extracted together to obtain a sample for NMR analysis. Though the sampling time scales are different for the Atlanta WSOC and biomass burning WSOC samples, their comparison here is justified as only their highly averaged compositions are being studied rather than diurnal trends. Efforts are underway to collect larger daily Atlanta WSOC samples using multiple Hi-Vol samplers in order to examine diurnal compositional variations.

It should be noted that this aerosol particle collection method is susceptible to sampling artifacts because the Hi-Vol air samples were not denuded of interfering gases. Positive artifacts can exist from vapor absorption to the quartz filter and collected aerosol. Also, loss of semi-volatile organic compounds during sampling can lead to negative artifacts, and these compounds will not be measured in this analysis. In another study, Sullivan and Weber [160], however, found fairly good agreement between WSOC extracted from 24 hr integrated Hi-Vol filters and an on-line 6-min denuded measurement of WSOC, (zero-intercept slope of 1.10, $R^2 = 0.83$). Assuming that the online system is influenced less by artifacts, there is some evidence to suggest Hi-Vol WSOC is fairly representative of the ambient aerosol.

7.3.2 Fractionation of WSOC.

To simplify the chemical analyses of this complex material, WSOC was fractionated into recovered hydrophobic and hydrophilic components. Reverse-phase solid phase extraction (SPE) with XAD-8 resin (composed of a polymerized methyl ester of polyacrylic acid) was used to partition the organic solutes from the sample filter extracts (mobile phase) into the non-polar stationary phase. Since the primary partitioning force is hydrophobic

interactions, the resin retains organics that are the most hydrophobic compounds among the WSOC components. The organics that pass through the column are hydrophilic.

SPE is used to isolate two components of the WSOC, hydrophilic and hydrophobic compounds. The hydrophilic compounds are those components of the filtered liquid sample that penetrate the column when sample pH is adjusted to 2 by the addition of 0.1 M HCl. A portion of the organic compounds retained on the column is then extracted with a pH 13 eluent of 0.1 M NaOH. The hydrophobic compounds that are extracted by this method are referred to as the recovered hydrophobic fraction.

Laboratory calibrations indicated that the hydrophilic fraction includes mono/di-carboxylic acids and carbonyls with less than 4 or 5 carbons, polysaccharides, polyols, and organic bases. The recovered hydrophobic fraction includes aromatic carboxylic acids and phenols. All aromatic compounds tested were recovered with 80 to 85% efficiency. A Suwannee River humic acid standard was recovered at 90% efficiency, which is expected since XAD-8 resin is used in the method to isolate humic acid [170]. A fraction of the hydrophobic WSOC was not efficiently recovered. Aliphatic and cyclic carboxylic acids and carbonyls with 5-9 carbons and organic nitrates had recoveries of less than 20%. A more in-depth discussion of this method, calibration, and results from an ambient study can be found in Sullivan and Weber [159].

Decesari et al. [45] performed liquid ^{1}H NMR on fractions using a different SPE method, and thus their results are not directly comparable to those discussed in this paper. Unlike Decesari et al. [45], we chose a SPE method that does not require organic eluents. This permits a direct measurement of the C concentrations in the isolated hydrophilic and hydrophobic WSOC fractions, along with the bulk WSOC, via a Total Organic Carbon (TOC) analyzer (Sievers, 800-Turbo, Boulder, CO). Table 10) summarizes the ambient concentrations of the OC, WSOC, and SPE-isolated WSOC fractions for the urban Atlanta and biomass burning samples. Note, for the Atlanta sample the results are for average conditions measured during the period over which the 24-hour Hi-Vol samples were pooled to obtain sufficient mass for the NMR analysis.

A small amount ($\sim$ 30-50 ppb) of carbon is present in the deionized water used for the

Table 10: Ambient concentrations of the urban Atlanta* and biomass burning samples.

	OC	WSOC	Hydrophilic	Recovered Hydrophobic
Urban Atlanta	4.30	3.12	1.87	0.72
Biomass Burning	934	659	368	230

- All units are in μg C m^{-3}
- OC is the concentration of organic carbon measured by the thermal/optical transmission method [18]. WSOC, hydrophilic, and recovered hydrophobic are all measured with a Sievers TOC analyzer.
- The individual urban Atlanta samples used for the NMR analysis were not measured; instead, average concentrations are given for the period over which the samples were pooled for the NMR analysis.

filter extractions. This is negligible compared to the carbon contents of the ambient samples of WSOC and its hydrophilic, and recovered hydrophobic fractions. From June to August 2004, the sampling period in Atlanta during which the 8 filters used for NMR analysis were collected, the average and standard deviation (bracketed) of the WSOC, hydrophilic, and recovered hydrophobic fractions from other extracted filters is 41000 (11000) ppb C, 24000 (9400) ppb C, and 30000 (11000) ppb C, respectively. Therefore, the background carbon interferences are negligible and do not interfere with the NMR analyses. It is also noted that the solubility of some specific organic compounds in the ambient aerosol may depend on the liquid concentrations produced by our extraction method. An assessment cannot be made of this effect since an individual compound analysis was not performed.

WSOC and the two fractions were freeze-dried prior to NMR analyses. The hydrophilic fractions from both sets of samples (urban and biomass burning) did not dry down completely after freeze-drying, most probably due to the presence of strongly hygroscopic compounds, such as sulfuric, and, nitric acids [156]. These samples were mixed with a small amount of organic-free powdered Kaolinite, an aluminosilicate mineral, in order to facilitate solid-state NMR analyses. A similar treatment was also required for the un-fractionated WSOC from the biomass burning samples.

7.3.3 Solid-state ^{13}C NMR Spectroscopy

All NMR experiments were performed at the Georgia Tech NMR center in the School of Chemistry and Biochemistry. ^{13}C NMR spectra were acquired on a Bruker DSX 400 spectrometer using Cross Polarization-Magic Angle spinning (CP-MAS) at a ^{13}C frequency of 100 MHz. Samples containing 20-35 mg of carbon (40 to 70 mg of dry sample or 45 to 100 mg of sample plus Kaolinite) were packed in 4mm-diameter cylindrical zirconia rotors fitted with Kel-F caps and spun at 10,000 $\pm$ 10Hz in a Bruker magic angle spinning probe. For all three fractions, an optimized cross polarization pulse sequence was used with a 1.0 msec contact time and recycle delay of 5 seconds. Cross polarization is achieved by creating a second variable magnetic field to equalize energy levels of protons and carbons [180]. Because protons relax quickly with a time constant $T_{1\rho}H$, also known as the spin-lattice relaxation time, it is not possible to hold the net magnetizations of protons in this field indefinitely. If $T_{1\rho}H$ is much smaller than the contact time needed for the slowest carbons to cross-polarize, then these carbons will not be observed. In complex material such as aerosol WSOC, where compounds with a range of $T_{1\rho}H$'s are present, NMR optimization experiments have to be performed to determine an optimal value of contact time so that carbon in all carbon functional groups will be observed without bias. We performed a series of 6 experiments on two natural organic matter samples, in which the contact time was varied from 50 to 5000 μsec and the peak areas for all the functional groups were compared. The samples for the optimization experiments were freeze dried samples of dissolved marine organic matter that had a similar diversity of carbon functional groups as the WSOC samples [141]. It was found that using a pulse delay of 5 seconds and a contact time of 1.0 msec consistently gave the highest values of peak area for all the functional groups. Typical results of these optimization experiments are shown for one sample (Figure 5).

The value of 1.0 msec for contact time determined during our optimization experiments has also been found to be optimal by other researchers for a wide variety of natural organic matter samples [39]. For the WSOC samples, a total of 10,240 transients were collected for each and the spectra processed with 100 Hz exponential line broadening. Identification of functional groups by ^{13}C NMR is based on their chemical shift relative to an external

tetramethylsilane (TMS) standard set at 0 ppm. The ^{13}C NMR spectra were split into seven spectral regions on the ppm scale (0-45, 45-60, 60-95, 95-110, 110-140, 140-160, 160-190), and the integrated areas in each were determined. Data processing and calculation of integrated peak areas were carried out off-line using the Mestre-C software package (Mestrelab Research, Santiago de Compostela, Spain). Using this software package, peak areas between selected ppm ranges corresponding to different C functional groups can be integrated. The software returns absolute peak areas relative to a reference peak (whose area is set as 1). The integrated peak areas and signal to noise ratios for all samples are available as Supplemental Information (Tables 12 and 13). Percentage peak areas of individual peaks are then calculated by dividing their areas by the total spectral peak area of the sample. Using the Mestre-C software rather than manual integrations ensures that the spectral limits are chosen precisely for all spectra. The integrated NMR peak areas are a semi-quantitative ($\pm$10%) measure of the relative contributions of different functional groups to the organic C present in a sample. These values allow us to understand the major overall trends in organic C composition, such as whether a sample contains a prevalence of aliphatic, aromatic or carboxylic compounds.

7.4 Results and Discussion

7.4.1 Composition of Atlanta Aerosol WSOC

Solid-state ^{13}C NMR spectra of the bulk WSOC and its recovered hydrophobic and hydrophilic fractions, extracted using XAD-8 resins, from the Atlanta aerosol samples are presented in Figure 20. The major C functional groups identified in these spectra are alkyl (0-45 ppm), O-alkyl (60-95 ppm), alkyl substituted aromatics (110-140 ppm) and carboxylic acids (160-190 ppm). Very minor peaks corresponding to anomeric/acetal C (95-110 ppm) and aromatic C bonded to N or O (140-160 ppm) may be present in the bulk WSOC and recovered hydrophobic fractions. Table 11 gives the relative abundance (as % total peak area) of the C functional groups in WSOC and its fractions as calculated from integrated peak areas.

The most noticeable feature in these spectra is the large alkyl peak in the bulk WSOC as

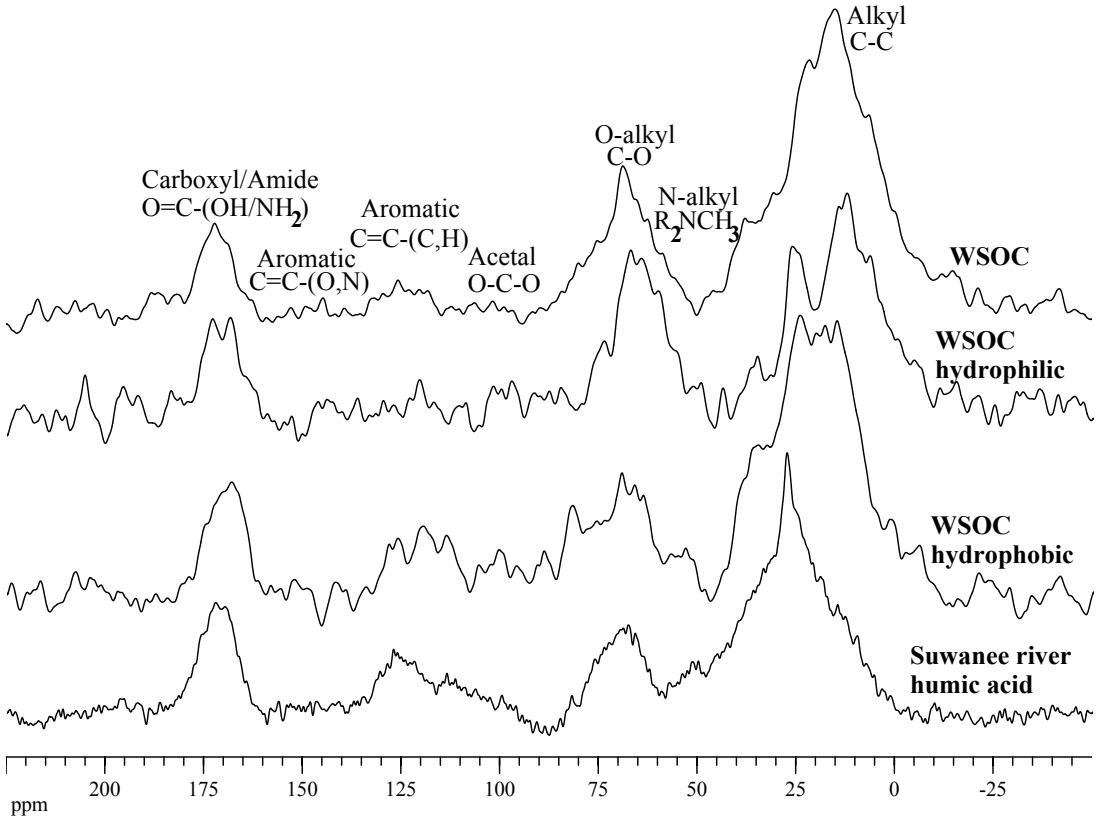

Figure 20: Solid-state ^{13}C NMR spectra of urban Atlanta water-soluble organic carbon (WSOC) and its recovered hydrophobic and hydrophilic fractions. Also presented for comparison is the spectrum from the Suwannee River Humic acid standard. Note: For a given spectrum, the peak areas represent the relative distributions of C bond types in the sample. Comparison of peak areas between samples is not straightforward due to the differences in their C contents.

Table 11: Percentage of total NMR peak area measured under each spectral region for Atlanta WSOC and its fractions; Suwannee River humic acid and biomass burning WSOC and its fractions.

	% total peak area in each region on the ppm scale						
	0-45	45-60	60-95	95-110	110-140	140-160	160-190
Atlanta WSOC							
Total	64.0	3.5	17.4	0.7	4.2	0.7	9.7
Hydrophilic	60.0	6.6	24	0.0	0.0	0.0	9.6
Recovered Hydrophobic	59.5	3.0	18.0	1.8	8.3	0.0	9.5
Suwannee river humic acid	56.6	7.4	9.1	1.7	10.3	0.5	14.3
Biomass burning WSOC							
Total	50.3	7.9	30.2	6.4	3.2	1.0	1.0
Hydrophilic	0.0	24.3	75.7	0.0	0.0	0.0	0.0
Recovered Hydrophobic	35.5	7.5	9.9	12.0	21.6	8.9	4.6

- Functional groups in the different spectral regions are as follows: 0-45 (Alkyl); 45-60 (N-alkyl); 60-95 (O-alkyl); 95-110 (Acetal/anomeric); 140-160 (Aromatic); 160-190 (Carboxylic acid/ester, amide).

well as its recovered hydrophobic and hydrophilic fractions. The largely aliphatic nature of WSOC is in agreement with results obtained from ^{1}H NMR spectroscopy on aerosols [45,67]. A number of unresolved peaks can be seen in the alkyl region indicating the presence of different forms of aliphatic C (Figure 20). These alkyl carbons can be part of a large variety of aliphatic as well as aromatic organic C compounds in WSOC including carboxylic acids, amides, and alcohols.

The second most prominent peak in terms of area is in the 60-95 ppm region. This peak can be attributed to C atoms associated with O-alkyl (C-O), CH(OH) or CH_2(OH) functional groups. These oxygenated aliphatic carbons may be found in polysaccharides, alcohols, or anhydrosugars. However, if significant amounts of 5 or 6-C ring polysaccharides (pentose or hexose sugars) are present, a slightly less prominent peak corresponding to acetal/anomeric (O-C-O) functional groups would be observed in the 95-110 ppm region. The ratio of O-alkyl to anomeric peak areas should have a value of 4:1 or 5:1 if all the

carbohydrates present are in the form of ring polysaccharides. Our data show that a small signal corresponding to anomeric C is seen only in the recovered hydrophobic fraction (Figure 20, Table 11). The 10:1 area ratio of the O-alkyl peak with this small anomeric peak suggests that most of these anomeric carbons are not associated with ring polysaccharides. Other possibilities to explain the oxygenated aliphatic C functional groups seen in these spectra include anhydrosugars such as levoglucosan, galactosan, and xylosan. These compounds, especially levoglucosan, are often used as tracers for biomass burning in aerosol C source apportionment studies [67]. They are only produced during the combustion of biomass and cannot be generated by non-combustive processes such as hydrolysis or microbial degradation, making them suitable as tracers for biomass burning [67]. The results of experiments investigating the retention and recovery of chemical compound classes by the XAD-8 resins indicate that anhydrosugars, such as levoglucosan, are present only in the hydrophilic fraction [159]. Therefore, anhydrosugars, sugar alcohols, and short-chain polyols probably account for the O-alkyl peak detected in the hydrophilic fraction. This peak in the recovered hydrophobic fraction may be due to other polyhydroxy (carbohydrate) compounds, which are only partially recovered in the XAD-8 column wash.

About 10% of the C in WSOC is associated with carboxylic acid functional groups (Figure 20, Table 11). Given the predominance of aliphatic C in these samples, most of the carboxylic acids appear to be aliphatic in nature. Another group of biomolecules that could contribute to this signal are amino acids. A small N-alkyl signal (usually a component of amino acids) is seen in all the spectra (Figure 20). Breakdown of biogenic fatty acids such as oleic acid can give rise to carboxylic acids and aliphatic carbons. Dicarboxylic acids can be produced by direct emission from fossil fuel or biomass combustion and the photochemical oxidation of hydrocarbons [106]. Theoretical and laboratory studies have shown that secondary organic aerosol formation through gas-phase reactions can produce low molecular weight organic compounds such as carboxylic acids, alcohols, and other single and multi-functional oxygenated compounds [59]. Among the different carboxyl/carbonyl compounds likely to occur in the WSOC fraction of aerosols [144], our ^{13}C NMR spectra do not show any evidence for the presence of ketones. These functional groups usually appear

in the 200-220 ppm region in ^{13}C NMR spectra. Thus, at the levels of sensitivity of our solid-state ^{13}C NMR spectra, keto-carboxylic acids are not detected in this urban aerosol WSOC.

A measurable amount of aromatic C is present in the bulk WSOC and recovered hydrophobic fraction, but none is detected in the hydrophilic fraction (Table 11). From the peak position in the NMR spectra, these aromatic carbons appear to be unsubstituted or substituted by alkyl, carboxylic acid, or O-alkyl. Thus, some or all of the alkyl functional groups observed in the recovered hydrophobic fraction are associated with aromatic C compounds. Previous work involving ^{1}H NMR spectra of chromatographically separated fractions of WSOC have indicated the presence of aromatic C substituted by carboxyl and nitro groups rather than alkyl groups [45, 47]. Aromatic C substituted by oxygen and nitrogen, such as phenols, would appear in the 140-160 ppm region of the ^{13}C NMR spectra. No peaks are observed in that region in the Atlanta WSOC spectra (Figure 20); however, significant levels were observed in the biomass samples (discussed later). These results are consistent with those of [52], who observed a small phenol signal in their WSOC sample collected during late autumn, but none from the summer sample. Possible sources of aromatic C to aerosols include motor vehicle exhaust, secondary organic aerosol (SOA) formation, and degradation of the lignin component of biomass during combustion. Since lignin degradation mostly gives rise to phenols, the aromatic carboxylic acids possibly present in our samples appear to be mainly a product of motor vehicle emissions or SOA producing reactions. For example, aromatic acids, such as phthalic acid, have been thought to be secondary products of oxidation of polycyclic aromatic hydrocarbons [62, 92].

7.4.2 Comparison to Suwannee River Humic Acid Standard

Studies of aerosol WSOC composition have often reported that a fraction of this material is similar in composition to aquatic humic substances [45,69]. Solid-state ^{13}C spectrum of the Suwannee River humic acid standard material was acquired using the same experimental conditions as the bulk WSOC and its fractions (Figure 20). The humic acid standard was extracted from natural waters using an XAD-8 resin and the same procedure we have used

to isolate the recovered hydrophobic WSOC fraction of the urban Atlanta aerosol. When comparing these two spectra, an interesting observation is that, while the C functional group resonances appear at exactly the same positions, they differ in terms of the relative proportions (Figure 20; Table 11). The Suwannee River humic acid has higher carboxylic acid and aromatic, and lower O-alkyl and alkyl content than the recovered hydrophobic WSOC fraction of the urban Atlanta aerosol. Therefore, urban Atlanta fine particle WSOC and its hydrophobic fraction appear to be only qualitatively similar to aqueous humic substances in terms of functional group distribution, as seen by ^{13}C NMR.

7.4.3 Comparison to Biomass Burning WSOC

^{13}C NMR spectra of bulk biomass burning WSOC and its XAD-8 recovered hydrophobic and hydrophilic fractions are presented in Figure 21. All the functional groups present in the Atlanta WSOC samples are also seen in these samples, but their relative abundances are different (Table 11). However, unlike the urban Atlanta sample, the biomass sample has a prominent peak at ∼145 ppm, corresponding to aromatic C attached to O or N (such as phenols), which is only seen in the spectra of biomass burning WSOC and its recovered hydrophobic fraction. These phenolic compounds are likely a product of the breakdown of biomass lignin components. Other differences between these two sets of samples include the larger N-alkyl peak observed in the biomass burning WSOC samples. N-alkyl functional groups may be present in compounds such as aliphatic amines.

The C functional groups observed in the biomass burning WSOC can form as a result of the combustion of cellulose, hemicellulose, and lignin, the major constituents of vegetation [134]. Sugar derivatives such as levoglucosan are produced during the pyrolysis of cellulose and hemicellulose, whereas the combustion of lignin produces methoxyphenols. The O-alkyl functional groups observed in all the biomass burning WSOC spectra (Figure 21) can be partly attributed to sugar derivatives as well as methoxyphenols. The ratio of the areas of the O-alkyl and acetal peaks for the biomass burning total WSOC sample has a value of 5:1, indicating the presence of ring polysaccharides. Aliphatic carboxylic acids are also present in these samples. ^{1}H NMR spectra from biomass burning aerosols in Amazonia have also

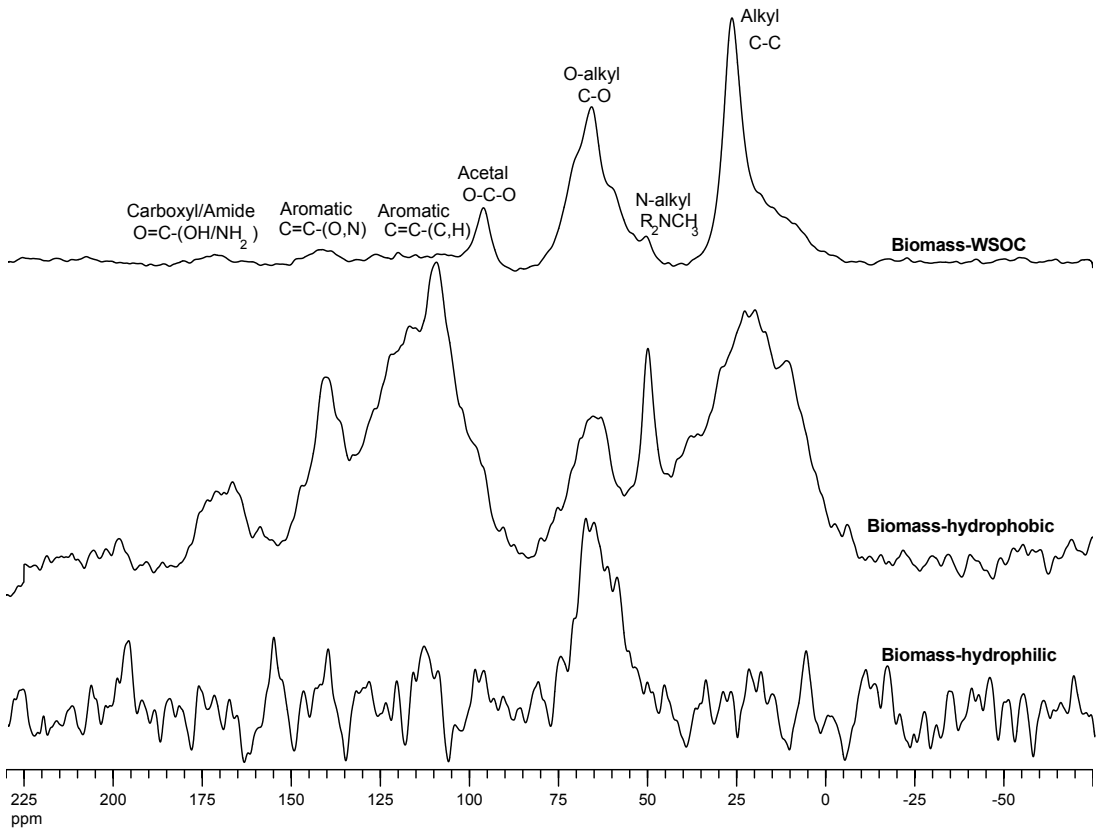

Figure 21: Solid-state ^{13}C NMR spectra of biomass burning water-soluble organic carbon (WSOC) and its recovered hydrophobic and hydrophilic fractions. Note: For a given spectrum, the peak areas represent the relative distributions of C bond types in the sample. Comparison of peak areas between samples is not straightforward due to the differences in their C contents.

revealed the presence of functional groups similar to those observed here [67]

7.4.4 Comparison between Hydrophobic and Hydrophilic Fractions of WSOC

As discussed earlier, laboratory experiments with the elution of synthetic, but possible, WSOC constituent compounds through the XAD-8 column have shown that it is possible to divide aerosol WSOC into chemically distinct recovered hydrophobic and hydrophilic components [159]. The ^{13}C NMR spectra confirmed our inference from the laboratory experiments that aromatic C functional groups occur only in the recovered hydrophobic fraction of WSOC (Figures 20, 21; Table 11). About 8% and 30% of the carbon in the recovered hydrophobic fraction of the Atlanta WSOC and biomass burning WSOC, respectively, can be attributed to aromatic functional groups, but there is no aromatic C signal in the hydrophilic fraction (Table 11). Therefore, the aromatic C observed in the bulk WSOC spectrum is associated exclusively with the recovered hydrophobic fraction. Further, the hydrophilic fraction appears to be enriched in O-alkyls and N-alkyls compared to the recovered hydrophobic fraction. This may be a result of higher carbohydrate and amino acid contents of the hydrophilic fraction. This difference between the two fractions is even more pronounced in the biomass burning WSOC where O-alkyl and N-alkyl are the only functional groups discernable in the hydrophilic fraction (Table 11). These results are also in agreement with those obtained from a new method to broadly speciate bulk WSOC and its hydrophilic and recovered hydrophobic fractions based on size-exclusion chromatographic analyses performed on these samples [160].

7.5 Conclusions

Solid-state ^{13}C NMR spectroscopy has been used to characterize the WSOC fraction of an urban carbonaceous aerosol, and the results have been compared to a biomass burning sample and Suwannee River humic acid standard. The aerosol samples were collected on quartz filters and the particles extracted into water. The results indicate that the urban Atlanta WSOC is predominantly composed of alkyl, O-alkyl, carboxylic acid and aromatic functional groups. Bulk WSOC as well as its recovered hydrophobic and hydrophilic fractions, isolated using a SPE method involving XAD-8 resin, are mostly aliphatic in nature.

The recovered hydrophobic fraction is different from the hydrophilic in that it contains aromatic C. These solid-state ^{13}C NMR results are validated by comparing them to those from a biomass burning sample, which is significantly different from urban Atlanta WSOC, and is composed of substantial amounts of sugar derivatives and phenolic compounds, as expected. Also, comparison with spectra from Suwannee River humic acids reveals that WSOC, and more importantly, the hydrophobic WSOC fraction, are only qualitatively similar to aqueous humic material. Overall, these results demonstrate that solid-state ^{13}C NMR spectroscopy is an excellent technique for studying the bulk organic C composition of WSOC. This method has the potential to investigate variations in WSOC composition in relation to changes in parameters such as aerosol sources.

CHAPTER 8

CONCLUSIONS

This dissertation demonstrates the scope and versatility of solid-state NMR spectroscopy in studying natural organic material from different environments. The results presented relate to particular aspects of natural organic matter composition and cycling in the marine environment and atmospheric aerosols. Some of the problems that have been studied include:

- composition and cycling of carbon and phosphorus in water column dissolved and particulate organic matter
- the mechanisms behind enhanced phosphorus fluxes in marine sediments overlain by anoxic bottom waters
- the composition of water-soluble organic C in urban and biomass burning aerosols

The major findings of this dissertation are summarized below:

8.1 Carbon and Phosphorus cycling in Water column Dissolved and Particulate Organic Matter

Despite increasing analytical sophistication, a major fraction of NOM remains unidentified in the form of specific biomolecules. In the marine water column, the molecularly uncharacterized fraction constitutes an increasing proportion of the organic carbon in deeper waters. This is the first study to use ^{13}C NMR spectroscopy to characterize ultrafiltered UPOM and also the first direct comparison of NMR results to molecular analyses on different size fractions from the same site. The agreement between carbohydrate to amino acid ratios obtained from molecular level analyses to those from modeling of ^{13}C NMR results indicates that the molecularly uncharacterized fraction is similar in composition to the characterized

fraction. The small fraction characterized in the form of specific biomolecules is inferred to be representative of the entire organic C.

Results from solid-state ^{13}C and ^{31}P NMR spectroscopy coupled with elemental and isotopic analyses indicate that ultrafiltered dissolved and particulate organic matter (UDOM and UPOM) in the water column differ in terms of their source and bulk chemical composition. Both UDOM and UPOM are composed of carbohydrates, lipids and amino acids but their relative abundances differ for the two size fractions and also change with depth in the water column. ^{31}P NMR spectroscopy shows that UDOM and UPOM also have distinct organic P composition. ^{31}P NMR spectra of UDOM reveal that P esters (75%) and phosphonates (25%) are the major P functional groups present, however, P esters were the only P bond type in UPOM. Compilation of evidence from different analyses lead to the conclusion that aggregation of UDOM does not result in significant production of UPOM, and conversely, UDOM is not produced simply by the solubilization of UPOM.

Comparison of ^{13}C and ^{31}P NMR findings suggest that P in UDOM and UPOM is associated with carbohydrates and amino acids. In UPOM, P is associated with lipids as well. These association suggest that P in UDOM and UPOM is present in the form of DNA, RNA, sugar phosphates and phosphoamino acids. Phospholipids and lipopolysaccharides also contribute to the P in UPOM. However, it appears that the P functional groups are somehow balanced in their distribution among molecular classes, because they remain in relatively constant proportion throughout the ocean.

8.2 Mechanisms behind Enhanced P Fluxes in Anoxic Sediments

^{31}P NMR spectra showing the presence of polyphosphates only in sediments from oxygenated environments, give some of the first evidence for potential cycling of polyphosphates by sediment microorganisms. This provides a new mechanism to explain enhanced benthic P fluxes from sediments overlain by anoxic bottom waters. ^{31}P NMR spectra also provide information on the composition and transformation of sediment organic P under different redox conditions. P-esters and phosphonates are the major organic P species present in

both oxic and anoxic sediments. There is no evidence for the preferential remineralization of either organic P species in these sediments.

8.3 Composition of WSOC in Urban Aerosols

This work is one of the first to successfully demonstrate the applicability of ^{13}C NMR to study aerosol WSOC. ^{13}C NMR spectra of urban Atlanta WSOC reveal that it is mostly aliphatic in nature and the minor aromatic component is associated with its hydrophobic fraction. The composition of WSOC from biomass burning aerosols is significantly different from urban Atlanta WSOC, and it is composed of substantial amounts of sugar derivatives and phenolic compounds. WSOC has been hypothesized to contain significant amounts of aqueous 'humic-like' material. However, comparison with spectra from Suwannee River humic acids reveals that WSOC, and more importantly, the hydrophobic WSOC fraction, are only qualitatively similar to aqueous humic material.

8.4 Future Research Directions

As the results of this dissertation demonstrate, solid-state NMR spectroscopy along with isotopic and elemental analyses, has yielded many new insights into the bulk composition and cycling of natural organic matter. In order to further improve our understanding of the composition and structure of natural organic matter, two avenues of research that can be explored are: 1) the use of advanced analytical techniques which can yield more specific compositional and structural information than solid-state 1D NMR; 2) obtaining spatially resolved compositional information. Advanced analytical techniques such as 2D NMR can be used to improve upon the compositional information gained from 1D NMR and examine the connectivities between different functional groups in a sample. High resolution mass spectrometric techniques such as Fourier Transform-Ion Cyclotron Resonance (FT-ICR) can also aid in understanding NOM composition by providing information on molecular weight distributions and possible molecular formulas of the compounds present. These kinds of analyses can potentially help bridge the gap between molecular level analyses of individual compound classes and bulk spectroscopic analyses.

Organic matter is produced with chemical heterogeneity on nanoscales and much of this heterogeneity survives degradation during NOM cycling. However, most analytical techniques used in NOM characterization, including NMR, assume homogenous distribution of organic compounds within samples. Spectromicroscopic techniques such as X-ray microscopy and X-ray absorption near edge structure (XANES) spectroscopy can be used to obtain spatially resolved structural and compositional information on NOM. These spectromicroscopic analyses can provide information on the distribution of functional groups within NOM samples with high spatial resolution ($\sim$ 30 nm). X-ray microscopy can also be used to detect the presence of structures such as cell walls in NOM samples. The protection of organic matter by mineral matrices, which is often invoked as a mechanism for organic matter preservation, can also be studied using spectromicroscopy.

APPENDIX A

SUPPLEMENTARY INFORMATION 1

Matlab code to calculate the proportions of Lipid, Protein and Carbohydrate in marine organic matter samples using optimization.

```
l= lipids, p= protein, c= carbohydrates, d=NMR results.
%End-member functional group distribution
l=[94.4 0 0 0 0 0 5.6];
p=[36.3 21 6.6 0 8.0 1.6 26.5];
c=[0 0 83.3 16.7 0 0 0];
% peak area from NMR spectra and MaxP = 3.8/(C/N)
% e.g. for the 20 m UDOM sample from Aloha,
d=[19.2 7.2 56.8 8.8 0 0 8]; MaxP=23.9;
sum(d)
% Optimization
A=[sum(l.*l) sum(l.*c) 1 0;
   sum(l.*p) sum(p.*c) 1 1;
   sum(l.*c) sum(c.*c) 1 0;
   1         1         0 0 ];
% Constraining the amino acid content
B=[sum(d.*l)-sum(l.*p)*MaxP, sum(d.*p)-sum(p.*p)*MaxP  sum(d.*c)-
sum(c.*p)*MaxP  1-MaxP]';
X=inv(A)*B
% Calculate the error
err=d-(l*X(1)+p*MaxP+c*X(2));
sum(err.^2)
```

APPENDIX B

SUPPLEMENTARY INFORMATION 2

Integrated peak areas and signal to noise ratios for peaks in each spectral region for urban Atlanta and biomass burning WSOC NMR spectra presented in Chapter 7 are given in Tables 12 and 13.

Table 12: Integrated peak areas in each spectral region for urban Atlanta and biomass burning NMR spectra

	Integrated peak area						
	0-45	45-60	50-95	95-110	110-140	140-160	160-190
Atlanta WSOC							
Total	1.0	0.05	0.27	0.01	0.065	0.01	0.15
Hydrophobic acid	1.0	0.1	0.3	0.03	0.14	0.0	0.16
Hydrophilic	1.0	0.11	0.04	0.0	0.0	0.0	0.16
Suwanee river humic acid	1.0	0.13	0.16	0.03	0.18	0.01	0.25
Biomass-burning WSOC							
Total	1.0	0.15	0.6	0.13	0.06	0.02	0.02
Hydrophobic acid	1.0	0.21	0.3	0.3	0.6	0.25	0.13
Hydrophilic	0.0	1.0	3.11	0.0	0.0	0.0	0.0

Table 13: Signal to noise ratio for peaks in each spectral region for urban Atlanta and biomass burning NMR spectra

	Signal to noise ratio						
	0-45	45-60	50-95	95-110	110-140	140-160	160-190
Atlanta WSOC							
Total	27.9	7.0	8.4	1.3	4.1	1.1	10.3
Hydrophobic acid	17.3	6.2	3.7	3.7	4.3	0.0	7.02
Hydrophilic	13.3	7.5	4.1	0.0	0.0	0.0	5.6
Suwanee river humic acid	26.8	3.9	12.1	3.4	9.1	1.4	6.5
Biomass-burning WSOC							
Total	67.7	43.2	43.2	2.1	2.4	3.7	0.6
Hydrophobic acid	24.4	14.0	14.1	29.2	22.9	7.3	5.9
Hydrophilic	0.0	2.5	3.1	0.0	0.0	0.0	0.0

REFERENCES

[1] Allen, D. and Palen, E., "Recent advances in aerosol analysis by infrared spectroscopy," *Journal of Aerosol Science*, vol. 20, pp. 441–455, 1989.

[2] Altabet, M. A., "Organic C, N, and stable isotopic composition of particulate matter collected on glass-fiber and aluminum-oxide filters," *Limnology and Oceanography*, vol. 35, no. 4, pp. 902–909, 1990.

[3] Aluwihare, L., Repeta, D., and R.F., C., "A major biopolymeric component to dissolved organic carbon in surface sea water.," *Nature*, vol. 387, pp. 166–169, 1997.

[4] Aluwihare, L., Repeta, D., and R.F., C., "Chemical composition and cycling of dissolved organic matter in the Mid-Atlantic bight," *Deep-Sea Research II*, vol. 49, pp. 4421–4437, 2002.

[5] Aminot, A. and Kerouel, R., "Dissolved organic carbon, nitrogen and phosphorus in the N-E Atlantic and the N-W Mediterranean with particular reference to non-refractory fractions and degradation," *Deep Sea Research I*, vol. 51, pp. 1975–1999, 2004.

[6] Amon, R. and Benner, R., "Rapid cycling of high molecular weight dissolved organic matter in the oceans.," *Nature*, vol. 369, pp. 549–552, 1994.

[7] Amon, R. and Benner, R., "Bacterial utilization of different size classes of dissolved organic matter," *Limnology and Oceanography*, vol. 41, pp. 41–51, 1996.

[8] Anderson, L. D., Delaney, M. L., and Faul, K. L., "Carbon to phosphorus ratios in sediments: Implications for nutrient cycling," *Global Biogeochemical Cycles*, vol. 15, pp. 65–79, 2001.

[9] Aspila, K., Agemian, H., and Chau, A., "A semi-automated method for the determination of inorganic, organic and total phosphate in sediments.," *Analyst*, vol. 101, pp. 187–197, 1976.

[10] Bauer, J., Ruttenberg, K., Wolgast, D., Monaghan, E., and Schrope, M., "Cross-flow filtration of dissolved and colloidal organic nitrogen and phosphorus in sea water: Results from an intercomparison study," *Marine Chemistry*, vol. 55, pp. 33–52, 1996.

[11] Benitez-Nelson, C., O'Neill, L., Kolowith, L., Pellechia, P., and Thunell, R., "Phosphonates and particulate organic phosphorus cycling in an anoxic marine basin," *Limnology and Oceanography*, vol. 49, no. 5, pp. 1593–1604, 2004.

[12] Benner, R., "Chemical composition and reactivity," in *Biogeochemistry of marine dissolved organic matter* (Hansell, D. and Carlson, C., eds.), pp. 59–90, London: Academic Press, 2002.

[13] Benner, R., "Molecular indicators of the bioavailability of dissolved organic matter.," in *Aquatic ecosystems: Interactivity of dissolved organic matter* (Findlay, S. and Sinsabaugh, R., eds.), pp. 121–137, Amsterdam: Elsevier Science, 2003.

[14] Benner, R., Biddanda, B., Black, B., and McCarthy, M., "Abundance, size distribution, and stable carbon and nitrogen isotopic compositions of marine organic matter isolated by tangential-flow ultrafiltration," *Marine Chemistry*, vol. 57, pp. 243–263, 1997.

[15] Benner, R., Pakulski, J., McCarthy, M., Hedges, J., and Hatcher, P., "Bulk chemical characteristics of dissolved organic matter in the ocean.," *Science*, vol. 255, pp. 1561–1564, 1992.

[16] Benner, R. and s Kaiser, K., "Abundance of amino sugars and peptidoglycan in marine particulate and dissolved organic matter," *Limnology and Oceanography*, vol. 48, no. 1, pp. 118–128, 2003.

[17] Bieleski, R., "Phosphate pools, phosphate transport, and phosphate availability," *Annual reviews in plant physiology*, vol. 24, pp. 225–252, 1973.

[18] Birch, M. and Cary, R., "Elemental carbon-based method for monitoring occupational exposures to particulate diesel exhaust," *Aerosol Science and Technology*, vol. 35, pp. 221–241, 1996.

[19] Bjorkman, K. and Karl, D., "Bioavailability of inorganic and organic phosphorus compounds to natural assemblages of microorganisms in Hawaiian coastal waters," *Marine Ecology Progress Series*, vol. 111, pp. 265–273, 1994.

[20] Bjorkman, K. and Karl, D., "Presence of dissolved nucleotides in the north Pacific subtropical gyre and their role in cycling DOP," *Aquatic Microbial Ecology*, vol. 39, no. 2, pp. 193–203, 2005.

[21] Bjorkman, K. and Karl, D. M., "Bioavailability of dissolved organic phosphorus in the euphotic zone at Station Aloha, North Pacific Subtropical Gyre," *Limnology and Oceanography*, vol. 48, no. 3, pp. 1049–1057, 2003.

[22] Blando, J., Porcja, R., Li, T.-H., Bowman, D., Lio, P., and Turpin, B., "Secondary formation and the Smoky Mountain organic aerosol: An examination of aerosol polarity and functional group distribution during SEAVS," *Environmental Science and Technology*, vol. 32, pp. 604–613, 1998.

[23] Bostrom, B., andersen, J., Fleischer, S., and Jansson, M., "Exchange of phosphorus across the sediment-water interface," *Hydrobiologia*, vol. 170, pp. 229–244, 1988.

[24] Cade-Menun, B. J., "Using phosphorus-31 nuclear magnetic resonance spectroscopy to characterize phosphorus in environmental samples," in *Organic phosphorus in the environment* (Turner, B., Frossard, E., and Baldwin, D., eds.), p. 432, CABI publishing, 2004.

[25] Cade-Menun, B. and Preston, C., "A comparison of soil extraction procedures for 31P NMR spectroscopy," *Soil Science*, vol. 161, pp. 101–114, 1996.

[26] Campbell, L. and Vaulot, D., "Photosynthetic picoplankton community structure in the subtroopical North Pacific Ocean near Hawaii (stationALOHA," *Deep-Sea Research I*, vol. 40, pp. 2043–2060, 1993.

[27] Carman, R., Edlund, G., and Damberg, C., "Distribution of organic and inorganic phosphorus compounds in marine and lacustrine sediments: a 31P NMR study," *Chemical Geology*, vol. 163, pp. 101–114, 2000.

[28] Cavender-Bares, K., Karl, D., and Chisholm, S., "Nutrient gradients in the western North Atlantic Ocean: Relationship to microbial community structure and comparison to patterns in the Pacific Ocean," *Deep-Sea Research I*, vol. 48, pp. 2373–2395, 2001.

[29] Cembella, A. D. and Antia, N., "The determination of phosphonates in sea water by fractionation of the total phosphorus," *Marine Chemistry*, vol. 19, pp. 205–210, 1986.

[30] Chang, A. and Patterson, R., "Seasonal sediment and diatom record from late Holocene laminated sediments, Effingham Inlet, British Columbia, Canada," *Palaios*, vol. 18, pp. 477–494, 2003.

[31] Chesselet, R., Fontugne, M., Baut-Menard, P., Ezat, U., and Lambert, C., "The origin of particulate organic carbon in the marine atmosphere as indicated by its stable carbon isotope composition.," *Geophysical Research Letters*, vol. 8, pp. 345–348, 1981.

[32] Chow, J., Watson, J., D.H., L., Solomon, P., Magliano, K., Ziman, S., and RIchards, L., "PM10 and PM2.5 compositions in California's San Joaqin valley.," *Aerosol Science and Technology*, vol. 18, pp. 105–128, 1993.

[33] Church, M., Ducklow, H., and Karl, D. M., "Multiyear increases in dissolved organic matter inventories at Station Aloha in the North Pacific subtropical gyre.," *Limnology and Oceanography*, vol. 47, no. 1, pp. 1–10, 2002.

[34] Clark, L., *Composition and cycling of marine organic phosphorus*. Ph.d., University of Texas at Austin, 2000.

[35] Clark, L., Ingall, E., and Benner, R., "Marine phosphorus is selectively remineralized," *Nature*, vol. 393, p. 426, 1998.

[36] Clark, L., Ingall, E., and Benner, R., "Marine organic phosphorus cycling: Novel insights from nuclear magnetic resonance," *American Journal of Science*, vol. 299, pp. 724–737, 1999.

[37] Colman, A. S., Blake, R., Karl, D. M., Fogel, M., and Turekian, K., "Marine phosphate oxygen isotopes and organic matter remineralization in the oceans.," *Proceedings National Academy of Sciences*, vol. 102, no. 37, pp. 13023–13028, 2005.

[38] Colman, A. S. and Holland, H. D., "The global diagenetic flux of phosphorus from marine sediments to the oceans: Redox sensitivity and the control of atmospheric oxygen levels," *SEPM special publication*, vol. 66, pp. 53–75, 2000.

[39] Cook, R., "Coupling NMR to NOM," *Analytical and Bioanalytical Chemistry*, vol. 378, pp. 1484–1503, 2004.

[40] Cowie, G. and Hedges, J., "Improved quantification of amino acids in natural samples: charge-matched recovery standards and reduced analysis time.," *Marine Chemistry*, vol. 37, pp. 223–238, 1992.

[41] Cowie, G. and Hedges, J., "Biochemical indicators of diagenetic alteration in natural organic matter mixtures," *Nature*, vol. 369, no. 304-307, 1994.

[42] Davelaar, D., "Manganese: A necessary micronutrient to enhance biological phosphorus removal?," *Water Science and Technology*, vol. 21, pp. 1711–1716, 1989.

[43] de Haas, D., Wentzel, M., and Ekama, G., "The use of simultaneous chemical precipitation in modified activated sludge systems exhibiting biological excess phosphate removal Part 2: Method development for fractionation of phosphate compounds in activated sludge," *Water SA*, vol. 26, no. 4, pp. 453–466, 2000.

[44] de Montigny, C. and Prairie, Y., "The relative importance of biological and chemical processes in the release of phosphorus from a highly organic sediment," *Hydrobiologia*, vol. 253, pp. 141–150, 1993.

[45] Decesari, S., Facchini, M., Fuzzi, S., and Tagliavini, E., "Characterization of water-soluble organic compounds in atmospheric aerosol: A new approach," *Journal of Geophysical Research*, vol. 105, no. D1, pp. 1481–1489, 2000.

[46] Decesari, S., Facchini, M., Matta, E., Lettini, F., Mircea, M., Fuzzi, S., Tagliavini, E., and Putaud, J., "Chemical features and seasonal variation of fine aerosol water-soluble organic compounds in the Po Valley, Italy," *Atmospheric Environment*, vol. 35, pp. 3691–3699, 2001.

[47] Decesari, S., Facchini, M., Matta, E., Mircea, M., Fuzzi, S., Chughtai, A., and Smith, D., "Water soluble organic compound formed by oxidation of soot.," *Atmospheric Environment*, vol. 36, no. 1827-1832, 2002.

[48] Deinema, M., Habets, L., Scholten, J., Turkstra, E., and Webers, H., "The accumulation of polyphosphate in Acinetobacter spp.," *FEMS microbiology letters*, vol. 9, no. 1-4, pp. 275–279, 1980.

[49] Delaney, M., "Phosphorus accumulation in marine sediments and the oceanic phosphorus cycle," *Global Biogeochemical Cycles*, vol. 12, pp. 563–572, 1998.

[50] Druffel, E., Bauer, J., Williams, P., Griffin, S., and Wolgast, D., "Seasonal variability of particulate organic radiocarbon in the northeast Pacific Ocean," *Journal of Geophysical Research*, vol. 101, pp. 20543–20552, 1996.

[51] Druffel, E., Griffin, S., Honjo, S., and Manganini, S., "Evidence of old carbon in the deep water column of the Panama Basin from natural radiocarbon measurements," *Geophysical Research Letters*, vol. 25, pp. 1733–1736, 1998.

[52] Duarte, R., Pio, C., and Duarte, A., "Spectroscopic study of the water-soluble organic matter isolated from atmospheric aerosols collected under different atmospheric conditions.," *Analytica Chimica Acta*, vol. 530, pp. 7–14, 2005.

[53] Duer, M., *Introduction to solid-state NMR spectroscopy*. Blackwell publishing, 2005.

[54] DuRand, M., Olson, R., and Chisholm, S., "Phytoplankton population dynamics at the Bermuda Atlantic Time-series Station in the Sargasso Sea," *Deep-Sea Research II*, vol. 48, pp. 1983–2003, 2001.

[55] Facchini, M., Decesari, S., Mircea, M., Fuzzi, S., and Loglio, G., "Surface tension of atmospheric wet aerosol and cloud/fog droplets in relation to their organic carbon content and chemical composition," *Atmospheric Environment*, vol. 34, pp. 4853–4857, 2000.

[56] Fearnside, P., "Fire in the tropical rain forests of the Amazon basin," in *Fire in the tropical biota (Ecological studies 84)* (Goldammer, J., ed.), pp. 106–115, New York: Springer-Verlag, 1990.

[57] Fillippelli, G., "Carbon and phosphorus cycling in anoxic sediments of the Saanich Inlet, British Columbia.," *Marine Geology*, vol. 174, no. 1-4, pp. 307–321, 2001.

[58] Fillippelli, G. and Delaney, M., "Phosphorus geochemistry of equatorial Pacific sediments," *Geochimica et Cosmochimica Acta*, vol. 60, pp. 1479–1495, 1996.

[59] Finlayson-Pitts, B. and Pitts Jr, J., *Atmospheric Chemistry: Fundamentals and Experimental Techniques*. New York: John Wiley, 1986.

[60] Finlayson-Pitts, B. and Pitts Jr, J., *Chemistry of the upper and lower atmosphere*. New York: Academic Press, 1999.

[61] Fogel, M. and Cifuentes, L., "Isotope fractionation during primary production," in *Organic Geochemistry* (Engel, M. and Macko, S., eds.), pp. 73–98, New York: Plenum Press, 1993.

[62] Fraser, M., Cass, G., and Simoneit, B., "Air quality model evaluation data for organics. 6. C3-C24 organic acids," *Environmental Science and Technology*, vol. 37, pp. 446–453, 2003.

[63] Froelich, P., Klinkhammer, G., Bender, M., Luedtke, N., Heath, G., Cullen, D., Hartman, B., and Maynard, V., "Early oxidation of organic matter in pelagic sediments of the eastern equatorial Atlantic: Suboxic diagenesis," *Geochimica et Cosmochimica Acta*, vol. 43, pp. 1075–1090, 1979.

[64] Fyfe, C., *Solid-state NMR for chemists*. Guelph, ON: C.F.C Press, 1983.

[65] Gachter, R., Meyer, J., and Mares, A., "Contribution of bacteria to release and fixation of phosphorus in lake sediments," *Limnology and Oceanography*, vol. 33, pp. 1542–1558, 1988.

[66] Gelinas, Y., Baldock, J., and Hedges, J., "Demineralization of marine and freshwater sediments for CP/MAS 13C NMR analysis," *Organic Geochemistry*, vol. 32, pp. 677–693, 2001.

[67] Graham, B., Mayol-Bracero, O., Guyon, P., Roberts, G., Decesari, S., Facchini, M., Artaxo, P., Maenhaut, W., Koll, P., and andreae, M., "Water-soluble organic compounds in biomass burning aerosols over Amazonia 1. characterization by NMR and GC-MS," *Journal of Geophysical Research*, vol. 107, no. D20, p. 8047, 2002.

[68] Hamilton, J., Webb, P., Lewis, A., Hopkins, J., Smith, S., and Davy, P., "Partially oxidized organic components in urban aerosol using GCXGC-TOF/MS," *Atmospheric Chemistry Physics Discussions*, vol. 4, pp. 1393–1423, 2004.

[69] Havers, A., Burba, P., Lambert, J., and Klockow, D., "Spectroscopic characterization of humic-like substances in airborne particulate matter," *Journal of Atmospheric Chemistry*, vol. 29, pp. 45–54, 1998.

[70] Hedges, J., Baldock, J., Gelinas, Y., Lee, C., Peterson, M., and Wakeham, S., "Evidence for non-selective preservation of organic matter in sinking marine particles," *Nature*, vol. 409, pp. 801–804, 2001.

[71] Hedges, J., Baldock, J., Gelinas, Y., Lee, C., Peterson, M., and Wakeham, S., "The biochemical and elemental compositions of marine plankton: A NMR perspective.," *Marine Chemistry*, vol. 78, pp. 47–63, 2002.

[72] Hedges, J., Eglington, G., Hatcher, P., Kirchman, D., Arnosti, C., Derenne, S., Evershed, R., Kogel-Knabner, I., de Leeuw, J., Littke, R., Michaelis, W., and Rullkotter, J., "The molecularly uncharacterized component of nonliving organic matter in natural environments," *Organic Geochemistry*, vol. 31, pp. 945–958, 2000.

[73] Hedges, J. and Oades, J., "Comparative geochemistries of soils and sediments," *Organic Geochemistry*, vol. 27, pp. 319–361, 1997.

[74] Hedges, J. and Stern, J., "Carbon and nitrogen determinations of carbonate-containing solids," *Limnology and Oceanography*, vol. 29, pp. 657–663, 1984.

[75] Hernes, P. and Benner, R., "Transport and diagenesis of dissolved and particulate terrigenous organic matter in the North Pacific Ocean," *Deep-Sea Research I*, vol. 49, pp. 2119–2132, 2002.

[76] Hernes, P., Hedges, J., Peterson, M., Wakeham, S., and Lee, C., "Neutral carbohydrate geochemistry of particulate material in the central equatorial Pacific," *Deep-Sea Research II*, vol. 43, no. 4-6, pp. 1181–1204, 1996.

[77] Hodson, R. and Azam, F., "Occurrence and characterization of a phosphoenolpyruvate: Glucose phosphotransferase system in a marine bacterium, Serratia marinorubra.," *Applied Environmental Microbiology*, vol. 38, pp. 1086–1091, 1979.

[78] Hong, A., Zhou, Y., and Diwu, Z., "Phosphopeptides and their biological applications," *Chemistry Today*, pp. 57–60, 2003.

[79] Hopkinson, C. S., Vallino, J., and Nolin, A., "Decomposition of dissolved organic matter from the continental margin," *Deep Sea Research II*, vol. 49, pp. 4461–4478, 2002.

[80] Hopkinson, C. and Vallino, J., "Efficient export of carbon to the deep ocean through dissolved organic matter," *Nature*, vol. 433, pp. 142–145, 2005.

[81] Hupfer, M. and Gachter, R., "Polyphosphate in lake sediments: 31P NMR spectroscopy as a tool for its identification," *Limnology and Oceanography*, vol. 40, pp. 610–617, 1995.

[82] Hupfer, M., Rube, B., and Schmeider, P., "Origin and diagenesis of polyphosphate in lake sediments: A 31P NMR study," *Limnology and Oceanography*, vol. 49, no. 1, pp. 1–10, 2004.

[83] Hurtgen, M., Lyons, T., Ingall, E., and Cruse, A., "Anomalous enrichments of iron monosulfide in euxinic marine sediments and the role of H2S in iron sulfide transformation: Examples from Effingham Inlet, the Orca Basin and the Black Sea," *American Journal of Science*, vol. 299, pp. 556–588, 1999.

[84] Hwang, J. and Druffel, E., "Lipid-like material as the source of the uncharacterized carbon in the ocean.," *Science*, vol. 299, pp. 881–884, 2003.

[85] Ingall, E. D. and Jahnke, R. A., "Evidence for enhanced phosphorus regeneration from marine sediments overlain by oxygen depleted waters," *Geochimica et Cosmochimica Acta*, vol. 58, pp. 2571–2575, 1994.

[86] Ingall, E. D. and Jahnke, R. A., "Influence of water column anoxia on the elemental fractionation of carbon and phosphorus during sediment diagenesis," *Marine Geology*, vol. 139, pp. 219–229, 1997.

[87] Ingall, E. D. and Van Cappellen, P., "Relation between sedimentation rate and burial of organic phosphorus and organic carbon in marine sediments," *Geochimica et Cosmochimica Acta*, vol. 54, pp. 373–386, 1990.

[88] Ingall, E., Kolowith, L., Lyons, T., and Hurtgen, M., "Sediment carbon, nitrogen and phosphorus cycling in an anoxic fjord, Effingham Inlet, British Columbia," *American Journal of Science*, vol. 305, pp. 240–258, 2005.

[89] Ingall, E., Schroeder, P., and Berner, R., "The nature of organic phosphorus in marine sediments: new insights from 31P NMR," *Geochimica et Cosmochimica Acta*, vol. 58, pp. 2571–2575, 1990.

[90] Jackson, G. and Williams, P., "Importance of dissolved organic nitrogen and phosphorus to biological nutrient cycling," *Deep-Sea Research*, vol. 32, pp. 223–235, 1985.

[91] Jacobson, M., Hansson, H., Noone, K., and Charlson, R., "Organic atmospheric aerosols: Review and state of the science," *Reviews of Geophysics*, vol. 38, pp. 267–294, 2000.

[92] Jang, M. and McDow, S., "Products of Benz[a]anthracene photodegradation in the presence of known organic constituents of atmospheric aerosols," *Environmental Science and Technology*, vol. 31, pp. 1046–1053, 1997.

[93] Kaplan, L. and Newbold, J., "The role of monomers in sream ecosystem metabolism," in *Aquatic Ecosystem: Interactivity of dissolved organic matter* (Findlay, S. and Sinsabaugh, R., eds.), pp. 97–119, Amsterdam: Elsevier Science, 2003.

[94] Karl, D. M., "A sea of change: Biogeochemical variability in the North Pacific subtropical gyre," *Ecosystems*, vol. 2, pp. 181–214, 1999.

[95] Karl, D. M., Bidigare, R. R., and Letelier, R., "Long-term changes in plankton community structure and productivity in the subtropical North Pacific Ocean: The domain shift hypothesis.," *Deep Sea Research II*, vol. 48, pp. 1449–1470, 2001.

[96] Karl, D. M., Bjorkman, K., Dore, J., Fujieki, L., Hebel, D., and Houlihan, T., "Ecological nitrogen-to-phosphorus at Station ALOHA," *Deep Sea Research II*, vol. 48, pp. 1529–1566, 2001.

[97] Karl, D. and Bailiff, M., "The measurement and distribution of dissolved nucleic acids in aquatic environments," *Limnology and Oceanography*, vol. 34, pp. 543–558, 1989.

[98] Karl, D. and Bjorkman, K., "Dynamics of dop," in *Biogeochemistry of marine dissolved organic matter* (Hansell, D. and Carlson, C., eds.), pp. 249–366, London: Academic Press, 2002.

[99] Karl, D. and Yanagi, K., "Partial characterization of the dissolved organic phosphorus pool in the oligotrophic North Pacific Ocean," *Limnology and Oceanography*, 1997.

[100] Kiss, G., Varga, B., Galambos, I., and Ganszky, I., "Characterization of water-soluble organic matter isolated from atmospheric fine aerosol.," *Journal of Geophysical Research*, vol. 107, no. D21, pp. 8339, doi: 10. 1029/2001JD00063, 2002.

[101] Kitteredge, J., Horiguchi, M., and Williams, P., "Aminophosphonic acids: Biosynthesis by marine phytoplankton," *Comparative Biochemistry and Physiology*, vol. 29, pp. 859–863, 1969.

[102] Kolowith, L., Ingall, E., and Benner, R., "Composition and cycling of marine organic phosphorus," *Limnology and Oceanography*, vol. 46, pp. 309–320, 2001.

[103] Kononova, S. and Nesmeyanova, M., "Phosphonates and their degradation by microorganisms," *Biochemistry-Moscow*, vol. 67, pp. 187–195, 2002.

[104] Krivacsy, Z., Molnar, E., Tarjanyi, E., Gelencser, G., Kiss, G., and Hlavay, J., "Investigation of inorganic ions and organic acids in the atmospheric aerosol by capillary electrophoresis," *Journal of Chromatography A*, vol. 781, pp. 223–231, 1997.

[105] Laarkamp, K., *Organic phosphorus in marine sediments: Chemical structure, diagenetic alteration and mechanisms of preservation.* Ph.d., Massachusetts Institute of Technology, 2000.

[106] Lawrence, J. and Koutrakis, P., "Measurement and speciation of gas and particulate phase organic acidity in an urban environment 2," *Journal of Geophysical Research*, vol. 101, pp. 9171–9184, 1996.

[107] Lee, C., Wakeham, S., and Arnosti, C., "Particulate organic matter in the sea: The composition conundrum," *Ambio*, vol. 33, no. 8, pp. 565–575, 2004.

[108] Lee, C., Wakeham, S., and Hedges, J., "Composition and flux of particulate amino acids and chloropigments in equatorial Pacific sea water and sediments," *Deep-Sea Research I*, vol. 47, pp. 1535–1568, 2000.

[109] Lenton, T. M. and Watson, A. J., "Redfield revisited 1. regulation of nitrate, phosphate, and oxygen in the ocean," *Global Biogeochemical Cycles*, vol. 14, pp. 225–248, 2000.

[110] Lenton, T. M. and Watson, A. J., "Redfield revisited 2. what regulates the oxygen content of the atmosphere?," *Global Biogeochemical Cycles*, vol. 14, pp. 249–268, 2000.

[111] Lim, H.-J. and Turpin, B., "Origins of primary and secondary organic aerosol in atlanta: Results of time-resolved measurements during the Atlanta supersite experiment.," *Environmental Science and Technology*, vol. 36, pp. 4489–4496, 2002.

[112] Loh, A. and Bauer, J., "Distribution, partitioning and fluxes of dissolved and particulate organic C, N and P in the eastern North Pacific and Southern Oceans," *Deep-Sea Research I*, vol. 47, pp. 2287–2316, 2000.

[113] Loh, A., Bauer, J., and Druffel, E., "Variable ageing and storage of dissolved organic components in the open ocean," *Nature*, vol. 430, pp. 877–881, 2004.

[114] Malcolm, R., "Applications of solid-state 13C NMR spectroscopy to geochemical studies of humic substances," in *Humic Substances II* (Hayes, M., MacCarthy, P., Malcolm, R., and Swift, R., eds.), New York: John Wiley and sons, 1989.

[115] Malm, W., Molenar, J., Eldred, R., and Sisler, J., "Examining the relationship among atmospheric aerosols and light scattering and extinction in the Grand Canyon area," *Journal of Geophysical Research*, vol. 101, pp. 19,251–19,265, 1996.

[116] Mao, J., Hu, W., Schmidt-Rohr, K., Davies, G., Ghabbour, E., and Xing, B., "Quantitative characterization of humic substances by solid-state 13C nuclear magnetic resonance.," *Journal Soil Science Society of America*, vol. 64, pp. 873–884, 2000.

[117] Mayol-Bracero, O., Guyon, P., Graham, B., Roberts, G., Andreae, M., Decasari, S., Facchini, M., Fuzzi, S., and Artaxo, P., "Water-soluble organic compounds in biomass burning aerosols over Amazonia 2. apportionment of the chemical composition and importance of the polyacidic fraction," *Journal of Geophysical Research*, vol. 107,891, p. 10.1029/2001JD000522, 2002.

[118] McCarthy, M., Hedges, J., and Benner, R., "The chemical composition of dissolved organic matter in sea water," *Chemical Geology*, vol. 107, pp. 503–507, 1993.

[119] McCarthy, M., Hedges, J., and Benner, R., "Major biochemical composition of dissolved high molecular weight organic matter in sea water," *Marine Chemistry*, vol. 55, pp. 281–297, 1996.

[120] McCarthy, M., Hedges, J., and Benner, R., "Major bacterial contribution to marine dissolved organic nitrogen," *Science*, vol. 281, pp. 231–234s, 1998.

[121] McCarthy, M., Pratum, T., Hedges, J., and Benner, R., "Chemical composition of dissolved organic nitrogen in the ocean," *Nature*, vol. 390, pp. 150–154, 1997.

[122] McManus, J. M., Berelson, W. M., Coale, K. H., Johnson, K. S., and Kilgore, T. E., "Phosphorus regeneration in continental margin sediments," *Geochimica et Cosmochimica Acta*, vol. 61, pp. 2891–2907, 1997.

[123] Murphy, A. E., Sageman, B. B., and Hollander, D. J., "Eutrophication by decoupling of the marine biogeochemical cycles of C, N, and P: A mechanism for the Late Devonian mass extinction," *Geology*, vol. 28, pp. 427–430, 2000.

[124] Murphy, A. E., Sageman, B. B., Hollander, D. J., Lyons, T. W., and Brett, C. E., "Black shale deposition and faunal overturn in the Devonian Appalachian basin: Clastic starvation, seasonal water-column mixing and efficient biolimiting nutrient recycling," *Paleoceanography*, vol. 15, pp. 280–291, 2000.

[125] Murphy, J. and Riley, J., "A modified single solution method for the determination of phosphate in natural waters," *Analytica Chimica Acta*, vol. 27, pp. 31–36, 1962.

[126] Myneni, S., "Soft x-ray spectroscopy and spectromicroscopy studies of organic molecules in the environment," in *Applications of synchotron radiation in low-temperature geochemistry and environmental science.* (Fenter, P., Rivers, M., Sturchio, N., and Sutton, S., eds.), vol. 49 of *Reviews in Mineralogy and Geochemistry*, pp. 485–579, The Geochemical society, 2002.

[127] Nanny, M. and Minear, R., "Characterization of soluble unreactive phosphorus using 31P nuclear magnetic resonance spectroscopy," *Marine Geology*, vol. 139, pp. 77–94, 1997.

[128] Nesmeyanova, M., "Polyphosphates and enzymes of polyphosphate metabolism in Escherichia coli," *Biochemistry-Moscow*, vol. 65, no. 3, pp. 309–314, 2000.

[129] Novakov, T. and Corrigan, C., "Cloud condensation nucleus activity of the organic component of biomass smoke particles," *Geophysical Research Letters*, vol. 23, pp. 2141–2144, 1996.

[130] Pakulski, J. and Benner, R., "Abundance and distribution of dissolved carbohydrates in the ocean.," *Limnology and Oceanography*, vol. 39, pp. 930–940, 1994.

[131] Paytan, A., Cade-Menun, B. J., McLaughlin, K., and Faul, K. L., "Selective phosphorus regeneration of sinking marine particles: evidence from P-31NMR," *Marine chemistry*, vol. 82, pp. 55–70, 2003.

[132] Perdue, E. and Ritchie, J., "Dissolved organic matter in fresh waters," in *Surface and ground water, weathering and soils.* (Drever, J., ed.), vol. 5 of *Treatise on Geochemistry*, Elsevier, 2003.

[133] Petsch, S. T. and Berner, R. A., "Coupling the geochemical cycles of C, P, Fe and S: The effect on atmospheric O2 and the isotopic records of carbon and sulfur," *American Journal of Science*, vol. 298, pp. 246–262, 1998.

[134] Petterson, R., "The chemical composition of wood," *Chemistry of solid wood*, vol. Advanced Chemistry Series, no. 207, pp. 57–126, 1984.

[135] Pettersson, K., "Alkaline phosphatase activity and algal surplus phosphorus as phosphorus-deficiency indicators in Lake Erken.," *Archiv fur Hydrobiologie*, vol. 89, pp. 54–87, 1980.

[136] Repeta, D., Quan, T., Aluwihare, L., and Accardi, A., "Chemical characterization of high molecular weight dissolved organic matter in fresh and marine waters.," *Geochimica et Cosmochimica Acta*, vol. 66, no. 6, pp. 955–962, 2002.

[137] Ruttenberg, K. and Berner, R., "Authigenic apatite formation and burial in sediments from non-upwelling continental margin environments," *Geochimica et Cosmochimica Acta*, vol. 57, pp. 991–1007, 1993.

[138] Ruttenberg, K. and Goni, M, A., "Phosphorus distribution, C:N:P ratios and delta13C subOC in arctic, temperate, and tropical coastal sediments: Tools for characterizing bulk sedimentary organic matter.," *Marine Geology*, vol. 139, pp. 123–145, 1997.

[139] Sanders, J. and Hunter, B., *Modern NMR spectroscopy: A guide for chemists*. Oxford: Oxford university press, 2nd. ed., 1993.

[140] Sannigrahi, P. and Ingall, E. D., "Polyphosphates as a source of enhanced P fluxes in marine sediments overlain by anoxic waters: Evidence from 31P NMR," *Geochemical Transactions*, vol. 6, no. 3, pp. 52–59, 2005.

[141] Sannigrahi, P., Ingall, E. D., and Benner, R., "Cycling of dissolved and particulate organic matter at station Aloha: Insights from 13C NMR spectroscopy coupled with elemental, isotopic and molecular analyses.," *Deep Sea Research I*, vol. 52, no. 8, pp. 1429–1444, 2005.

[142] Sannigrahi, P., Sullivan, A. P., Weber, R. J., and Ingall, E., "Characterization of water-soluble organic carbon in urban atmospheric aerosols using solid-state 13C NMR spectroscopy," *Environmental Science and Technology*, vol. In press, 2005.

[143] Sanudo-Wilhelmy, S., Kustka, A., Gobler, C., Hutchins, D., Yang, M., Lwiza, K., Burns, J., Capone, D. G., Raven, J., and Carpenter, E. J., "Phosphorus limitation of nitrogen fixation by Trichodesmium in the central Atlantic Ocean.," *Nature*, vol. 411, pp. 66–69, 2001.

[144] Saxena, P. and Hildemann, L., "Water-soluble organics in atmospheric particles: A critical review of the literature and application of thermodynamics to identify candidate compounds.," *Journal of Atmospheric Chemistry*, vol. 24, pp. 57–109, 1996.

[145] Saxena, P., Hildemann, L., McMurry, P., and Seinfeld, J. H., "Organics alter hygroscopic behavior of atmospheric particles," *Journal of Geophysical Research*, vol. 100, pp. 18,755–18,770, 1995.

[146] Schauer, J. J. and Cass, G., "Source apportionment of wintertime gas-phase and particle-phase air pollutants using organic compounds as tracers.," *Environmental Science and Technology*, vol. 34, pp. 1821–1832, 2000.

[147] Schlesinger, W., *Biogeochemistry: An analysis of global change*. London: Academic Press, 1991.

[148] Schnitzer, M., "Soil organic matter- the next 75 years," *Soil Science*, vol. 151, pp. 41–48, 1991.

[149] Schuffert, J., Jahnke, R., Kastner, M., Leather, J., Sturz, A., and Wing, M., "Rates of formation of modern phosphorite off western Mexico," *Geochimica et Cosmochimica Acta*, vol. 58, no. 22, pp. 5001–5010, 1994.

[150] Schulz, H. and Schulz, H., "Large sulfur bacteria and the formation of phosphorite," *Science*, vol. 307, pp. 416–418, 2005.

[151] Schwartzenbach, R., Gschwend, P., and Imboden, D., *Environmental organic chemistry*. New York: John Wiley, 1993.

[152] Seinfeld, J. and Pandis, S., *Atmospheric chemistry and physics*. New York: John Wiley and Sons, 1996.

[153] Sharp, J., "Size classes of organic carbon in sea water.," *Limnology and Oceanography*, vol. 42, pp. 1803–1813, 1973.

[154] Skoog, A. and Benner, R., "Aldoses in various size fractions of marine organic matter: Implications for carbon cycling," *Limnology and Oceanography*, vol. 42, no. 8, pp. 1803–1813, 1997.

[155] Slomp, C., Thomson, J., and De Lange, G., "Enhanced regeneration of phosphorus during the formation of the most recent eastern Mediterranean sapropel (s1)," *Geochimica et Cosmochimica Acta*, vol. 66, pp. 1171–1184, 2002.

[156] Solomon, P., Baumann, K., Edgerton, E., Tanner, R., Eatough, D., Modey, E., Marin, H., Savoie, D., Natarajan, S., Meyer, M., and Norris, G., "Comparison of integrated samplers for mass and composition during the 1999 Atlanta supersites project," *Journal of Geophysical Research*, vol. 108 (D7), p. 10.1029/2001JD001218, 2003.

[157] Solorzano, L. and Strickland, J., "Polyphosphate in sea water," *Limnology and Oceanography*, vol. 13, pp. 515–518, 1968.

[158] Sullivan, A. P., Weber, R. J., Clements, A. L., Turner, J. R., Bae, M. S., and Schauer, J. J., "A method for on-line measurement of water-soluble organic carbon in ambient aerosol particles: Results from an urban site," *Geophysical Research Letters*, vol. 31, no. 13, 2004. L13105.

[159] Sullivan, A. and Weber, R. J., "Chemical characterization of the ambient organic aerosol soluble in water Part 1: Isolation of hydrophobic and hydrophilic fractions," *Journal of Geophysical Research*, vol. In review, 2005a.

[160] Sullivan, A. and Weber, R. J., "Chemical characterization of the ambient organic aerosol soluble in water Part 2: Analysis of hydrophobic and hydrophilic fractions by size exclusion chromatography with TOC analysis," *Journal of Geophysical Research*, vol. In review, 2005b.

[161] Sundareshwar, P., Morris, J., Pellechia, P., Cohen, H., Porter, D., and Jones, B., "Occurrence and ecological implications of pyrophosphate in estuaries," *Limnology and Oceanography*, vol. 46, pp. 1570–1577, 2001.

[162] Sundby, B., Anderson, L., Hall, P., Iverfeldt, A., Van Der Loeff, M., and Westerlund, S., "The effect of oxygen on release and uptake of cobalt, manganese, iron and phosphate at the sediment-water interface," *Geochimica et Cosmochimica Acta*, vol. 50, pp. 1282–1288, 1986.

[163] Sundby, B., Gobeil, C., Silverberg, N., and Mucci, A., "The phosphorus cycle in coastal marine sediments," *Limnology and Oceanography*, vol. 37, no. 6, pp. 1129–1145, 1992.

[164] Suzuki, Y., Imai, S., Kawakami, M., Masuda, Y., and Akasaka, K., "Identification and determination of low-molecular weight organic compounds in fog water using proton NMR spectroscopy," *Bulletin of Environmental Contamination and Toxicology*, vol. 60, pp. 355–362, 1998.

[165] Suzuki, Y., Kawakami, M., and Akasaka, K., "H-1 NMR application for characterizing water-soluble organic compounds in urban atmospheric particles," *Environmental Science and Technology*, vol. 35, no. 13, pp. 2656–2664, 2001.

[166] Suzumura, M. and Ingall, E., "Distribution and dynamics of various forms of phosphorus in sea water: Insights from filed observations in the Pacific Ocean and a laboratory experiment," *Deep-Sea Research I*, vol. 51, pp. 1113–1130, 2004.

[167] Ternan, N., McGrath, J., McMullan, G., and Quinn, J., "Organophosphonates: Occurrence, synthesis and biodegradation by microorganisms," *World Journal of Microbiology and Biotechnology*, vol. 14, pp. 635–647, 1998.

[168] Thomson-Bulldis, A. and Karl, D. M., "Application for a novel method of phosphorus determinations in the oligotrophic NNorth Pacific Ocean," *Limnology and Oceanography.*, vol. 43, pp. 1565–1577, 1998.

[169] Thurman, E., *Organic geochemistry of natural waters.* Lancaster: Martinus Nijhoff/Dr. W. Junk, 1985.

[170] Thurman, E. and Malcolm, R., "Preparative isolation of aquatic humic substances," *Environmental Science and Technology*, vol. 14, pp. 463–466, 1981.

[171] Turner, B., Maheiu, N., and Condron, L., "Phosphorus-31 nuclear magnetic resonance spectral assignments of phosphorus compounds in soil NaOH-EDTA extracts," *Soil Science Society of America Journal*, vol. 67, pp. 497–510, 2003.

[172] Van Cappellen, P. and Berner, R., "Flourapatite crystal growth from modified sea water solutions," *Geochimica et Cosmochimica Acta*, vol. 55, pp. 1219–1234, 1991.

[173] Van Cappellen, P. and Ingall, E., "Benthic phosphorus regeneration, net primary production, and ocean anoxia: A model of the coupled marine biogeochemical cycles of carbon and phosphorus," *Paleoceanography*, vol. 9, pp. 677–692, 1994.

[174] Van Cappellen, P. and Ingall, E., "Redox stabilization of the atmosphere and oceans by phosphorus-limited marine productivity," *Science*, vol. 271, pp. 493–496, 1996.

[175] Wakeham, S. and Lee, C., "Organic geochemistry of particulate matter in the ocean: the role of particles in oceanic sedimentary cycles.," *Organic Geochemistry*, vol. 14, pp. 83–96, 1989.

[176] Wakeham, S. and Lee, C., "Production, transport and alteration of particulate organic matter in the marine water column.," in *Organic geochemistry: Principles and applications* (Engel, M. and Macko, S., eds.), pp. 145–169, New York: Plenum Press, 1993.

[177] Wakeham, S., Lee, C., Hedges, J., Hernes, P., and Peterson, M., "Molecular indicator of diagenetic status in marine organic matter," *Geochimica et Cosmochimica Acta*, vol. 61, pp. 5363–5369, 1997.

[178] Wallmann, K., "Feedbacks between oceanic redox states and marine productivity; a model perspective focused on benthic phosphorus cycling," *Global Biogeochemical Cycles*, vol. 17, no. 3, p. 18, 2003.

[179] Wang, X.-C., Altabet, M., Callahan, J., and Chen, R., "Stable carbon and nitrogen isotopic compositions of high molecular weight dissolved organic matter from four U.S. estuaries," *Geochimica et Cosmochimica Acta*, vol. 68, no. 12, pp. 2681–2691, 2004.

[180] Wilson, M., *NMR techniques and applications in geochemistry and soil chemistry*. Oxford: Pergamon, 1987.

[181] Wilson, M., "Solid-state nuclear magnetic resonance spectroscopy of humic substances: Basic concepts and techniques," in *Humic Substances II* (Hayes, M., MacCarthy, P., Malcolm, R., and Swift, R., eds.), New York: John Wiley and Sons, 1989.

[182] Yan, J., Packer, N., Gooley, A., and William, K., "Protein phosphorylation: Technologies for the identification of phosphoamino acids," *Journal of Chromatography A*, vol. 80, no. 1-2, pp. 23–41, 1998.